3D printing of Geopolymer Concrete

Author:	Zainab Aldin
Date:	08 January 2019

Graduation Committee:

Dr. Guang Ye, MSc	TU Delft, CiTG
Prof. dr. ir. E.Schlangen	TU Delft, CiTG
Dr. H. Nugteren, MSc	TU Delft, TNW
Ir. Lambert Houben, MSc	TU Delft, CiTG

Delft University of Technology

3D printing of Geopolymer Concrete

By
Zainab Aldin

A thesis submitted to the Faculty of Civil Engineering and Geosciences
in partial fulfilment of the requirements for the degree of
Master of Science in Civil Engineering at the Technical University of Delft, The Netherlands

DELFT UNIVERSITY OF TECHNOLOGY FACULTY OF CIVIL ENGINEERING AND GEOSCIENCES
STEVINWEG 1
2628 CN
DELFT
THE NETHERLANDS

Graduation Committee:

Chairman:
Dr. G. Ye, Materials- Mechanics- Management & design, Faculty of Civil Engineering and Geosciences, TU Delft

Committee members:
Prof. dr. ir. H.E.J.G.Schlangen , Materials- Mechanics- Management & design, Faculty of Civil Engineering and Geosciences, TU Delft

Dr. H. Nugteren, Faculty of applied sciences, TU Delft

Ir. Lambert Houben, Faculty of Civil Engineering and Geosciences, TU Delft

Table of Contents

Acknowledgement

My thesis could not be accomplished without the constructive guidance, advice, and support by my supervisor Dr. Guang Ye. You have been my daily supervisor of this M.Sc thesis project . I would like extend my heartfelt gratitude for all your help and encouragement.

I would like to sincerely thank my co-advisors Prof. Eric Schlangen and Dr. Henk Nugteren for their discrete advises, tips and guidance during this work.
Thanks are also extended to my colleague PhD candidate Stefan Chaves Figueiredo for his tips.

I would also like to thank Maiko van Leeuwen and Ton Blom at the department of Civil Engineering for their technical support during conducting of some experiments in the concrete laboratory.

My thanks and gratitude are extended to Dr. Khadija El Cheikh and PhD candidate Dengwu Jiao at the University of Gent, Belgium for their technical support during the conducting of some 3D printing measurements.

Acknowledgement are also due to my family for their encouragement, moral and financial support.

List of Abbreviations

AAB	Alkaline activated binders
BFS	Blast furnace slag
C_2S	Calcium silicates (Belite)
C_3A	Tricalcium aluminate (C_3A)
C_3S	Calcium silicates (Alite)
C_4AF	Tetra calcium aluminoferrite
C-H	Calcium hydroxide/Portlandite
CSHs	Calcium-silicate hydrates
DP	Degree of polymerization
FA	Fly ash
GPC	Geopolymer concrete
LPA	Laser particle analyser
MK	Metakaolin
NH	Sodium hydroxide (NaOH)
OPC	Ordinary Portland cement
OPCC	Ordinary Portland cement concrete
SCM	Supplementary cementitious materials
SF	Silica fume
WG	Waste glass
XRD	X-ray powder diffraction
XRF	X-ray fluorescence

Abstract

In spite of the fact that there are many advantages of alkali activated materials (also called geopolymers) over the cement-based materials, geopolymer concrete has been used in the past for construction purposes on a very limited level. Among the many advantages of geopolymers compared with the cement-based materials is less CO_2 emission, it uses byproducts as a binder, less energy consumption during its production, more durable as a material, fast setting time and high strength development.

This work is an attempt to exert some light on the usability and applicability of geopolymers in the field of construction with concentration on its use in the 3D printing. The main aim of this study is to propose a design methodology for geopolymer paste mixture to be used in 3D printing process.

For achieving this goal, one paste mixture design was selected among six ones on the bases of longer workability/flowability, suitable extrudability and specific setting time. These six designs have different binder ratios. The selected mixture design, named S20, was tested further to find out its suitability for 3D printing process. This S20 mixture was tested on compressive strength, setting time, rheological properties, open time, buildability and 28 days tensile bonding strength of two layers.

To find the best suitable design, modifications were done on the S20 mixture by changing the ratios between the used alkaline solutions Na_2SiO_3 and NaOH (0.25 was selected). These alkaline solutions played a major role in delaying the initial setting time for rheological tests (90 minutes were selected) and the extrudability for the 3D printing process. Another factor for the best design is the Acti-gel as an additive. This additive has a direct link with the buildability, extrudability and viscosity when added with different percentages. The best selected percentage of the Acti-gel was 0.75% for this mixture design. The open time and the 28 days tensile bonding strength tests were selected to be 33 minutes and 1.32 MPa respectively. Comparing the measured plastic viscosity to the open time test, the extrudability of the mixture is not anymore valid beyond 8.8 Pa.s plastic viscosity. This short open time of 33 minutes for such geopolymer mixture design needs a fast-performing 3D printer. This might help in achieving construction projects within short time.

Chapter 1

1 General introduction

1.1 Background

Pollution is considered to be responsible of the destruction of the natural land which we live on, the water we drink and the air we breathe. The rapid developments in the technology is aimed to make our lives easier. However, the rapid developments started to inflict negative affects in our globe environment by destroying the natural resources of the earth. Many researchers have proven that the massive increase in pollution growth is due to the rapid growth of the technology and other areas. Based on the data collected from the European Commission (Figure 1.1), the total waste that is produced in Europe from the industry in the year 2014 was around 10.2%. [1] As for the CO_2-emission from cement production and the use of fossil-fuel was in the year 2016 around 3.5 gigatons (Figure 1.2). [2]

The data in Figure 1.2 shows that the largest CO_2 emitting countries are China, United States and some countries in the middle east and North Africa. European countries standing on the fourth place of the largest CO_2 producers.

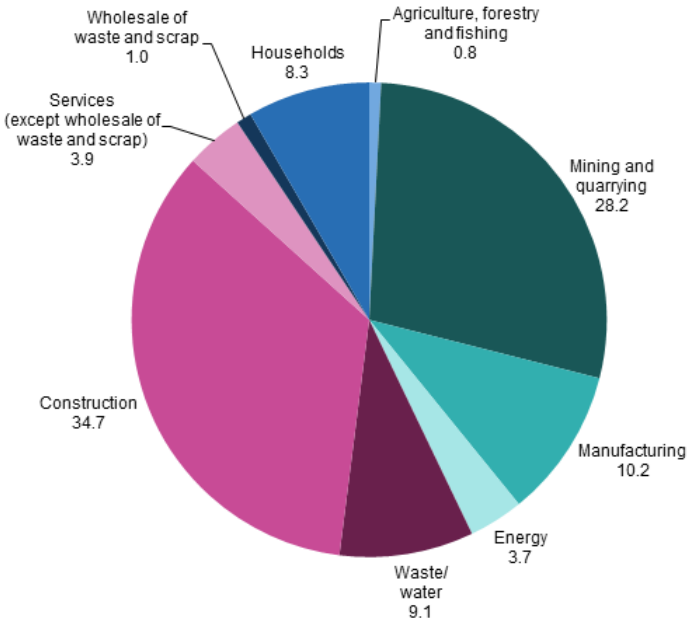

Fig. 1. 1: Waste production, broken down by economic activity and households in the Europe [1]

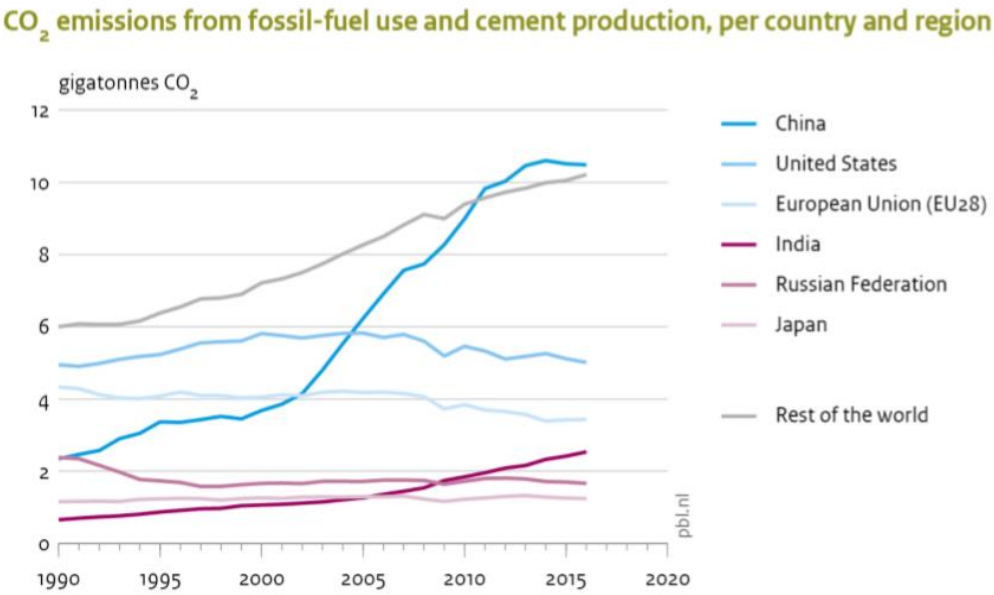

Fig. 1. 2: CO_2 emission from cement production and fossil-fuel use, per country [2]

Turning waste into a resource is fundamental to the economy. If it is possible, in the near future, to re-manufacture, re-use and recycle waste products than there is no need anymore to exhaust natural resources for human activities. Waste can be eliminated and re-used in a sustainable and more efficient way.

Among the byproducts that are produced every year by the industry are Fly-Ash (FA) and Blast furnace slag (BFS). Fly-Ash (FA) and Blast furnace slag (BFS) are applied as a partial replacement of cement. Cement is the primary ingredient in concrete that most structures; such as bridges, roads and buildings are made of. The most coming known cement types are given in the overview in Table 1.1.

Table 1.1: Cement types [NEN-EN 197-1: 2011]

Cement type		
CEM I	Portland cement	Portland cement + max. 5% of minor additional constituents
CEM II	Portland-composite cement	Portland cement + max. 35% of other constituents (BFS, FA)
CEM III	Blast furnace cement	Portland cement and higher percentage BFS
CEM IV	Pozzolanic cement	Portland cement+ max 55% pozzolanic constituents
CEM V	Composite cement	Portland cement+ BFS, FA and pozzolanic constituents

Based on the data collected in the Netherlands for cement production and usage, about 50-60% of CEM III cement, 35% of CEM I and the rest of cement CEM II are used for decades. [3] Before the end of the year 2018, around 5.000 kT will be consumed in the Netherlands as it is shown in Figure 1.3.

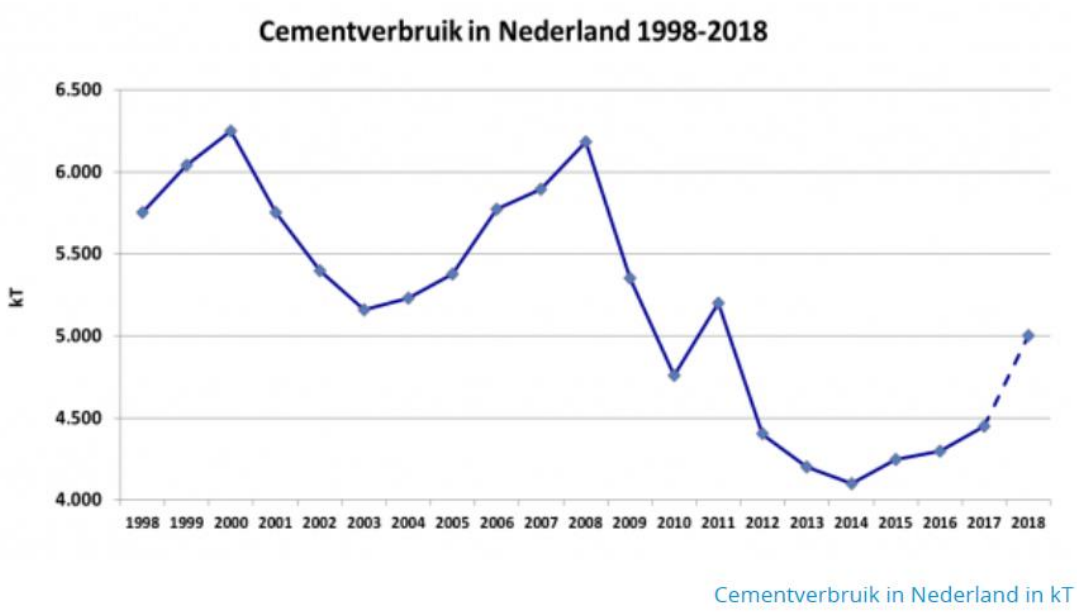

Fig. 1. 3: Cement consumption in the Netherlands 1998-2018 [3]

The production of Ordinary Portland cement concrete (OPCC) is characterized with its high emission of carbon dioxide (CO_2) due to calcination of limestone and combustion of fossil fuel, coupled with high energy consumption (kiln temperatures of 1450–1550 °C) for its production. [4] [7] Moreover, Portland cement consumption has grown nearly exponentially in the last two decades.

To produce 2.0 billion tons of Portland cement, over 3.0 billion tons of raw materials (70% of which are limestone) are consumed. [7] As a result, the amount of CO_2 released to the atmosphere increases due to the energy consumption for the production of cement. To minimize the depletion of natural resources, it is required to re-use and develop sustainable materials. The three pillars of sustainable development are economy and environmental protection as well as social development. The Earth's capacity to support people is determined by natural constraints and human priorities. [5] [6]
Around the world, researchers are focusing on finding new types of concretes that have better or similar rheological and mechanical properties as cement-based concrete. One of these concretes are the alkaline activated materials (also called geopolymers). Geopolymer concretes (GPC) were eventually developed with the aim to reduce the CO_2 footprint by eliminating the use of cement and reduce the costs by using industrial byproducts. [7]

Geopolymer concrete, which is characterized by low permeability, high mechanical properties and excellent heat resistance, has been receiving increasing attention in the building industry. However, there are some challenges regarding the structural application, such as production costs, adjusting the fast setting time and tailoring the workability. [8] [9]

1.2 GP Concrete vs. OPC Concrete

In this paragraph, a comparison is made between OPC concrete and alkaline activated materials (geopolymers). This comparison is important for having a better insight into the properties differences and how to improve it as an alternative future construction material. A summation of these properties is shown in Table 1.2 and Table 1.3.

1.2.1 Environmental impact

Greenhouse gasses emission, such as CO_2 and CO are the main reason for the global warming. The production of one ton of Ordinary Portland Cement emits nearly one ton of CO_2 in the atmosphere. [8] As reported, the cement industry contributes approximate a 5% to 8% global CO_2 emission. [12] [37] [38] [39] [40]

Based on researcher's findings, the application of byproducts, such as FA and BFS as alternative binders does not affect the environment negatively. [10] [11] [13] [14]
McLellan et al. (2011) proved a reduction of greenhouse gas emission by using Australian geopolymer products. The reduction in greenhouse gas was around 44%-64% compared with that of OPCC. [10] [11]
Mclellan has mention that the main reason of the reduction in CO_2 for geopolymer systems is due to the minimum processed natural minerals and industrial wastes are applied to form the binding agent. Besides Mclellan, Turner et al. mentioned in 2013 that GPC reduces 80% the production of CO_2 compared to OPCC. [41]

1.2.2 Compressive strength

The chemical composition of the GPC plays an important role in having different mechanical and rheological properties. The compressive strength of concrete is one of the most important characteristics. It depends on different factors such as liquid to binder ratio (l/b), coarse & fine aggregate ratio, type of binders, compaction of concrete, temperature, relative humidity and curing conditions. With addition to these factors, GPC is also affected by the molarity of alkaline activator solution(s) as well as the mixing ratios of both binders and alkaline activator solution(s).

Based on the findings of Guo et al. (2010), Hardjito et al. (2004), Nasvi et al. (2012), Kong & Sanjyan (2008) and Yost et al. (2013), GPC can develop high strength in the early ages under high curing temperature. [15] [16] [17] [18] [19] However other researchers like Kumar et al. (2010), Li & Liu (2007) and Manjunath & Giridhar (2011) reached to the conclusion that the addition of slag to the mixture helps GPC in gaining its target strength at 28 days of curing under ambient condition. [20] [21] [22] Based on the research of Akhilesh et al. (2012) GPC showed 1.5 times higher compressive strength when compared to OPCC with the same mixture design. [23]

1.2.3 Flexural and Tensile strength

Besides the higher compressive strength, GPC has a higher tensile strength when compared to OPCC. A higher tensile strength improves the capacity of a section by decreasing the amount of required reinforcement and delays the crack development. The work of Nikraz & Olivia (2012) reported that the tensile strength of GPC is about 8% to 12% greater than OPCC. [25] Furthermore Bhikshma et al. (2012) observed that the higher tensile strength of GPC is related to the chemical composition. [26] Based on the observation of their work shows that tensile strength can vary from 3.72 to 4.95 MPa for an alkaline liquid to FA ratio of 0.3 to 0.5. Another researcher (Hardjito et al. (2005)) found that the tensile and flexural strength is comparable to the OPCC. [27]

1.2.4 Modulus of elasticity

Based on the work of Nath et al. (2017) for a similar compressive strength the elastic modulus of GPC is 25% to 30% lower than of the OPCC at a curing age of 28 days. In addition to that, the value of modulus of elasticity of GPC is not affected by the increase of temperature. [32]

1.2.5 Fire resistance

The strength capacity of concrete decreases when it is subjected to high temperatures. GPC is considered as a fire-resistant material. The observation of Mane and Jadhav (2012) shows that when OPCC and GPC exposed to a temperature of 500 °C, GPC has less reduction in the strength capacity than OPCC. This reduction is due to the thermal expansion between aggregates and paste. [28] [29]

In general, GPC has a good fire resistance with respect to OPCC when it is exposed to a temperature more than 800 °C. [29] [30] [31]

1.2.6 Density and porosity

In addition to the mechanical strength, the work of Mohd et al. (2013) showed that the density of FA based GPC was between 2290 kg/m^3 and 2460 kg/m^3 but still similar to the OPCC. [24] whereas the work of Nath et al. (2017) found that the density of GPC is between 2323 kg/m^3 and 2400 kg/m^3, which is similar to the OPCC density range. [32]

For the porosity, Mohd et al. (2013) found in his work that the porosity of OPCC was around 3.0% to 5.1% and that for the GPC was around 1.0% to 1.9%. [24]

1.2.7 Shrinkage and creep

The GPC has low shrinkage and creep properties. The Drying shrinkage strains are extremely small in the order of 100 micro strains after one year compared with the range of values of 500 to 800 micro strains experienced by OPCC. Wallah et al. (2010) concluded that fly ash-based geopolymer concrete undergoes low creep. [33]

In fact, this behavior is caused by the lower amount of water used in producing GPC. [10] The value of creep deceases with the increase of compressive strength and it is estimated that GPC has not more than 0.4 compared with 0.7 for OPCC. [10]

1.2.8 Corrosion resistance

Shaikh et al. (2014) explained in his work that GPC exhibits better corrosion resistance than OPCC. The higher amount of the Sodium Silicate (Na_2SiO_3) and the higher concentration of Sodium Hydroxide (NaOH), gives better corrosion resistance of GPC. [34] Olivia et. al. (2011) concluded that after making a comparison with OPCC, FA based GPC take a long time to fail and has good corrosion resistance. [35]

1.2.9 Energy consumption

It is also important to make a comparison between the total embodied energy required to produce OPCC and GPC. Bennet et al. (2013) explained in his work that embodied energy of FA and GGBFS based GPC is 40% less than OPCC. In OPCC the cement contributes to 94% of the total embodied energy. While both Sodium Hydroxide (39%) and Sodium Silicate (49%)

together contribute a lion's share to the embodied energy of GPC (Figure 1.4 and Figure 1.5). [36]

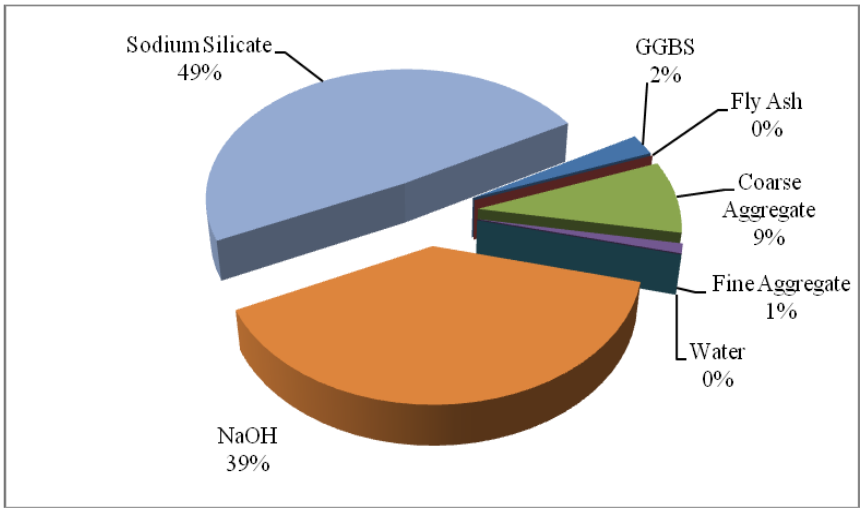

Fig.1. 4: Embodied energy contribution of each material on fly ash-GGBS based geopolymer concrete [36]

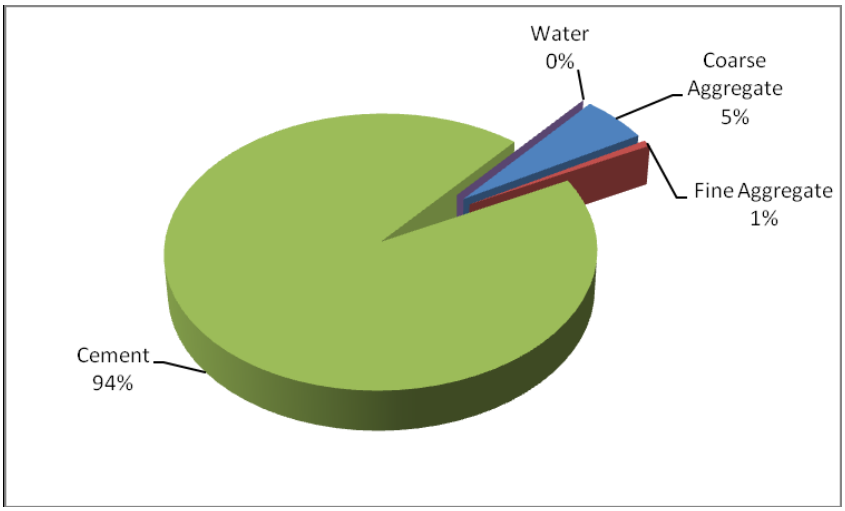

Fig.1. 5: Embodied energy contribution of each material on OPC concrete. [36]

Table 1. 2: Properties comparison between GPC and OPCC

Property	GPC	OPCC
Emission of CO_2	44 % to 80% reduction of human-generated atmospheric CO_2 worldwide.	Major contributor 5% to 8% of human-generated atmospheric CO_2 worldwide.
A major contributor to strength	Alumina (Al_2O_3), Silica (SiO_2) and calcium oxide (CaO).	Alite (C_3S) and Belite (C_2S) in cement.
Density	GPC has a density between 2290 kg/m^3 and 2460 kg/m^3, but still comparable to the OPCC.	
Porosity	The porosity of GPC is between 1.0% to 1.9%.	The porosity OPCC is between 3.0% to 5.1%.
Water absorption	GPC has a lower water absorption compared to OPCC.	
Durability of structures	High durability due to low porosity.	Lower durability due to higher porosity than GPC.
Setting time	Fast initial and final setting time.	Can be much easier adjusted compared to GPC.
Energy consumption for its production	The embodied energy of FA and GGBFS based GPC was 40% less than OPCC.	
Hydration Temperature development at an ambient temperature	Sets at room temperature. It has almost no temperature gain.	For high cement content mixtures, the temperature can rise up to 58 °C. [42]
Strength gain	Rapid strength gain. This depends also on the chemical reaction of the precursor(s) with the activator(s).	Takes more time to reach its strength. Especially the first week of curing.
Compressive Strength	GPC has 1.5 times higher compressive strength than OPCC.	
Tensile strength & Flexural strength	GPC has comparable tensile and flexural strength to 8% à 12% higher strength than OPCC.	
Elastic modulus	GPC has around 25% to 30% lower E-modulus than of the OPCC by a comparable compressive strength.	
Shrinkage and Creep	GPC has lower shrinkage of 100 micro strains compared to 500 to 800 micro strains to that of OPCC. The creep value of GPC has not more than 0.4 compared with 0.7 for OPCC. shrinkage.	
Corrosion resistance	GPC has a greater corrosion resistance than OPCC.	
Fire resistance	GPC has a good fire resistance compared to OPCC when exposed to more than 800 ºC.	

Table 1. 3: Properties of GPC based on Davidovits research [43]

Property	GPC performance compared to OPCC
Compressive Strength	equivalent
Tensile strength & Flexural strength	30% higher
Early age strength	Good
Shrinkage	lower (average 300 µm)
Acid resistance	Higher
Sulfate resistance	Higher
Chloride resistance	Higher
Heat of reaction	Very low
Fire resistance	Higher

1.3 Research aim and objective of this work

In recent years 3D printing has received more attention in various fields. One of these fields is concrete 3D printing. The main advantage of 3D concrete printing is that it can manufacture non-standard geometries, complex and details rapidly using a printer that contains a pump, hosepipe and a nozzle. The manufactured object is printed layer by layer without the need of a formwork and with a specific printing speed depending on the mixture properties and object design.
Even for cement-based concrete 3D printing concrete is still in its early stages of development, not much attention is paid to the development of 3D printing geopolymer concrete.

1.3.1 Research aim

The overall aim of this project is to propose a design methodology of geopolymer concrete mix which can be used for 3D printing process. More specifically, an optimal ratio between the binder (FA: BFS) and the alkaline solution (NaOH: Na_2SiO_3) will be studied explicitly, to compile with the 3D printing processes.

1.3.2 Objectives

In order to reach the research goal, following objectives are defined:

- To study the effect of binder ratio (FA: BFS) and alkaline ratio (NaOH: Na_2SiO_3) on specific setting time and mechanical strength development according to the technical specification of the 3D printing machine;
- To optimization the workability, extrudability and buildability for 3D printing. The fresh mixture properties, such as shear yield stress τ_0 and viscosity are considered;
- To test the open time and tensile bonding strength of two layers/filaments.

It is very important to point out that the fresh mixture has to be designed based on the type of 3D printer, because there are quite a few types of 3D printers with different kind of speeds, pressure and printing nozzles.

1.4 Outline of thesis

Chapter 1: General introduction

Chapter 2: Literature review

Chapter 3: Geopolymers as a material

Chapter 4: Geopolymer paste mixture design for 3D printing

Chapter 5: Rheological properties and 3D printing of geopolymer paste mixtures

Chapter 6: Conclusions

Chapter 7: Recommendations

Chapter 2

Google.com

2 LITERATURE REVIEW

2.1 INTRODUCTION TO 3D PRINTING

3D Printing is successfully applied in wide range of industries such as aerospace and automotive manufacturing. 3D printing can be divided to three techniques; contour crafting (CC), extrusion and powder printing (Figure 2.3). [67] Structural application of contour crafting was developed by Dr. Behrokh Khoshnevis. [68] However, its application in concrete construction is still in its early stages. Some of the reasons are unsuitability of available automated fabrication technologies for large scale products, limitations in the materials that could be used by an automated system and the economic unattractiveness of expensive automated equipments. On the other hand, construction industry is facing serious problems, such as:

- Accidents rate at construction sites is high;
- Labor efficiency is alarmingly low;
- Work quality is low;
- And controlled construction site is difficult and insufficient and skilled workforce is diminishing.

Worldwide researchers are trying to study and improve 3D printing on concrete, because it is one of the most widely used man-made construction materials on the planet. This technique extrudes the premixed materials through a nozzle to build structural elements layer upon layer based on a computer design without the need of a formwork and produces a laminated structure. It has become more popular in the building industry due to its flexibility in architectural and construction design.

Some of the known examples of 3D printed projects were executed are the five-story apartment 3D printed by WinSun [69] and the BigDelta project of a castle printed in situ [70] (Figure 2.1 and Figure 2.2). These projects have demonstrated a great potential and feasibility large-scale 3D printing of building components. For this growing innovative technique in the construction field, it is required to develop high performance building materials that are compatible with the 3D printers. Also, there are different types of small-scale 3D printers for laboratory tests and small-scale construction designs. The discussion of the large-scale 3D printers is beyond the scope of this work.

Fig. 2. 1: WinSun China build world's first tallest 3D printed apartment building [69]

Fig. 2. 2: BigDelta project of a 3D printed castle [70]

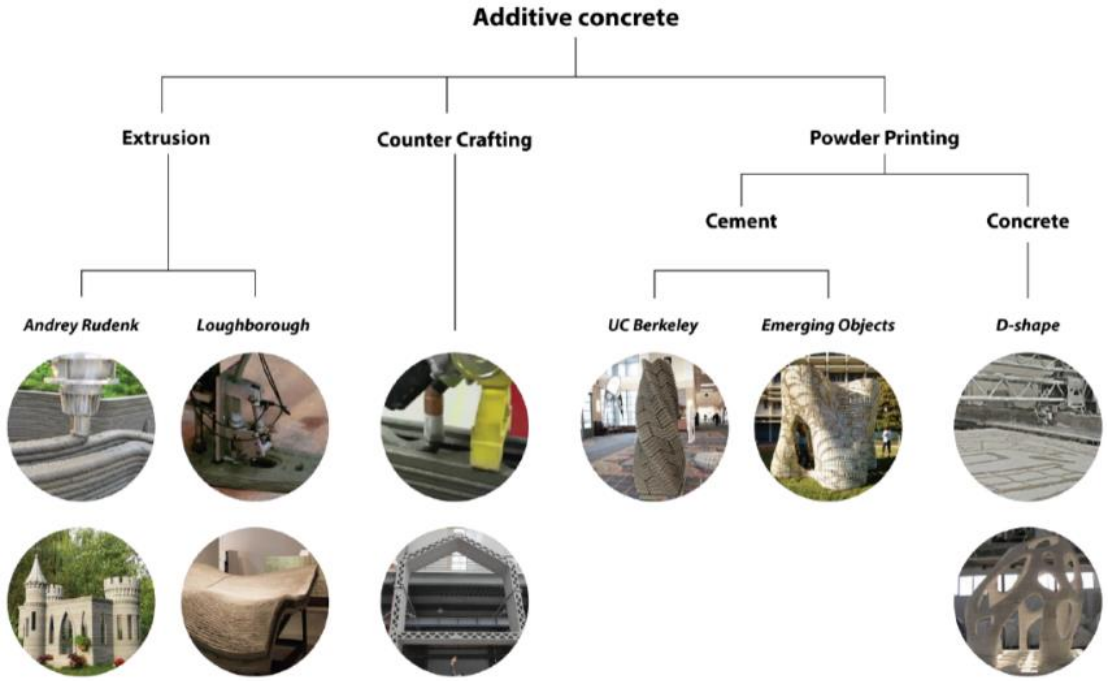

Fig. 2. 3: Digital manufacturing additive Concrete [67]

2.2 Advantages and disadvantages of 3D printing in construction

2.2.1 Advantages of 3D printing

The main advantages of 3D printing technology are the reduction of project construction costs, flexibility in the structural design and possibility of applying more than one type of construction material. [71]

2.2.2 Disadvantages of 3D printing

The main disadvantages of 3D printing are:

The size of the 3D printer is directly related to the scale and size of the printed structural design. Another limitation is the fact that multiple items cannot be simultaneously produced with one 3D printer and for the time being, the costs of buying and setting up a 3D printer is very high. Furthermore, large scale adoption of 3D printing will result in significant job loss. Nonetheless, new technologies almost always end up generating newer jobs. [72]

2.3 PREVIOUS EXPERIMENTAL LABORATORY WORK IN 3D PRINTING

Paul et al. (2017) examined in his work the fresh and hardened properties of 3D printed cementitious materials for building constructions. [75] Three mixture designs were examined on rheological properties, two mixtures contain cement as its binder and one mixture was a geopolymer mortar mixture, Table 2.1. The later (Mixture 1) contains fly ash and slag as its binders. To improve the workability and extrudability of Mix 1, Acti-gel as a rheological modifier and bentonite clay were used. Two alkaline solutions, Potassium Silicate (K_2SiO_3) and Potassium Hydroxide (KOH) were used to activate the binders. The workability of the mortars was examined by means of rheology test (Figure 2.4 and Figure 2.5). The plastic viscosity and shear stress where examined by applying the Bingham model for non-Newtonian fluids. The plastic viscosity of mixture 1, shown in Table 2.2, was around 186 Pa.s. Mixture 1 has a higher plastic viscosity than the cement-based mixtures 2 and 3.

Table 2. 1: materials composition for 3D printed concrete [75]

Mix	Materials compositions (kg/m^3)
Mix 1	Slag: 39, fly ash: 645, silica fume: 78, sand: 1168, actigel: 8, bentonite: 8, water: 47, K_2SiO_3: 250, KOH: 23
Mix 2	Cement: 290, fly-ash: 278, silica fume: 145, sand: 1211, water: 285, sodium lignosulfonate: 7
Mix 3	Cement: 289, fly-ash: 277, silica fume: 145, sand: 1209, water: 284, sodium lignosulfonate: 9, glass fiber: 13.5 (density: 2.7, tensile strength: 1.5 N/m^2, young's modulus: 74 GN/m^2, failure strain: 2%)

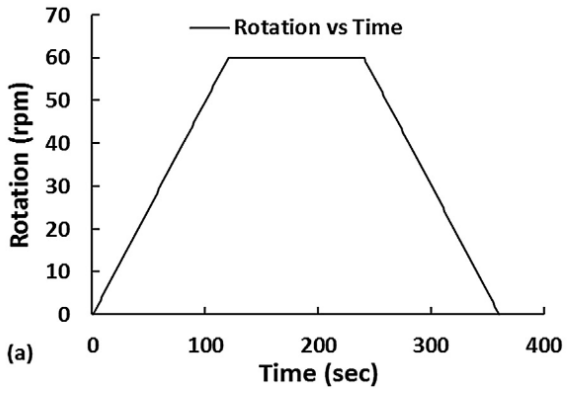

Fig. 2. 4: Applied rotation with time for rheology test [75]

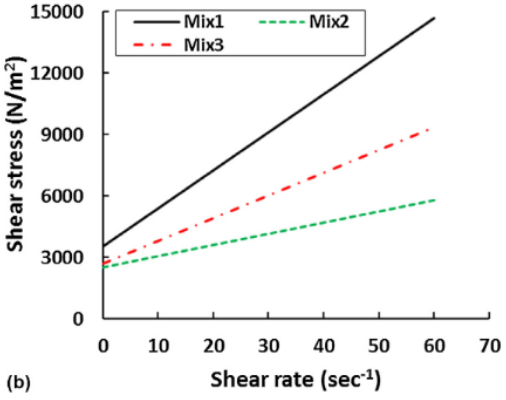

Fig. 2. 5: Calculated shears stress and shear rate of the three mortars using the Bingham model [75]

Table 2. 2: Rheological properties of the three mortar mixtures [75]

Mix	Viscomat value				Using calibration coefficients [22]		
	Static yield torque (N mm)	Dynamic yield torque (N mm)	Slope of the curve (N mm/min)	Thixotropy (N mm rpm)	Static yield stress	Dynamic yield stress	Plastic viscosity
					(N/m^2)	(N/m^2)	($N\ s/m^2$)
Mix1	1370	358	6.3	11 273	13 522	3534	186
Mix 2	1401	367	4.8	13 756	13 828	3622	144
Mix 3	1763	303	3.8	17 947	17 401	2991	113

Ma et al. (2018) work focused on different testing procedures of cementitious materials containing copper tailings for extrusion-based 3D printing. [68] In the fresh state, the mortar mixtures with different copper tailings are measured on open time, buildability and extrudability. The open time stands for the time interval of the mixture to have good workability/extrudability and printability without disruption of the printed filaments. The extrudability of the fresh mixture is evaluated by the continuity and stability of the filament from a printing nozzle of 8* 8 mm^2. There should be no liquid drainage and no blockage of the nozzle during the extrusion process of the fresh mixture.

The results in Figure 2.6 and Figure 2.7 show that the structural stability of the printed structures was decreased significantly with the increase of tailing dosage, especially the 30% and 40% of tailing. One of those mixtures was examined on open time test, see Figure 2.8 and Figure 2.9. In this test, the width of the filaments was measured every 5 minutes time interval. The data show that the optimal width of the filaments is obtained after (25- 80) minutes of mixing time and the optimal buildability was between (30-80) minutes. The mixture showed disruption of the filament after 90 minutes of mixing time.

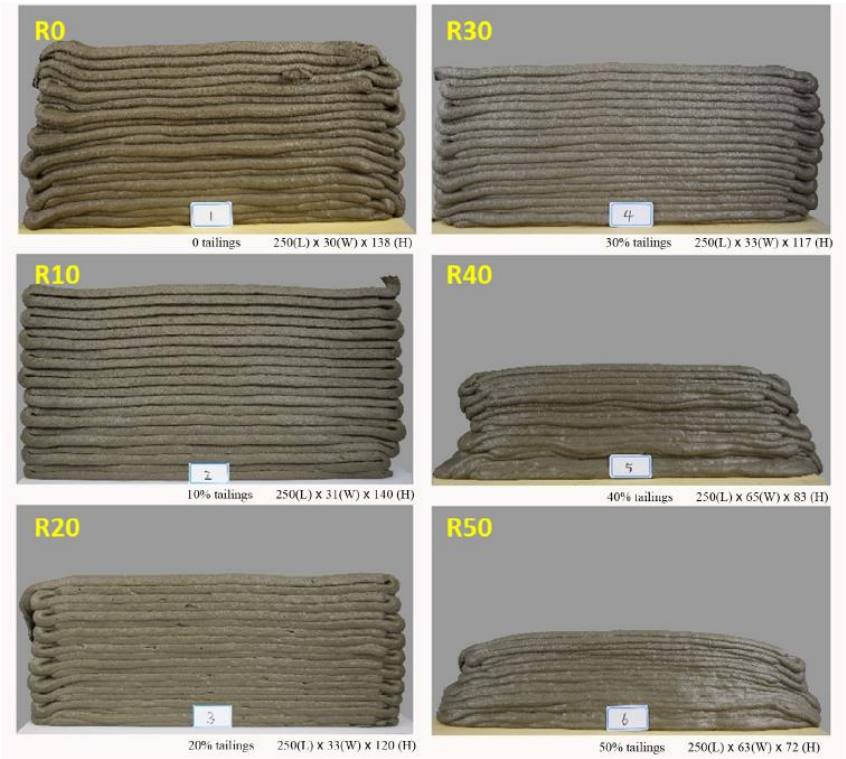

Fig. 2. 6: Image of structure built-up wit 20 layers of filament in a single process [68]

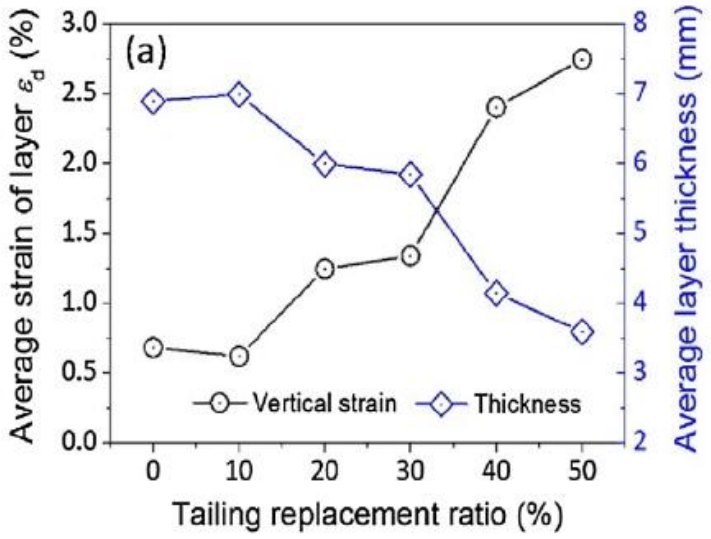

Fig. 2. 7: Average vertical strain (ε_d) and average layer thickness of the mixtures with different ratios of copper tailing [68]

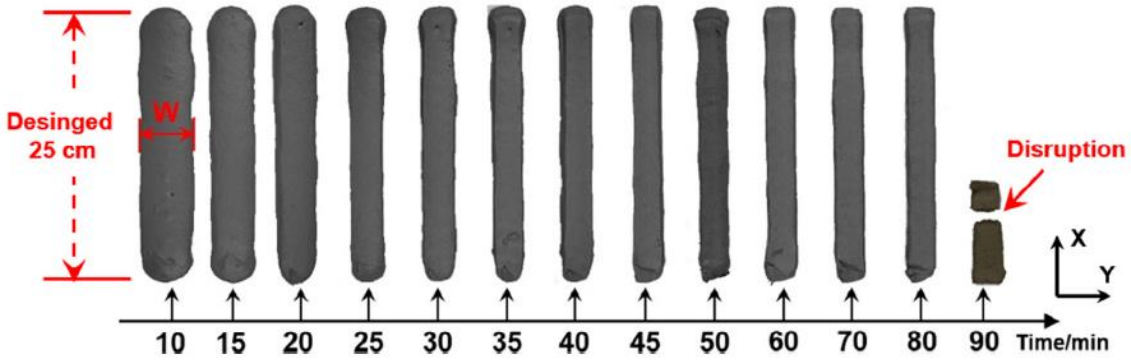

Fig. 2. 8: open time of R40 mixture [68]

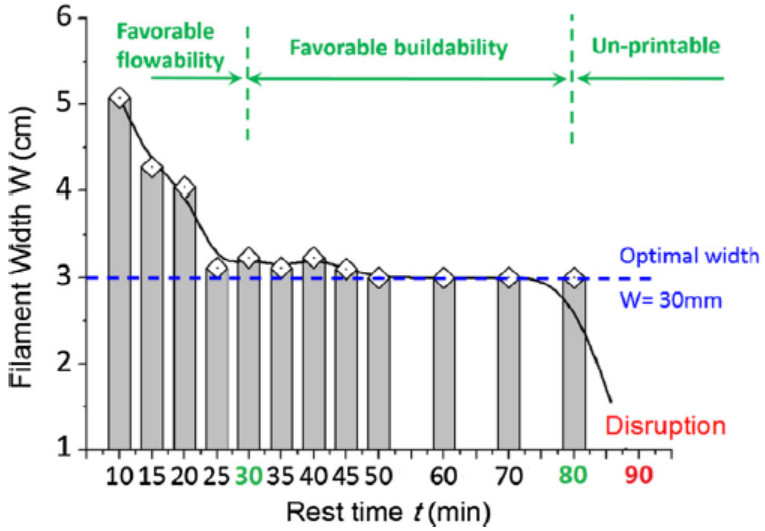

Fig. 2. 9: Open time of R40 mixture [68]

2.4 Concluding remarks

As it is mentioned before, the work of Paul et al. (2017) and Ma et al. (2018) gave preliminarily hint how to approach the procedure which has been adopted in this work for 3D printing. It is important to mention here that Paul et al. (2017) applied Acti-gel in his geopolymer mortar design. This Acti-gel was used in this experimental work because one of the properties of the Acti-gel provides shape stability to a mixture. It can be considered as an anti-settling agent and rheological modifier which it can results in lowering the shear stress during the extruding process through a nozzle and improving the buildability of the extruded mixture.

Therefore, combination of both types of experimental procedures are quite recommended to be adopted in the testing procedure of this work, such as testing the rheological properties (plastic viscosity and shear stress) and the open time test of a mixture design. By testing the rheological properties of a mixture, especially the plastic viscosity, with different time intervals and comparing it to the open time test, can give information about the values of the maximum time required for good extrudability.

Chapter 3

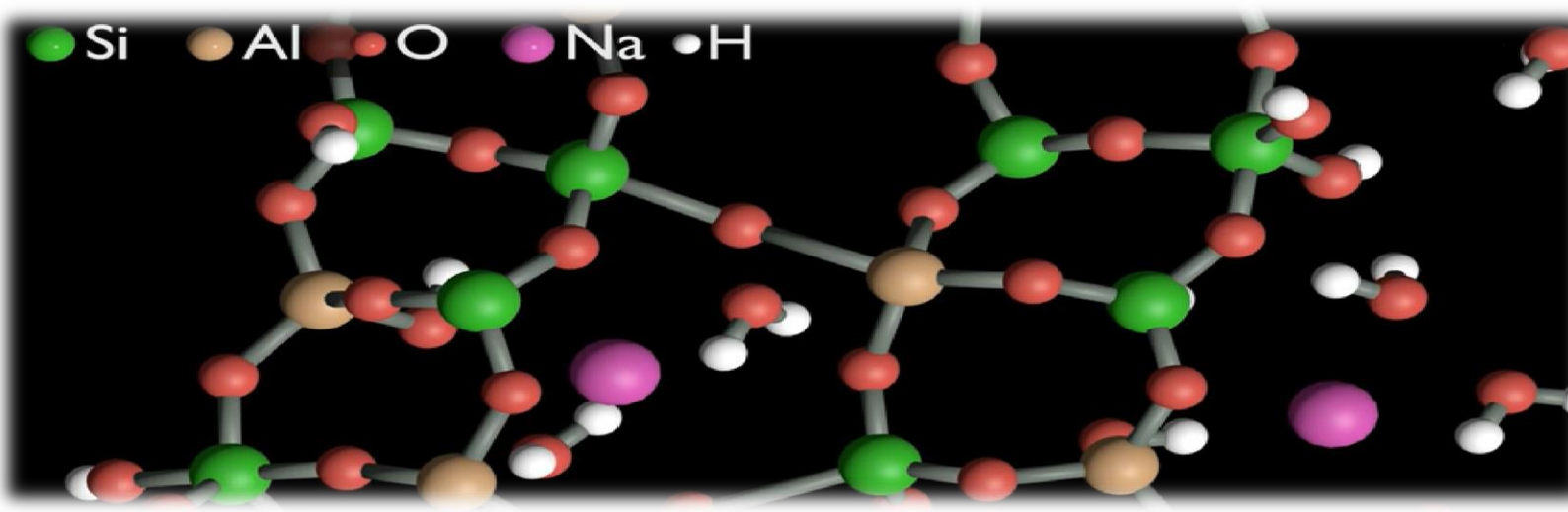

youtube.com

3 GEOPOLYMERS AS A MATERIAL

3.1 INTRODUCTION

The term geopolymer was first introduced by Davidovits in 1979 to describe a family of mineral binders that gave a chemical composition similar to zeolites but with an amorphous microstructure. [7] Geopolymers do not form calcium-silicate hydrates (CSHs) like the OPC to gain its strength but utilize the polycondensation of silica (SiO_2), alumina (Al_2O_3) to attain its structural strength. The known binders should be rich in Aluminium (Al), Silicon (Si), such as fly ash (FA) and metakaolin (MK). A third known binder is the blast furnace slag (BFS), which is rich in calcium (Ca) and silicon (Si). FA and BFS are known as supplementary cementitious materials (SCM) and are the most common applied cementitious components for concrete. [46]

Binders rich in Aluminum and Silicon can only be activated using alkaline solutions. According to Deventer and Provis in 2009 the alkaline activation first started when Purdon demonstrated in 1940 the synthesis of construction materials by alkaline activation of BFS that contains a high amount of calcium. [7] However, Shi et al. (2011) gave this credit to the achievements of the German cement chemist and engineer Kuhl in 1930. [7] [44]

In the year 1908 one of Kuhl patent was recognized as the first one that applied alkali activation of aluminosilicate binders in order to obtain an alternative binder material instead of OPC. [7] [39]

Except the work of Glukhovsky on alkaline cement, not much attention was paid to the field of alkali activation in the last few decades (Table 3.1).

According to the research of Davidovits, geopolymers generates around 0.184 tons of CO_2 per ton of binder. Duxson et al. (2007) stated that the production of disodium oxide (Na_2O) generates high amount of CO_2, whereas the alkaline activated materials generates lower amount of CO_2 than the production OPC. Based on the work of Duxson and van Deventer in 2009 alkaline activated materials shows 80% reduction in CO_2 emission compared to OPC. [7]

Table 3. 1: Bibliographic listing of some important events in the history of AAB [7]

Author	Year	Significance
Khul	1908	alkali activation of aluminosilicate binders
Khul	1930	alkaline activation of BFS
Feret	1939	Slags used for cement
Purdon	1940	Alkali-slag combinations
Glukhovsky	1959	Theoretical basis and development of alkaline cements
Glukhovsky	1965	First called 'alkaline cements'
Davidovits	1979	'Geopolimer' term
Malinowski	1979	Ancient aqueducts characterized
Forss	1983	F-cement (slag-alkali-superplasticizer)
Langton and Roy	1984	Ancient building materials characterized
Davidovits and Sawyer	1985	Patent of 'Pyrament' cement
Krivenko	1986	DSc Thesis, $R_2O - RO - SiO_2 - H_2O$
Malolepsy and Petri	1986	Activation of synthectic melilite slags
Malek *et al.*	1986	Slag cement-low level radioactive wastes forms
Davidovits	1987	Ancient and modern concretes compared
Deja and Malolepsy	1989	Resistance to chlorides shown
Kaushal *et al.*	1989	Adiabatic cured nuclear wastes forms from alkaline mixtures
Roy and Langton	1989	Ancient concretes analogs
Majundar *et al.*	1989	$C_{12}A_7$ – slag activation
Talling and Brandstetr	1989	Alkali-activated slag
Wu *et al.*	1990	Activation of slag cement
Roy *et al.*	1991	Rapid setting alkali-activated cements
Roy and Silsbee	1992	Alkali-activated cements: an overview
Palomo and Glasser	1992	CBC with metakaolin
Roy and Malek	1993	Slag cement
Glukhovsky	1994	Ancient, modern and future concretes
Krivenko	1994	Alkaline cements
Wang and Scrivener	1995	Slag and alkali-activated microstructure
Shi	1996	Strength, pore structure and permeability of alkali-activated slag
Fernández-Jiménez and Puertas	1997	Kinetic studies of alkali-activated slag cements
Katz	1998	Microstructure of alkali-activated fly ash
Davidovits	1999	Chemistry of geopolymeric systems, technology
Roy	1999	Opportunities and challenges of alkali-activated cements
Palomo	1999	Alkali-activated fly ash – a cement for the future
Gong and Yang	2000	Alkali-activated red mud-slag cement
Puertas	2000	Alkali-activated fly ash/slag cement
Bakharev	2001 2002	Alkali-activated slag concrete
Palomo and Palacios	2003	Immobilization of hazardous wastes
Grutzeck	2004	Zeolite formation
Sun	2006	Sialite technology
Duxson	2007	Geopolymer technology: the current state of the art
Hajimohammadi *et al.*	2008	One-part geopolymer
Provis and van Deventer	2009	Geopolymers: structure, processing, properties and industrial applications

3.2 Alkaline activated binders (AAB)

In the last few decades, a wide range of aluminosilicate and calcium rich binders have been developed. Some of these binders are formed by nature, other are industrial products and waste products, as illustrated in the pictures below.

Metakaolin (MK)

Blast furnace slag (BFS)

Fly Ash (FA)

Waste Glass (WG)

Silica Fume (SF)

Or a combination of two or more

- Natural products (metakaolin MK);
- Industrial by-products (FA , BFS);
- Wastes (Waste glass (WG);
- A mixture of them with or without OPC.

Alkaline activated components can be divided into pozzolanic and cementitious materials (Figure 3.2). However, the focus of this project will be on fly Ash (FA) and blast furnace slag (BFS). These components can be activated individually or in a combination of two or more. It is important to mention that the chemical composition, particle size and particle shape of the components influences the mechanical and rheological properties of the concrete. In Figure 3.3 a range of chemical composition of FA, BFS, SF, MK and OPC are shown.

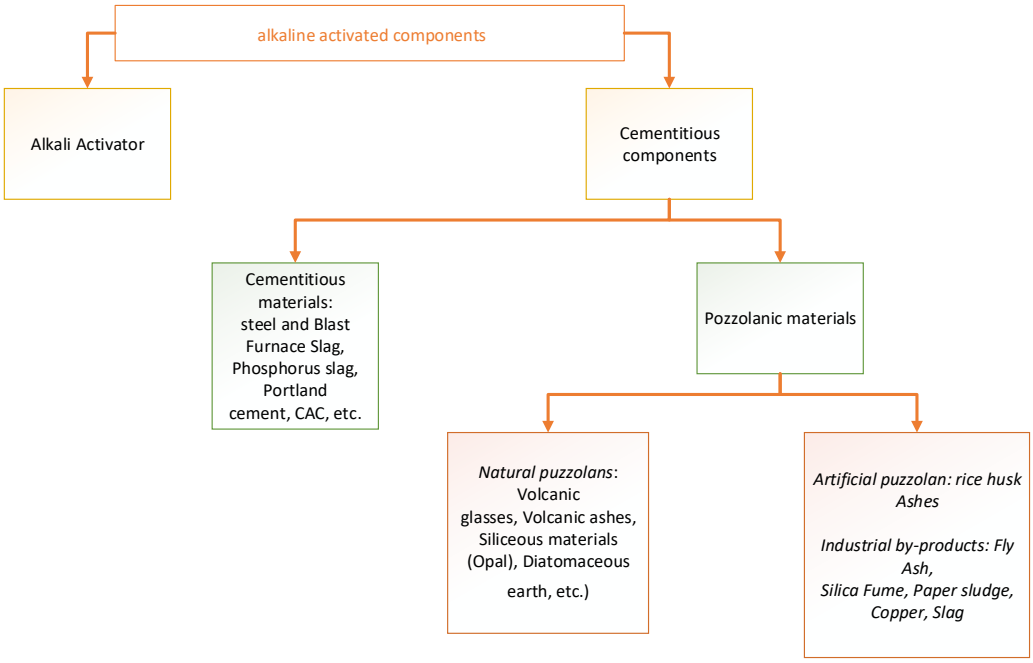

Fig. 3. 2: Alkali activated binders (AAB) [45]

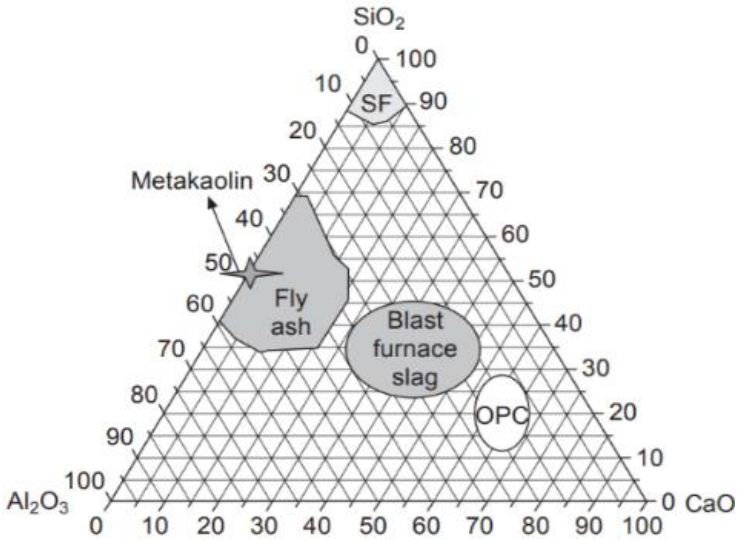

Fig. 3. 3: Range of compositions of the raw materials used to manufacture alkaline cements on a CaO-SiO_2-Al_2O_3 diagram [45]

3.2.1 Blast Furnace Slag (BFS)

Blast Furnace Slag is a pozzolanic by-product that is formed when iron ore or iron pellets, coke and flux (limestone or dolomite) are melted together in a blast furnace (Figure 3.4). During the melting of the raw materials, the lime in the flux is chemically combined with the aluminates and silicates of the ore and coke ash to form a non-metallic product called blast Furnace Slag (BFS). This non-metallic product can be cooled in several ways to form different types of blast furnace slag products.

Fig. 3. 4: Raw components for the formation of BFS [47] [48] [49]

BFS that comes from a particular furnace is fairly consistent with similar physical and chemical properties. [50]

The shape of the BFS particles are irregular with a glassy surface (Figure 3.5). The main requirement for BFS to be applied as supplementary cementitious materials (SCM) is to have CaO + MgO/SiO_2 ratio >1. It must be ground to specific surface of 400 - 600 [m^2/kg]. Specific surface plays an important role in the rate and intensity of the activation process. Furthermore, BFS can vary in composition between different furnaces and ores.

For this study BFS was supplied from ORCEM in the Netherlands. To understand the chemical composition, crystalline and amorphous phases and the fineness of the particles, the BFS was analysed by an X-ray fluorescence (XRF), X-ray powder diffraction (XRD) and laser particle analyser (LPA).

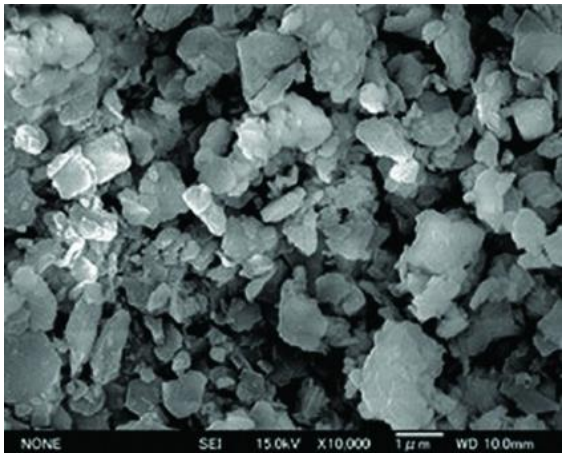

Fig. 3. 5: Microstructure of blast furnace slag through field emission scanning electron microscope (FESEM) [52]

3.2.2 Fly Ash (FA)

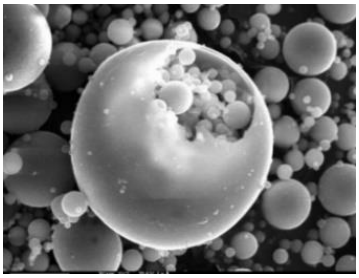

Fig. 3. 6: Fly Ash spherical particles though the scanning electron microscope (SEM) [54]

Fly Ash is a pozzolanic by-product that is formed during coal combustion (heated to 1500±200 ºC) and is driven out of the coal fired boilers together with flue gases. The ash that falls to the bottom of the boiler is called bottom ash. The FA is captured by special filters from the rest of the flue gases before it reaches the chimneys. Depending on the source and composition of the burned coal, the components of the FA vary considerably. However, all the type of fly ashes contains substantial amounts of silica (SiO_2) (both crystalline and amorphous phases), aluminium oxide (Al_2O_3) and lime (CaO).

The fly ash contains smaller amount of magnesia (MgO), sulphur oxide (SO_3), alkalis (Na_2O and K_2O) as well as traces of titanium, vanadium, manganese, phosphorus, germanium and gallium. The particles of fly ash have a spherical glassy shape (Figure 3.6). [53] The ash has specific surface ranges from 2500 [cm^2/g] to 5000 [cm^2/g] and has a density from 2.2 [g/cm^3] to 2.8 [g/cm^3].

According to (ASTM C618-08a) fly ash is divided into type F and C depending on the lime content:

- **Type F fly ash:** with lime (CaO) content lower than 7%. The majority oxides in this type of ash are SiO_2, Al_2O_3 and iron oxides. It is most abundant type of ash and frequently re-used. The material is basic with a pH over 10. This ash is added to OPC. Another alternative is activating the ash with an alkaline activator to form a gel that hardens in time (also called geo-polymerization/ alkaline activation). Class F fly ash is most widely used in geopolymer synthesis.
- **Type C fly ash**: Class C contains more than 20% of lime (CaO). In the presence of water, Class C fly ash hardens and gets stronger over time. It does not need any alkaline activators to form a gel that hardens in time.

For this study FA was supplied from VLIEGASUNIE BV in the Netherlands. To understand the chemical composition, crystalline and amorphous phases and the fineness of the particles; an X-ray fluorescence (XRF), X-ray powder diffraction (XRD) and laser particle analyser (LPA) was applied on FA.

3.3 ALKALINE ACTIVATOR SOLUTIONS

The second essential component in the geopolymer concrete is the alkaline activator solutions. Glukhovsky et al. (1994) classified six groups of activators by their chemical composition (Figure 3.7). [62] The most common alkaline activators used in the BFS and FA are alkaline hydroxides (caustic solutions), alkaline silicates or blends of the two to generate high alkalinity. The anions and cations play different roles in the alkaline activation. The anions in the activator solution are important in the geo-polymerization process and consequently in the mineralogical and microstructural characteristics of the materials. There are four different types of anions that are normally mixed with the raw materials. The most common used is the hydroxides, silicates and carbonates and to lesser extent the sulfates.

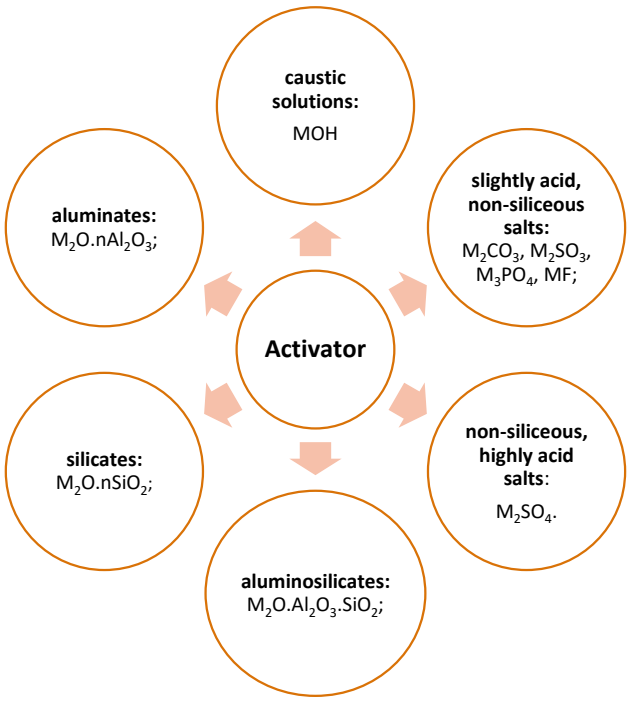

Fig. 3. 7: Alkaline activators [62]

3.3.1 Sodium hydroxide (NaOH)

Sodium hydroxide (NaOH) is an inorganic white solid compound (in a powder or pallets form) that consists of Na^+ and OH^- ions. It is a commonly used alkaline activator due to its availability, low price and low viscosity.

Sodium hydroxide is easy soluble in water that produces exotherm heat release [1].

Glukhovsky mentioned in his work that the OH^- ions catalyze the dissolution of Si^{4+} and Al^{3+} in the SCM by inducing the hydrolysis of Si-O-Si and Si-O-Al bonds. This OH^- ions catalysis the hydrolytic reaction in all the stages of the alkaline activation, but also raises the pH level

that is required in the dissolution of the SCM and subsequent condensation reaction. In scientific articles, the liquid NaOH is written as Na_2O and H_2O. When the concentration of Na_2O is around 4.8% C-A-S-H gel is formed. A concentration of 8% or higher, C-A-S-H gel is formed and possible some Ca $(OH)_2$ might appear. The concentration of the sodium hydroxide (molarity) influences the reaction degree and the mechanical strength development of the mixture.

$$\boldsymbol{NaOH\ (s) + H_2O\ (l) \rightarrow Na^+ + OH^- + H_2O + Heat} \quad [1]$$

3.3.2 Sodium Silicate (Na_2Sio_3)

The second most commonly used activator is the sodium silicate (also called waterglass). It is easy soluble compound that contains Disodium Oxide (Na_2O) and Silica (SiO_2) with chemical formula ($Na_{2x}SiO_{2+x)}$ or
$(Na_2O)_x \cdot SiO_2$. The Disodium Oxide content (Na_2O) is required for the geo-polymerization process because it affects the pH level. A solution which contains more Na_2O, the higher is the pH level. In addition to Na_2O, Silica (SiO_2) provides a denser matrix. Soluble silicate affects the workability, mechanical strength development and shortens the setting time of the mixture. [45]
The higher the concentration of SiO_2 and Na_2O, the more viscous the solution is. The viscosity is a product of the formation silicate polymers that consists of (Silicon (Si) and Oxygen (O)) atoms. These atoms are linked by covalent bonds into large negatively charged chains or ring structure that takes in the positively charged Na^+ and water-molecules H_2O. [63] It is believed that the waterglass contributes to formation of high Silica primary gel during the activation of the BFS. This gel is formed when soluble silicates reacts with the Ca^{2+} ions in the BFS to form C-A-S-H gel. For the purpose of this project a waterglass solution is used for the alkaline activation process. The solution contains a mol-ratio between SiO_2: Na_2O of 3.3: 3.5. The density and viscosity vary at a temperature of (20°C) between 1.34 - 1.36 kg/l and 80 -100 cp (Table 3.2 and Appendix C).

Table 3. 2: Sodium silicates (Na_2SiO_3) composition

SiO_2	27.5%
H_2O	64.25%
Na_2O	8.25%

3.4 Additives

3.4.1 Retarder

Depending on the required mechanical properties of a geopolymer mixture, the setting time can be adjusted from 5 minutes to more than 2 hours. The admixtures in the market are designed for cement-based materials and most of these admixtures are not suitable to geopolymer concrete. The setting time of a geopolymer paste mixtures can be delayed by adding Barium Chloride dehydrate retarder ($BaCl_2.2H_2O$). This retarder has a fine white power form that is easy soluble in water. When it is added to the paste mixture, it absorbs part of the moist which can reduce the workability and more liquid activator is required to improve it. Furthermore, the chloride is known to have corrosive effect on the steel reinforcing in a structure. More research is required on geopolymer paste mixture to be

able to understand the retardation process and how this can affect the formation of C-A-S-H and N-A-S-H gels in the matrix.

3.4.2 Acti-Gel ® 208

Acti-Gel® 208 is a highly purified clay based powdered product which can be made into a slurry suspension (Figure 3.8). It is a rheology modifier and anti-settling agent that stabilizes mixtures, provides superior aggregate suspension, and dramatically improves the performance and paste quality of concretes (Appendix D). The Acti-Gel consists of rod-shaped Magnesium Aluminium Silicate particles with pseudo-nano dimensions (Figure 3.10 and Table 3.3). The average particle size is between 1.5 to 2.0 microns and average diameter of 30 Angstroms (30* 10^{-10} meter) and are positively charged on the ends and negatively charged along the axis (Figure 3.9). This electrical interaction is what allow Acti-Gel® 208 to gel. When fully dispersed the particles form a unique lattice 'microstructure' that supports slightly higher yield stress and thixotropy (Figure 3.11). Under conditions of shear, flow conditions are enhanced resulting in improved pumpability and workability (lower viscosity upon shear force). Water-based liquids, slurries and suspensions with ions and/or solids (with charge) can become highly pseudo plastic by addition of 0.1-3.0% (wt.%) of Acti-Gel ® 208.

Fig. 3. 8: Acti-Gel Slurry Suspension

On removal of shear, the rate of thixotropic rebuilding of the lattice structure is exceptionally fast, which provides:

- Superior cohesion;
- The rapid development of green strength;
- Shape stability;
- Excellent anti-washout properties;
- Reduction in hydrostatic pressure.

The most important properties of the Acti-Gel are:

- Non-reactive;
- Non-swelling;
- Non- shrinking;
- Non-retarding;
- Temperature stable;
- pH tolerant between pH=2 to pH=13);
- Shear stable and bio-stable.

Table 3. 3: Acti-Gel chemical composition

SiO_2	49.57%
Al_2O_3	9.44%
Fe_2O_3	3.31%
MgO	8.81%
CaO	1.88%
Na_2O	0.59%
K_2O	0.66%

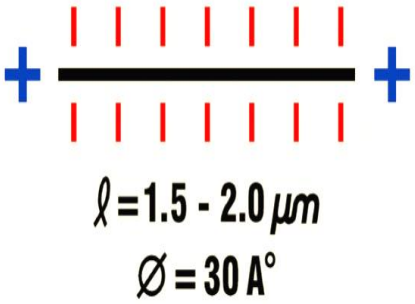

Fig. 3. 9: Acti-Gel particle positively charged on the ends and negatively charged along the axis

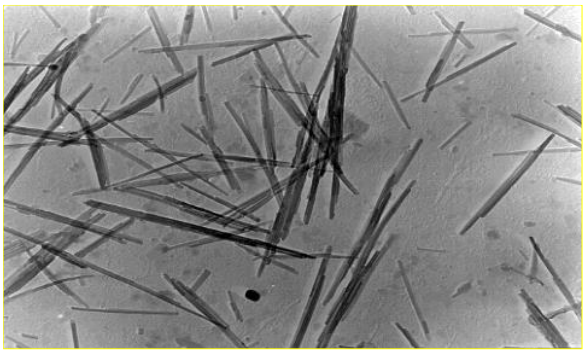

Fig. 3.10: Acti-Gel rod-shaped magnesium aluminium silicate particles

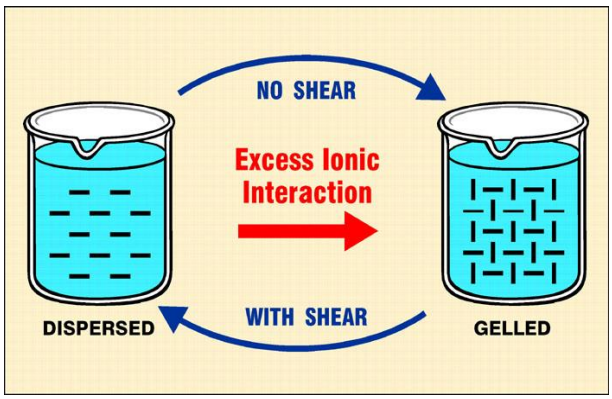

Fig. 3. 11: Ionic interaction of Acti-gel particles with and without shear force

3.5 Alkaline activation process

Alkaline activation of materials is relatively a new field compared to OPC. [50] [57] [58] [59] Based on the nature of BFS and FA that contain (CaO-SiO_2-Al_2O_3 system), BFS and FA are grouped into two main categories: (I) high Calcium and (II) low Calcium binders. The activation pattern differs in each when they are activated seperately. [56]

- **($Na,K)_2O$-CaO-Al_2O_3-SiO_2-H_2O system, Model I***:* In this model the binders that are rich in Calcium and Silicon such as BFS (SiO_2 + CaO > 70%) are activated under moderate alkaline conditions. The main product is **C-A-S-H** gel. The C-A-S-H gel differs slightly from the C-S-H gel that is formed in Portland cement paste, because it has a lower C/S- ratio (C/S= 0.9 to 1.2) and takes aluminium in its structure. The C-A-S-H gel provides the geopolymer concrete its mechanical strength and a room temperature curing without the need of external heating. [56]
- ***(*Na,K)_2O$-$Al_2O_3$-$SiO_2$-$H_2O$ system, Model II:** In this model the binders are rich in Aluminium and Silicon (Al_2O_3 + SiO_2). The binders used in this second alkaline activation procedure, such as MK and FA have low CaO content. The main reaction product formed in this case is a three-dimensional inorganic alkaline polymer, a **N-A-S-H** (alkaline aluminosilicate hydrate) gel. Because of the low CaO content, more aggressive working conditions (highly alkaline media and curing temperatures of 60–200 °C) are required to fasten the reaction process. [56]

- **Blended or hybrid alkaline system, Model III:** A combination of model I and model II. The binder is the result of alkaline activation of CaO, SiO_2 and Al_2O_3 contents > 20%. The main reaction products formed in this case is **C-A-S-H** and **N-A-S-H** gels. [56]

It is important to mention that the Calcium rich mixtures have a fast-early age strength development compared to the low calcium mixtures. Nedeljcovic et al. (2016) mentioned that the amorphous phases of BFS increases dissolution rate and consequently the hardening process is faster, favoring high amount of the products forming within first few days of the reaction. [74] The reaction products based on the used binder is shown in Table 3.4.

Table 3. 4: Products precipitating in different types of binders [56] [77]

Binder type		OPC	Alkaline materials	
			$(Na,K)_2O$-CaO-Al_2O_3-SiO_2-H_2O	$(Na,K)_2O$-Al_2O_3-SiO_2-H_2O
Reaction product	Primary	C-S-H	C-A-S-H	N-A-S-H
	Secondary	$Ca(OH)_2$ AF_m AF_t	Hydrotalcite $[Mg_6Al_2CO_3(OH)_{16}•4H_2O]$ C_4AH_{13} $CASH_8$ C_4AcH_{11} $C_8Ac_2H_{24}$	Zeolites: hydroxysodalite, zeolite P, Na-chabazite, zeolite Y, faujasite
C = CaO, S = SiO_2, A = Al_2O_3, N = Na_2O, H = H_2O, C = CO_2				

3.5.1 Fundamentals of alkaline activation in calcium-rich systems: $[(Na, K)_2O$-CaO-Al_2O_3-SiO_2-$H_2O]$

Number of research studies have shown that the phase of the components and their structure in the BFS effects the reactivity in alkaline conditions. It is believed that the C-A-S-H gel and C-S-H gels have a similar tobermorite structure (Figure 3.12). [60] The BFS reactivity is described by a parameter known as the degree of polymerisarion (DP) (Eq. 1). [61]

$$DP = n(CaO) - 2n(MgO) - n(Al_2O_3) - \frac{n(SO_3)}{n(SiO_2)} - 2n(MgO) - 0.5n(Al_2O_3) \quad [1]$$

The ranges of DP are from 1.3 - 1.5. The higher the number of DP, the higher is the degree of polymerization of BFS and thus the more material is reacted. [61] Glukhovsky and Krivenko proposed a model that would give an explanation to the alkaline activation of SiO_2 and CaO as shown in Eq. 2: [61]

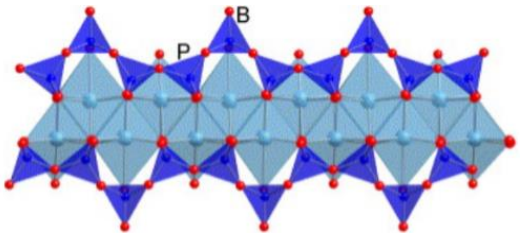

Fig. 3. 12: The chains have a kinked pattern where some silicate tetrahedra share O–O edges with the central Ca–O layer (called 'paired' tetrahedra, P) and others that do not (called 'bridging' tetrahedra, B). [60]

$$\equiv Si\text{-}O^- + R^+ \equiv\equiv Si\text{-}O\text{-}R$$

$$\equiv Si\text{-}O\text{-}R + OH^- \equiv\equiv Si\text{-}O\text{-}R\text{-}OH^- \quad [2]$$

$$\equiv Si\text{-}O\text{-}R\text{-}OH^- + Ca^{2+} \equiv\equiv Si\text{-}O\text{-}Ca\text{-}OH + R^+$$

In the initial phases of activation process, the alkaline cation [1] (R^+) acts as a catalyzer via cationic exchange with the Ca^{2+} ions. As the reactions advance, the alkaline cations are taken up into the structure. [61]

Garcia-Lodeiro et al. (2011) found that the presence of sufficient Calcium and a high pH values (pH ≥ 12), the

C-A-S-H gel is favored over N-A-S-H gel formation (see Figure 3. 13). [61] [66] The type and amount of liquid activator effects the structure and composition of the C-A-S-H gel and the presence of secondary phases. Simultaneously the particle size and structure (amorphous or crystalline) of the binder that is Calcium rich and the curing conditions plays an important role in the formation of the gel structure. A theoretical model for the reaction mechanism in alkaline activated slag is shown in Figure 3.14. [61]

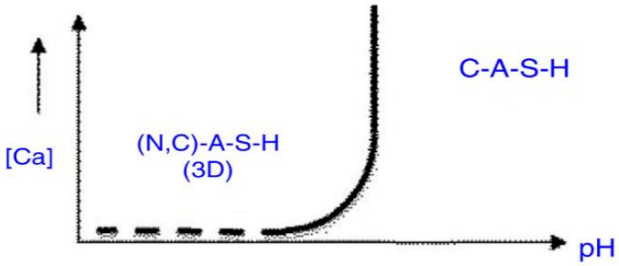

Fig. 3. 13: Formation of C-A-S-H and N-A-S-H gels depending of the pH value [61]

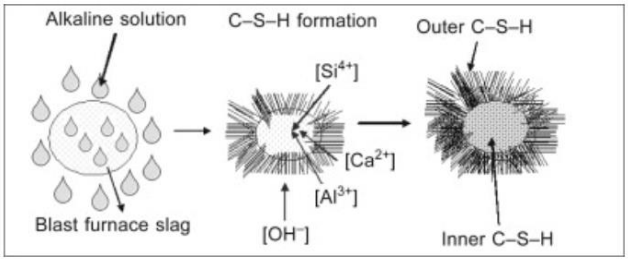

Fig. 3. 14: Theoretical model for the reaction mechanism in alkaline activated slag [61]

3.5.2 Fundamentals of alkaline activation in low-calcium systems: [(Na,K)2O-Al2O3-SiO2-H2O]

Fly ash and metakaolin are low Calcium materials mostly used in the manufacturing of concrete, although the higher cost of metakaolin constrains its use in concrete industry. This type of binders induces the precipitation of an amorphous alkaline aluminosilicate hydrate, known as N-A-S-H gel, during the alkaline activation. [56]

Palomo et al. (2005) introduced a structural model of N-A-S-H gel formation. It has been revised by various authors. [56] [64]

When a rich aluminosilicate source comes into contact with an alkaline solution, it starts to dissolve into several species with primary Silica and Alumina monomers. These monomers interact to form dimers, which in turn react with other monomers to form trimers, tetramers etc. The first intermediate reaction product which is rich in Aluminum, called gel 1, is formed when the solution has reached saturation. The Aluminum dissolves more quickly than the Silicon, because the Al-O bonds are weaker than Si-O bonds. When the reaction progresses, more Si-O groups dissolve raising the Silicon concentration in the reaction medium and increases its proportion in gel 2 (the N-A-S-H gel).

[1] the alkaline cation (R^+) can be Na^+ or K^+ depending on the activator composition and raw materials

The N-A-S-H gel (that is formed from low Calcium materials) has a three-dimensional (3D) structure that differs from the structure of the gels formed in the alkaline activation of Calcium-rich materials (Figure 3.15). [56]

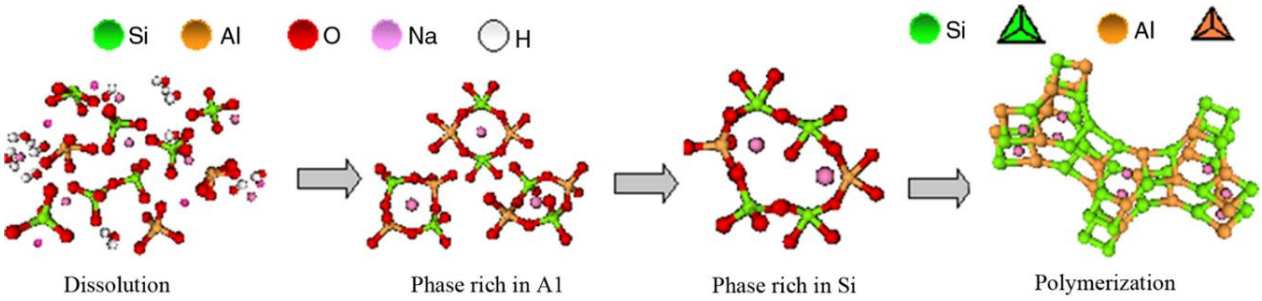

Fig. 3. 15: Model proposed for N-A-S-H gel formation [56] [64]

Another model of Fernández-Jiménez et al. (2005) was executed based on the scanning electron microscopy (SEM) that described the alkaline activation of FA, Figure 3.16. This model explains the chemical attack on the surface of the particles, Figure 3.16 (a). The alkaline activation process starts when the surface of the FA is chemically attacked by the alkaline solution, Figure 3.16 (a). This causes the formation of small cavities in the big spherical particle exposing the smaller inside particles to the alkaline solution, Figure 3.16 (b). The particles continue to dissolve from both inside and outside, which makes the reaction goes faster and reaction products would precipitate, Figure 3.16 (c). Not all the particles would be dissolved due to the precipitation of the reaction products, which causes the hindering of their contact with the alkaline solution, Figure 3.16 (d). The reaction would continue but in a slower phase and the unreacted particles can only be attacked through diffusion mechanism. The formed paste would have different morphologies (unreacted particles and reaction products (N-A-S-H, zeolites, etc.). [56]

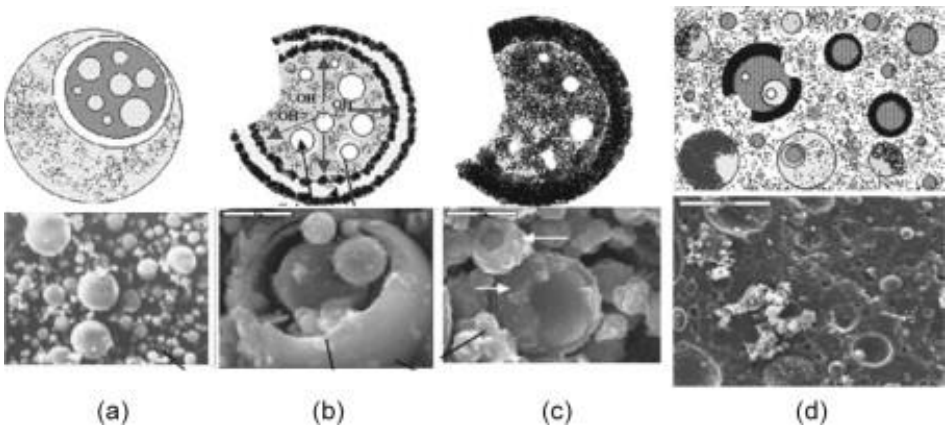

Fig. 3. 16: Model for the alkaline activation of fly ash over time [56]

3.5.3 Fundamentals of alkaline activation in hybrid systems: $(Na,K)_2O$-CaO-Al_2O_3-SiO_2-H_2O]–[$(Na,K)_2O$-Al_2O_3-SiO_2-H_2O]

The hybrid system is a combination of model I and II. Two or more binders are mixed together to activate CaO, SiO_2 and Al_2O_3. According to Provis and Bernal (2014), combining low and high Calcium rich binders together in a specific concentration, helps in achieving a good mechanical strength and more durable concrete. [65]
Nedeljcovic et al. (2016) mentioned that combination of FA and BFS, as a binder, gives more uniform development of the microstructure and counterbalance their properties. [74]

Due to the lack of reactivity of low Calcium binders (model II), the addition of rich Calcium binder improves the reactivity under ambient curing conditions. The curing conditions, the type of alkaline solutions and the concentration of both binder and alkaline solutions, affects the formation of the C-A-S-H and N-A-S-H gels. Recent research revealed that the C-A-S-H and N-A-S-H gels do not act as separate gels, but interact and undergo structural and composition change. [66]

A hybrid system of both low and high Calcium binders (Model III), are more beneficial for the development of stable microstructure and better mechanical properties. It can result in the reduction of the porosity and brittleness of a Calcium rich systems.

3.6 Concluding remarks

From what is mentioned above, combination of Calcium (BFS), Aluminium and Silicon rich materials (FA) were selected for this work, model III. This results in early age mechanical strength development of a mixture and simultaneously a room temperature curing without a need for external heating. This is due to the alkaline activation of CaO, SiO_2 and Al_2O_3 which forms the C-A-S-H and N-A-S-H gels.

This selected model is more beneficial for the development of stable microstructure, reduction of the porosity and brittleness of a calcium rich systems.

Chapter 4

4 GEOPOLYMER PASTE MIXTURE DESIGN FOR 3D PRINTING

4.1 INTRODUCTION

This chapter presents preliminary geopolymer paste mixture for 3D printing. In the first part, the physical and chemical properties of raw materials (FA and BFS) are examined by means of X-Ray fluorescence (XRF), X-Ray diffraction (XRD) and laser particle analyser (LPA). In the second part, the mixture designs are presented.

Compressive strength and setting time tests of the selected paste mixture designs are discussed for choosing the most suitable paste mixture compatible with the technical specifications of the specific 3D printer and ram extruder test

4.2 MATERIALS AND EXPERIMENTAL METHODS

4.2.1 Blast furnace slag (BFS)

4.2.1.1 BFS XRF- analyses

The used BFS consists of 30.72% Silica (SiO_2), 42.62% Lime (CaO), 13.32% Aluminum Oxide (Al_2O_3) and smaller concentrations of other compounds. The BFS is known to be a Calcium and Silicon rich material, Table 4.1 and Figure 4.1.

Table 4. 1: XRF- analyses of BFS

Compound	Concentration %
MgO	9.31
Al_2O_3	13.32
SiO_2	30.72
SO_3	1.45
K_2O	0.36
CaO	42.62
TiO_2	1.05
V_2O_5	0.02
MnO	0.34
Fe_2O_3	0.56
SrO	0.07
$Y2O_3$	0.01
ZrO_2	0.04
SnO_2	0.02
BaO	0.08

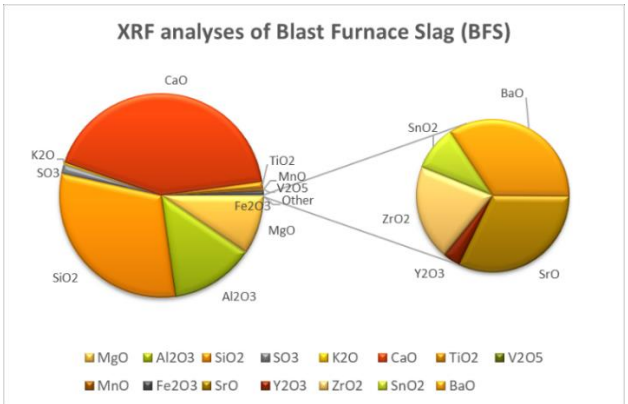

Fig. 4. 1: XRF-analyses of BFS

4.2.1.2 BFS XRD- analyses

The X-ray diffraction analyses (XRD) is used for the analyses and identification of the different crystalline phases of a material. It can be considered as a versatile non-destructive analytical technique. Identification is achieved by comparing the X-ray diffraction pattern obtained from unknown sample with internationally recognized database containing reference patterns for more than 70,000 phases.

The BFS contains mostly amorphous phases. However, it can contain crystalline peaks such as Gehlenite ($2CaO.Al_2O_3.SiO_2$) and Akermanite ($2CaO.MgO.2SiO_2$) (Figure 4.2). [55]

The XRD analyses of the BFS is shown in Figure 4.3. BFS contains mostly amorphous phases. The crystalline peaks are very small that the X'Pert highscore program could not identify them.

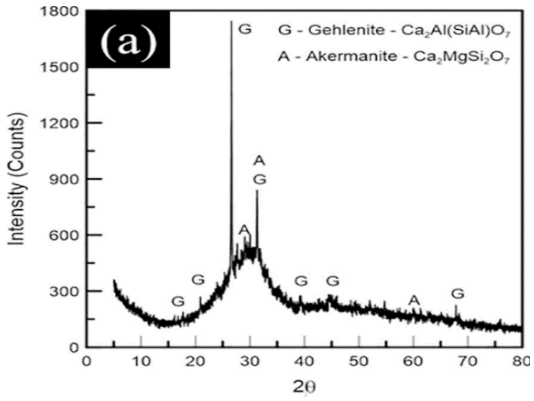

Fig. 4. 2: XRD analyses of BFS [55]

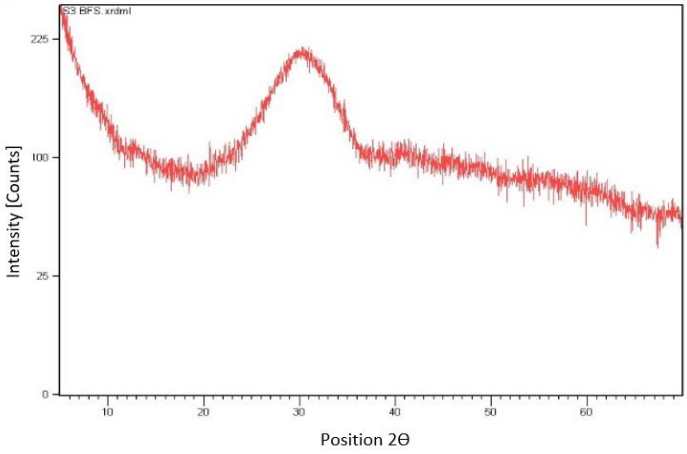

Fig. 4. 3: XRD analyses of BFS

4.2.1.3 BFS Particle size distribution (PSD)

The particle size of BFS influences the reactivity for the alkaline activation process. The reactivity of the big particles is less than the fine particles. Based on the research work of Wan in the year 2004, [51] the strength of the mortar is related to the surface area and PSD. When BFS, that is applied in the mortars, has the same surface area and contains more fine particles (diameter <3 µm), it shows a higher early mechanical strength development. Comparing these results to mortars that contain particles (diameter 3-20 µm), mortars with particles between 3.0 to 20 µm show higher long-term strength. [51]

Based on this information it can be concluded that the composition of the BFS and the particle size have a major influence on the alkaline activation process, setting time, workability and mechanical strength development. In Appendix A, the BFS volume percentage and cumulative undersize is shown by applying laser particle analyzer (LPA). The mean particles size of the BFS is 16.94 µm with a standard deviation (STD) of 9.75 µm. Furthermore, the particles size diameter ranges between 3.81 µm and 29.87 µm. From the obtained grain size results, it can be concluded that the general trend of the grain size of BFS goes towards the coarse size. This might influence the speed of alkaline activation reaction in a way that the coarse grains, which are the majority ratio in the BFS, would react much slower than the small grains.

4.2.2 Fly ash (FA)

4.2.2.1 FA XRF- analyses

The used FA in this work consists of 55.06% Silica (SiO_2), 26.74% Aluminum-Oxide (Al_2O_3), 8.09% Iron (III)Oxide (Fe_2O_3) and smaller concentration of other compounds. The FA is known to be an Aluminum (Al) and Silicon (Si) rich material (Table 4.2 and Figure 4.4). This FA can be classified as type F. To activate this type of FA an alkaline activator solution is required.

Table 4. 2: XRF- analyses of FA

Compound	Concentration %
MgO	1.25
Al_2O_3	26.74
SiO_2	55.06
P_2O_5	0.23
SO_3	0.73
K_2O	1.54
CaO	4.67
TiO_2	1.18
MnO	0.05
Fe_2O_3	8.09
ZnO	0.02
SrO	0.12
ZrO_2	0.05
BaO	0.12

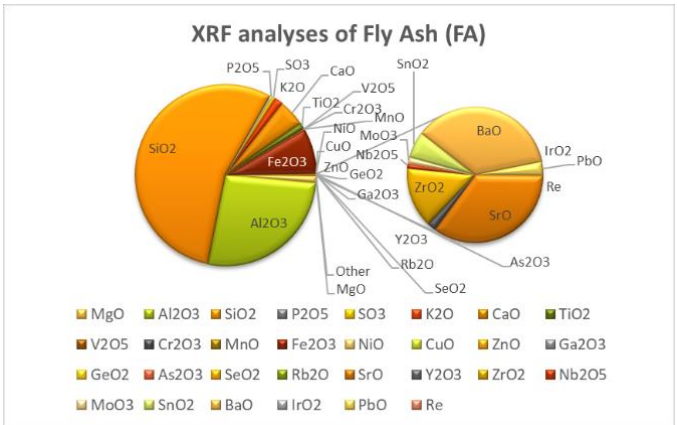

Fig. 4. 4: XRF-analyses of FA

4.2.2.2 FA XRD- analyses

Fly ash composition is expressed as bulk elemental oxide content that is determined by the XRF. However, this XRF-analyses does not show the crystalline and the highly reactive amorphous phases. To understand the phases of the class F FA, an X-ray powder diffraction (XRD) analyses is executed on a fine grinded sample. A comparison is made between the class F FA used in this work and the FA that is used in the research of Ma et al. (2013) [78]. The XRD results show mostly amorphous phases. Based on X'Pert highscore program, almost similar results were obtained in this work with that of Ma et al. (2013), see Figure 4.5. The intensities stand for Quartz (SiO_2), Mullite ($3Al_2O_3$. 2 SiO_2) and possibly Merwinitite (Ca_3Mg (SiO_4)$_2$) crystals. Based on Ma et al. (2013) work, the active amorphous Silica (SiO_2) and Alumina (Al_2O_3) are 34.9 wt.% and 16.2 wt.%. [78] These two percentages values might be close or similar to that of the Class F FA analyzed in this work.

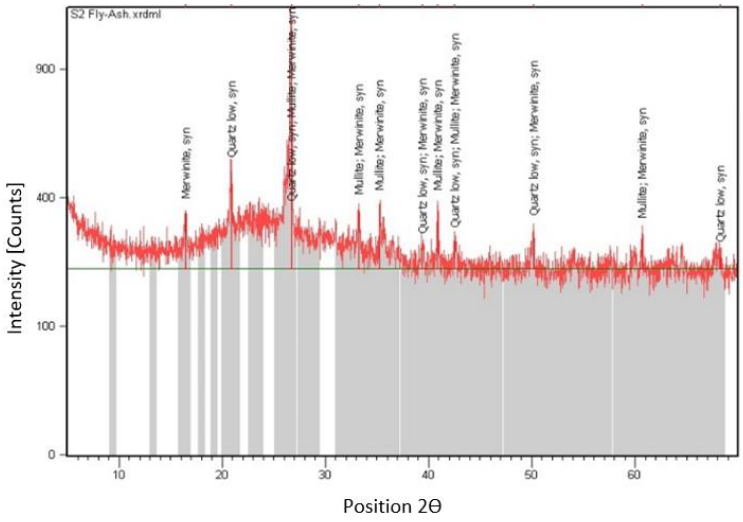

Fig. 4. 5: XRD analyses of FA

4.2.2.3 FA Particle size distribution (PSD)

In Appendix B, the laser particle analyzer (LPA) shows that the mean particle size of the FA is 54.30 µm, with a standard deviation (STD) of 34.25 µm. The particles size diameter ranges between 11.31 µm and 98.42 µm.

The mean particle size of FA of this work is larger than that of Ma et al. (2013) by 28.84 µm. [78] This would be inflicted negatively on the alkaline activation reaction speed of the FA grains. Larger particles would be slower reacted to the alkaline solutions.

4.2.2.4 Comparison between FA and BFS

Comparing the average particle size of BFS and FA, the BFS is finer than the FA by 37.5 µm, see Figure 4.6. Furthermore, both materials have reactive amorphous phases. However, the BFS particles reacts much faster than the FA due to its smaller grain sizes and amorphous phases although it requires more liquid activator for its workability.

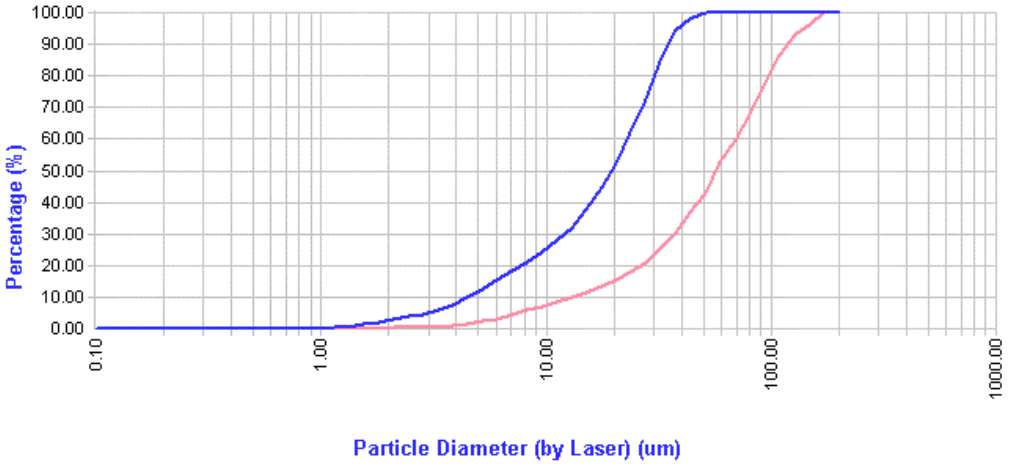

Fig. 4. 6: Cumulative volume percentage of BFS (blue line) and FA (pink line)

4.3 Paste mixture designs and test results

A mixture design suitable for 3D printing applications should have specific specifications. These specifications have direct link with the type of 3D printer machines, the type of construction to be built and the site construction environment. To fulfill these many conditions, a mixture should be designed carefully on many bases among which a suitable mechanical strength development, setting time, open time, buildability, extrudability and rheological properties (plastic viscosity) etc.

Having in mind the above-mentioned criteria about the different conditions that influence the mixture design to obtain the acceptable output from the specific 3D printer, many tests should be done to find a suitable mixture as follows:

4.3.1 Compressive strength and setting time of paste mixtures with different binder ratios

Six paste mixtures with different binder ratios between FA and BFS were tested on compressive strength and setting time. The mixture designs are presented in Table 4.3 and Table 4.4.

Table 4. 3: Geopolymer paste mixture designs S0, S10, S20, S30, S40 and S50

Mixture		S0	S10	S20	S30	S40	S50
	Density	Mass	Mass	Mass	Mass	Mass	Mass
	[gram/cm^3]	[gram]	[gram]	[gram]	[gram]	[gram]	[gram]
FA	2.44	1000	900	800	700	600	500
BFS	2.89	0	100	200	300	400	500
NaOH (4 M)		175	175	175	175	175	175
WGS	1.35	175	175	175	175	175	175
l/b-ratio		0.35	0.35	0.35	0.35	0.35	0.35
Ratio FA: BFS		100: 0	90: 10	80: 20	70: 30	60: 40	50: 50
Ratio NaOH: Na_2SiO_3		50: 50	50: 50	50: 50	50: 50	50: 50	50: 50

Table 4. 4: Mixture compositions of the pastes (with respect to 1 kg of binder (FA+BFS))

SiO_2	Na_2O	H_2O	l/b	SiO_2/Na_2O
[mol]	[mol]	[gram]	[-]	[-]
0.80	0.53	350	0.35	1.51

4.3.1.1 Compressive strength

The compressive strength results of the mixture designs in Table 4.3 and Table 4.4 shown in Figure 4.7. The compressive strength of the geopolymer paste mixtures were performed according to the [NEN 5988] on cubes with dimensions of 40 *40 *40 mm^3. The cubes were sealed in plastic bags and cured in a fog room with 20°C and 99% relative humidity until testing age of 1, 3, 7 and 14 days. Sealing the cubes in plastic bags prevents moisture exchange with the environment and limits the possibility of undesirable chemical reactions

in the specimens, for example a change in the formation of C-A-S-H and N-A-S-H gels or formation of micro-cracks in the paste.
The purpose of these different tests is to choose the most suitable paste mixture to be used in the 3D printing process. The basis of this choice depends on a longer workability and the most suitable extrudability of the mixture to be extruded with a 3D printer.
One of the main pillars to achieve that is by adopting the proper ratio of FA and BFS. For this project the NaOH molarity was kept constant at 4 mol/liter.

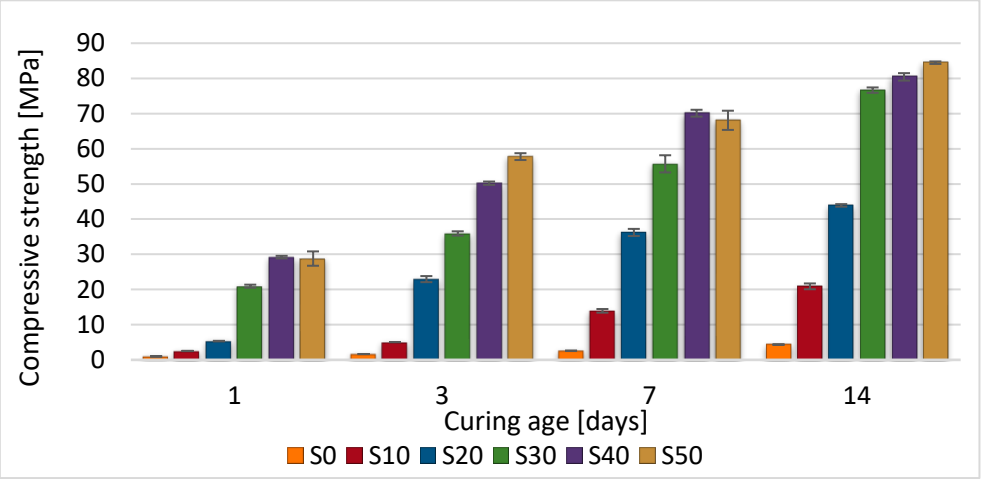

Fig. 4. 7: Compressive strength of S0, S10, S20, S30, S40 and S50 paste mixtures cured in fog room with 20°C and 99% relative humidity

As it is mentioned in section 3.5, the alkaline activation of higher concentration of BFS (more CaO content) forms more C-A-S-H gel, which in return causes the mixture to harden in ambient room temperature and develops early age mechanical strength. A higher percentage of BFS causes a linear increase in compressive strength of the tested specimens, see Figure 4.7. Among the different six selected paste mixtures, the S0 displayed a compressive strength of less than 5MPa on 14 days of curing. This mixture contains 0% of BFS and less than 5% CaO from the FA, Table 4.2. The S20 and S30 pastes, cured for 1 and 7 days, exhibited a difference of 15.6 MPa and 19.5MPa. Furthermore, comparing the S20 to the S10; the S20 has higher strength development with time than the S10, especially on the 3, 7 and 14 days of curing. The S20 displayed a compressive strength of 5.34 MPa for 1-day cured specimens.

4.3.1.2 Setting time

The main purpose of testing the setting time of the mixtures, is to find an optimized mixture with an initial setting time of 90 minutes that is compatible with the technical specifications of the specific 3D printer and ram extruder. This step will be discussed in chapter 5.

Meanwhile, the selected paste mixtures in Table 4.3 were examined on initial and final setting time. The setting time of the pastes is measured under a constant temperature of (20 ± 2) °C and relative humidity (RH) of (55.0± 2) % according to [NEN-EN 196-3]. The ratio between FA and BFS is examined on the setting time by using Vicamatic needle test. In Figure 4.7 and Figure 4.8, a relationship is noticed between the compressive strength and the setting time of the paste mixtures. The initial and final setting time has an exponential decrease. The initial setting time and final setting time between 30% and 50% of BFS is 3

and 6 minutes. An increase in the percentage of BFS beyond 45% would result in no drastic change in the setting time.

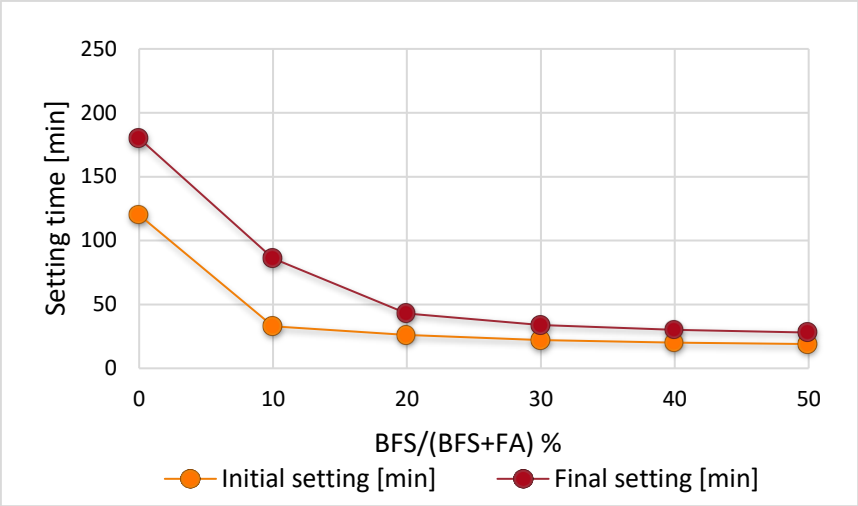

Fig. 4. 8: Geopolymer paste mixtures setting time with different binder ratios

From what is concluded from section 4.3.1.1, the S20 paste mixture will be chosen for further optimizing to be used later for 3D printing. The main reasons for choosing the S20 are:

- The binder contains 80% more spherical particles from the FA. This allows for lower l/b-ratio and it is better for extrudability due to the rolling of the spherical particles over each other;
- Comparison between the S10 and S20, the S20 gave a higher strength development between 3, 7 and 14 days of curing time. This mixture has a 1-day compressive strength of 5MPa.

4.3.2 Compressive strength and setting time of S20 paste mixtures with different percentage of retarder

Three S20 paste mixtures with 0.5%, 1% and 1.5% of Barium Chloride dehydrate retarder were compared to the S20 paste mixture with 0% of retarder on compressive strength and setting time, see Table 4.5. The percentage of the retarder is calculated with respect to the total binder weight.

Table 4. 5: S20 paste mixtures with 0%, 0.5%, 1% and 1.5% BaCl2. H2O retarder with respect to the total binder weight

Mixture	**S20**	**S20**	**S20**	**S20**
	Mass	**Mass**	**Mass**	**Mass**
	[gram]	**[gram]**	**[gram]**	**[gram]**
FA	800	800	800	800
BFS	200	200	200	200
NaOH (4 M)	175	175	175	175
WGS	175	175	175	175
Retarder ($BaCl_2$. H_2O)	0 (wt.% of the binder)	5 (0.5 wt.% of the binder)	10 (1 wt.% of the binder)	15 (1.5 wt.% of the binder)
l/b-ratio	0.35	0.35	0.35	0.35
FA: BFS	80: 20	80: 20	80: 20	80: 20
NH: WG	50: 50	50: 50	50: 50	50: 50

4.3.2.1 Compressive strength

The compressive strength of the S20 paste mixtures were performed according to the [NEN 5988] on cubes with a dimension of 40 * 40 * 40 mm^3. The cubes were sealed in plastic bags and cured in a fog room with 20°C and 99% relative humidity for the testing age of 1, 3 and 7 days. The compressive strength results are shown in Figure 4.9.

The early age strength of the hardened mixtures is dramatically lowered when the percentage of retarder increases. Addition of 0.5% of Barium Chloride dehydrate retarder lowered the 1-day cured specimens to 1.33 MPa. Specimens with 1% and 1.5% of retarder showed a compressive strength less than 1 MPa after 7 days of curing. The Barium Chloride dehydrate absorbs the moisture from the mixtures which results in reduction in the workability, especially for using it for 3D printing purposes. Furthermore, for early age mechanical strength development, it is not recommended to add more than 0.5% of Barium Chloride dehydrate to a mixture design. Therefore, there are two main reasons not to use the Barium Chloride dehydrate as a retarder to delay the setting time.

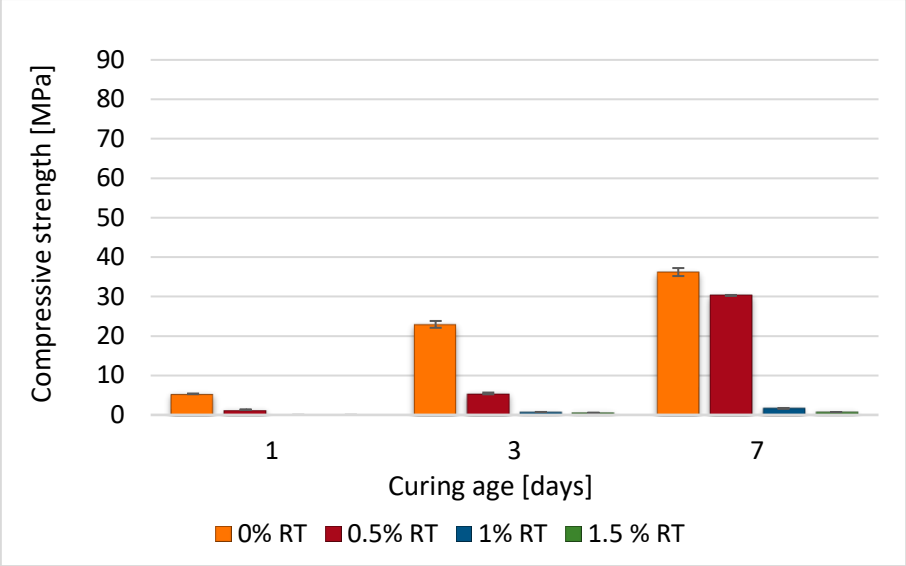

Fig. 4. 9: Compressive strength of S20 paste mixtures with the addition of $BaCl_2$. H_2O retarder (RT) cured in fog room with 20°C and 99% relative humidity

4.3.2.2 Setting time

The setting time of the S20 paste mixtures are measured under a constant temperature of (20 ± 2) °C and relative humidity (RH) of (55±2) % according to [NEN-EN 196-3]. The setting time results are shown in Figure 4.10. Depending on the percentage of added Barium Chloride dehydrate, the setting time can be delayed, however the compressive strength is negatively affected, as can be seen in Figure 4.9. The addition of 0.5% Barium Chloride dehydrate delays the initial setting time to 57 minutes and reduced the compressive strength from 5.34 MPa to 1.33 MPa.

In section 4.3.3, S20 paste mixtures will be further tested on compressive strength and setting time by changing the ratio of the alkaline activator solutions (NaOH and Na_2SiO_3).

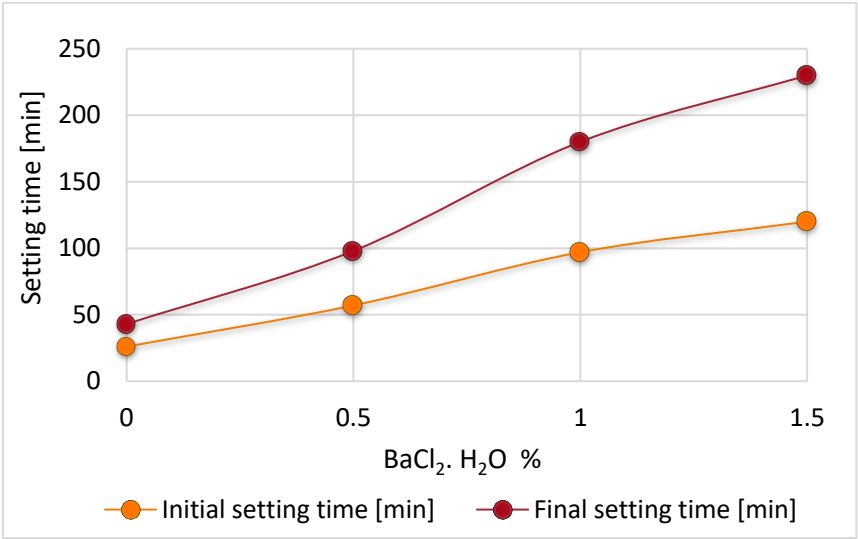

Fig. 4. 10: Setting time of S20 paste mixtures with 0%, 0.5%, 1% and 1.5% BaCl2. H2O retarder

4.3.3 Compressive strength and setting time of S20 paste mixtures with different concentration of alkaline activator solutions.

The concentration of the alkaline solutions has a major role in the formation of the C-A-S-H and the N-A-S-H gels. In section 3.3 is mentioned that the OH^- ions catalyze the dissolution of Si^{4+} and Al^{3+}, as well as the Ca^{2+} ions in the binders to form C-A-S-H gel. Furthermore, the Sodium Silicate solution (Na_2SiO_3) influences the dissolution of the Ca^{2+} ions in the BFS to form C-A-S-H gel and affects the workability and the setting time.

In Table 4.6, six S20 paste mixtures were tested on compressive strength and setting time. The differences between the mixtures are the ratios of the Sodium Hydroxide (NaOH) and Sodium Silicate (Na_2SiO_3) solutions. The studied Na_2SiO_3/NaOH ratios are 0, 0.25, 0.43, 1, 2.33 and 4. For each mixture the amount of mol SiO_2 and Na_2O is calculated with respect to 1 kg of binder and a l/b-ratio of 0.35.
The concentration of the Silica (SiO_2) influences the density of the matrix. More SiO_2 in the binder and/or alkaline activator solution makes the matrix more dense and higher mechanical properties can be obtained.
As it is mentioned before in section 4.3.1.2, the main reason of this step is to find a paste mixture with an initial setting time of around 90 minutes.
The results of the S20 paste mixture are shown in Table 4.6 and Figure 4.11. From all the six tested mixtures, mixture 5 and 6 displayed initial setting time of 85 and 125 minutes. The higher is the SiO_2/Na_2O ratio, the faster is the setting time. Based on the theoretical understanding, a greater SiO_2/Na_2O ratio should give a higher mechanical strength property. However, it has been noticed that mixture 3 exhibited a higher early strength development compared to mixture 1 and 2. This can be explained due to the fact of abundance of entrapped air in the mixture, which cannot be avoidable in the extruding process as in the case of conventional compaction method on mortars and concrete. Mixture 5 is chosen for further testing on rheological properties and 3D printing. The initial setting time of mixture 5, with Na_2SiO_3/NaOH and SiO_2/Na_2O ratio of 0.25 and 0.82, is around 85 minutes. The compressive strength of 1, 3 and 7- days cured specimens is around 0.77, 9.22 and 20.55 MPa. The compressive strength of 5MPa was obtained after 3 days of curing.

Table 4. 6: S20 paste mixtures with different ratios of NaOH and Na_2SiO_3 solutions with respect to 1 kg of total binder

Mix	Alkaline solution ratio	WGS/NH	SiO_2	Na_2O	SiO_2/Na_2O	l/b	Setting time		Compressive strength [MPa]		
		[-]	[mol]	[mol]	[-]	[-]	Initial [min]	Final [min]	1 [day]	3 [days]	7 [days]
1	4M NH: WGS= 20: 80	4.0	1.28	0.67	1.91	0.35	23	37	6.68	11.26	19.86
2	4M NH: WGS= 30: 70	2.33	1.12	0.63	1.78	0.35	31	40	2.85	13.71	27.71
3	4M NH: WGS= 50: 50	1.0	0.80	0.53	1.51	0.35	26	43	5.34	22.95	36.21
4	4M NH: WGS= 70: 30	0.43	0.48	0.44	1.1	0.35	75	180	0.64	4.87	14.90
5	**4M NH: WGS= 80: 20**	**0.25**	**0.32**	**0.39**	**0.82**	**0.35**	**85**	**190**	**0.77**	**9.22**	**20.55**
6	4M NH: WGS= 100: 0	0	0.00	0.30	0	0.35	125	245	0.53	7.88	12.55
NH: Sodium hydroxide solution (NaOH) WGS: Sodium silicate solution (Na_2SiO_3) / Waterglass											

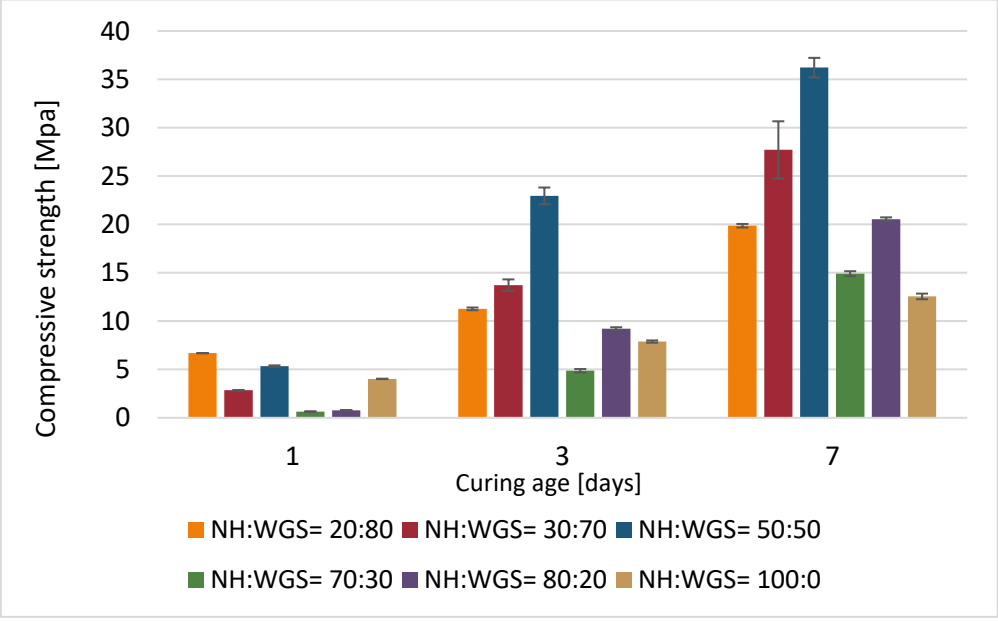

Fig. 4. 11: Compressive strength of S20 paste mixtures with different ratios of NaOH (NH) and Na_2SiO_3 (WGS) solutions
cured in fog room with 20°C and 99% relative humidity

4.4 Concluding remarks

In this chapter, different experimental tests were carried out on the binders (FA and BFS), compressive strength and setting time of the selected mixture designs to choose a suitable mixture for 3D printing and rheological properties using a ram extruder.
From these tests, it has been concluded that, the BFS is amorphous and consists of 42,62% lime (CaO) and 30.72% Silica (SiO_2). The mean particle size of BFS is 16.94 µm. It can be considered to have coarse grains size.
The FA has crystalline phases of Quartz (SiO_2), Mullite ($3Al_2O_3$. $2\ SiO_2$) and possibly Merwinitite ($Ca_3Mg\ (SiO_4)_2$). It is a Class F fly ash (FA) and consists mainly of 55.06% Silica and 26.74% Aluminium Oxide. The mean particle size of the FA is 54.30 µm. It can be considered coarse grains size. The grain size of BFS is finer than the FA by 37.5 µm. This might lead to slower reaction of FA than the BFS in the alkaline medium.

Six paste mixture designs with different ratios between FA and BFS were tested on compressive strength and setting time. The obtained results show higher percentage of BFS in the total binder which causes a linear increase of the early age compressive strength and an exponential decrease in the setting time. An increase in the percentage of BFS beyond 45% might results in no drastic change in the setting time. The S0 paste mixture with 0% BFS displayed, after 14 days of curing, less than 5MPa in compressive strength whereas the S20 (with 20% BFS) displayed a compressive strength of 5.34 MPa for 1-day cured specimens. The S20 paste mixture was chosen for further optimization to be more suitable in the 3D printing process and rheological tests.
The early age strength of the hardened S20 paste mixtures are dramatically lowered when the percentage of Barium Chloride dehydrate retarder increases. However, in spite of the fact that the Barium Chloride dehydrate is delaying the setting time, it is not recommended to be used in the mixture because of its absorption to the moisture of the mixtures. This results in the reduction of the workability by using it for 3D printing purposes.

The S20 paste mixture was further tested on compressive strength and setting time by changing the ratios between Sodium Hydroxide (NaOH) and Sodium Silicate (Na_2SiO_3) solutions. The selected Na_2SiO_3/NaOH ratios are 0, 0.25, 0.43, 1, 2.33 and 4. Therefore, from the six S20 paste mixtures, mixture 5 has been chosen for further testing on rheological properties and 3D printing. This is due to the fact that mixture 5, with ratios of Na_2SiO_3/NaOH and SiO_2/Na_2O of 0.25 and 0.82, has an initial setting time around 85 minutes. This mixture has a compressive strength of 0.77, 9.22 and 20.55 MPa for 1, 3 and 7- days cured specimens. The compressive strength of 5MPa was obtained after 3 days of curing.

Chapter 5

5 Rheological properties and 3D printing of geopolymer paste mixtures

5.1 Introduction

In this chapter, the rheological properties of selected paste mixtures will be discussed. Two kinds of rheology measurements were carried out using a plate rheometer and a ram extruder. A chosen mixture was further optimized to be suitable for the specific 3D printer and examined on mixture fresh state 4 layers buildability, open time and 28 days tensile bonding strength tests.

5.2 Rheological properties of paste mixtures

5.2.1 Introduction

Rheology is the study of flow and deformation of materials under applied forces which can be measured by using a rheometer or a ram extruder. The geopolymer pastes can be considered to be a non-Newtonian material. [75] For the rheological properties of the mixtures (plastic viscosity and shear yield stress τ_0), the Bingham model was adopted for the plate rheometer test. [75] The rheological properties of the fresh geopolymer mixtures are important for selecting the processing conditions and enabling a smooth extrusion process for 3D printing. The ability of the first layer to support itself and subsequent layers is a link to its rheological properties, more precisely its yield stress. [73] Therefore, geopolymer mixture must be designed to meet certain criteria that have direct relationship with the 3D printer. It is critical to ensure a complementary connection between the designs of the mixture and the printing machine on the following bases:

- The mixture should be easy extrudable, workable and at the same time it should have maximum buildability upon pouring;
- Maintaining an appropriate setting rate to ensure bonding with the subsequent layer and
- The mixture should have low percentage of pores (high density) and a fast-early age strength development.

Geopolymer paste mixtures have a sticky texture, which indicates possible good bonding strength depending on the time gap of extrusion between two successive layers during the 3D printing process. A successive extrusion process is highly dependent on the fresh paste

properties, the equipment wall and the forming system (nozzle). The paste is forced to flow in a certain conveying system to be extruded out of the nozzle.

For the purpose of this work, the selected S20 paste mixture was examined on rheological properties by using the plate rheometer and the ram extruder.

5.2.2 Plate rheometer

5.2.2.1 Testing procedure

The rheological measurements were carried out with a plate rheometer. The test setup is shown in Figure 5.1.
Six S20 paste mixtures were measured on shear stress versus shear rate by applying the Bingham model, Table 5.1. The difference between the mixtures is the percentage of added Acti-gel, calculated with respect to the total binder weight.
The pastes are mixed with a mechanical stirrer for 5 minutes (2 minutes binder and 3 minutes alkaline activator solutions) and immediately moved to the rheometer plate. The experiments are conducted in a constant room temperature of 20 °C. The test procedure used for the mixtures is shown in Figure 5.2.
Every 10 seconds the shear rate is changed by 20 s^{-1}. From 0 to 50 seconds, the shear rate is gradually increasing to a maximum of 100 s^{-1}, then gradually decreases to the original value of 20 s^{-1}. The gradual increase of the shear rate refines the shear stress, apparent viscosity and plastic viscosity. The apparent viscosity of non-Newtonian fluids depends on the shear rate. For a specific shear rate, the shear stress is measured and the slope of the two values gives the apparent viscosity (Figure 5.3 a). The apparent viscosity clarifies that when the shear rate increases, the analyzed material has a shear thickening behavior and vice versa. The plastic viscosity η is the slope of the shear stress and shear rate line above the shear yield stress τ_0 (Figure 5.3 b).

Table 5. 1: S20 geopolymer paste mixtures with different percentage Acti-gel with respect to total binder weight

Mix	1	2	3	4	5	6
	Mass [gram]	Mass [gram]	Mass [gram]	Mass [gram]	Mass [gram]	Mass [gram]
FA	400	400	400	400	400	40
BFS	100	100	100	100	100	100
Total Binder	500	500	500	500	500	500
NaOH	126	126	126	126	126	126
WGS	31.5	31.5	31.5	31.5	31.5	31.5
Total liquid activator	157.5	157.5	157.5	157.5	157.5	157.5
l/b-ratio	0.315	0.315	0.315	0.315	0.315	0.315
Acti-gel %	**0**	**0.2**	**0.5**	**0.75**	**1**	**1.5**
Acti-gel in gram	**0**	**1**	**2.5**	**3.75**	**5**	**7.5**
Total Solids	500	500	500	500	500	500
FA: BFS- ratio	80:20	80:20	80:20	80:20	80:20	80:20
NH: WGS- ratio	80:20	80:20	80:20	80:20	80:20	80:20

(a)

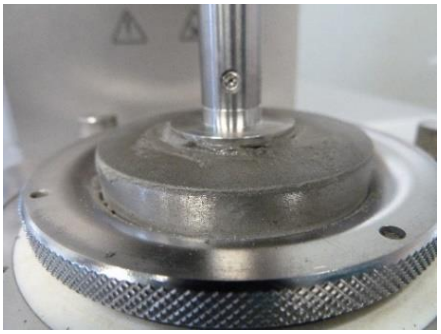

(b)

Fig. 5. 1: Rheometer test setup (a) and (b)

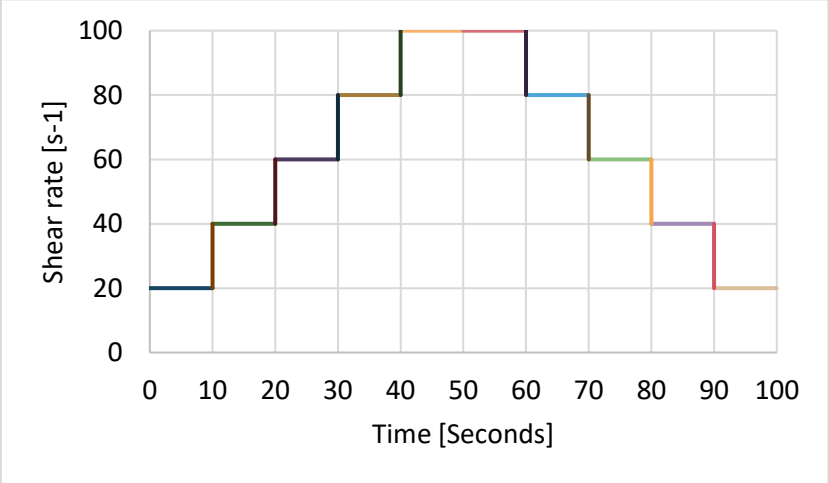

Fig. 5. 2: Shear rate versus time for the plate rheometer test

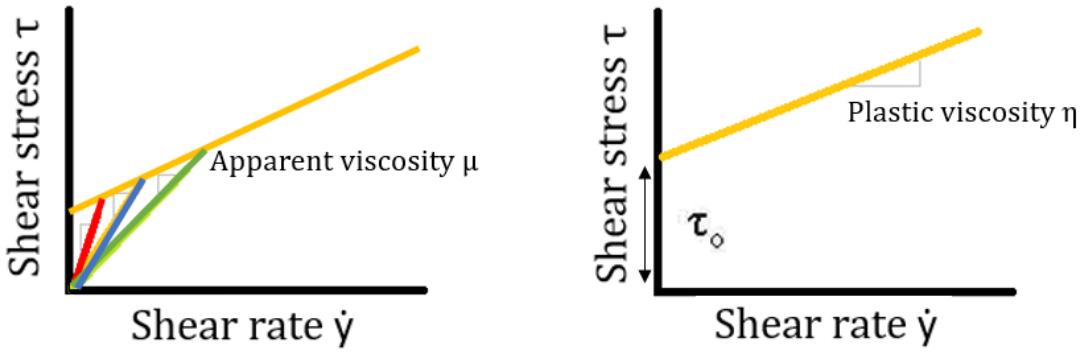

(a) (b)

Fig. 5. 3: Apparent viscosity and plastic viscosity for non-Newtonian material

5.2.2.2 Rheometer results

Tables E.1 to E.24, Appendix E and Figures 5.4 to Figure 5.9 show the rheometer test results of the six S20 paste mixtures samples. Each mixture was tested four times with a time interval of 10 minutes subsequently. The obtained results from the plate rheometer show, for similar value of shear rate, that the values of the shear stress increase linearly with time. It has also been noticed that for each specific time interval, the mixtures exhibited a shear thinning behavior. This is due to a slightly decrease in the apparent viscosity μ with the increase of the shear rate.

When comparing the shear stress and plastic viscosity of all the six mixtures on time interval of 30 minutes, the plastic viscosity and shear stress slightly decreases by increasing the concentration of Acti-gel. In addition to that, the shear yield stress τ_0 on the four-time intervals (shown in the rheo-grams) starts gradually to have similar shear yield stress. When the shear rate equals zero, it gives an indirect indication of the value of the shear yield stress. Even though the value of the shear yield stress is quite small, close to zero value, it is important to obtain the shear yield stress and the plastic viscosity to characterize the flow properties of any specific material. This means that such kind of material requires very slight stress to make it flowable which inflict its applicability in the extruding process for the purpose of 3D printing.

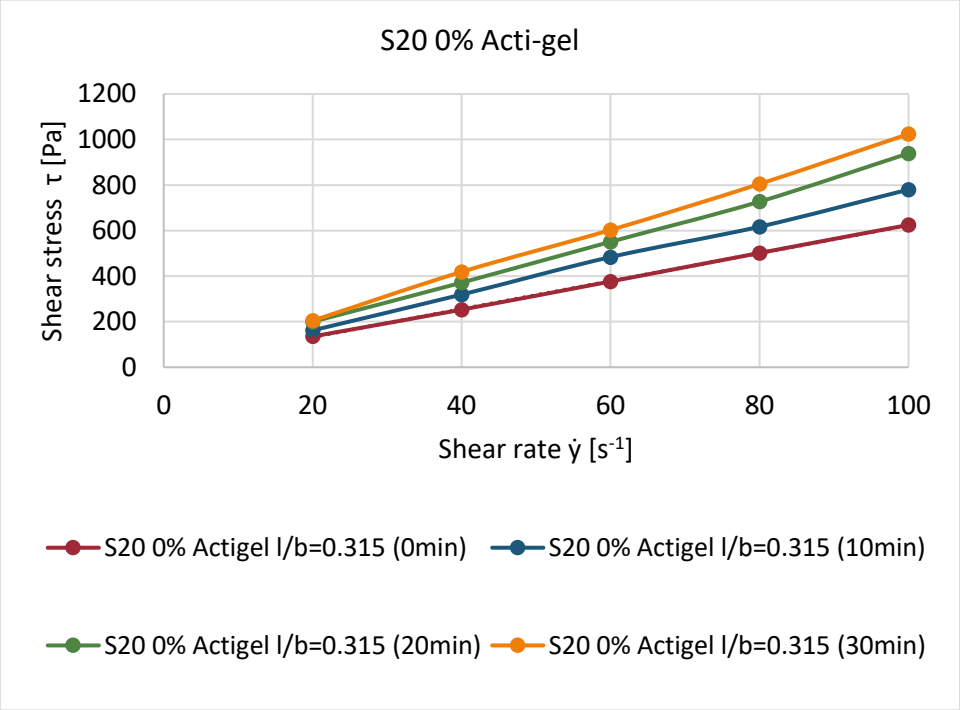

Fig. 5. 4: Mixture 1 S20 with 0% Acti-gel and l/b-ratio of 0.315 (shear stress vs shear rate)

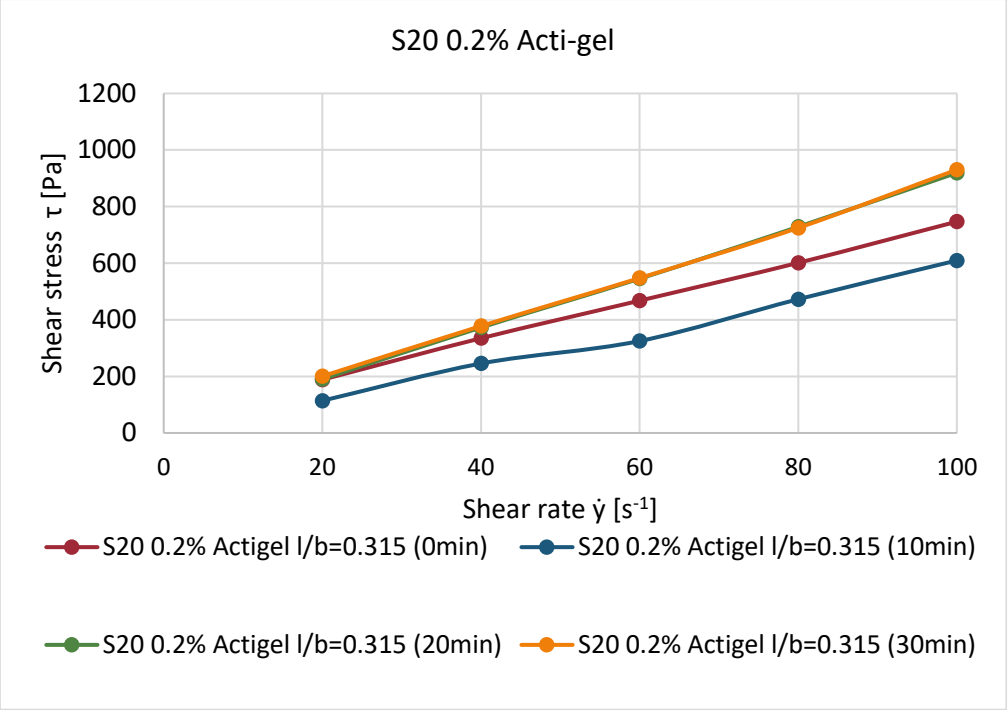

Fig. 5. 5: Mixture 2 S20 with 0.2% Acti-gel and l/b-ratio of 0.315 (shear stress vs shear rate

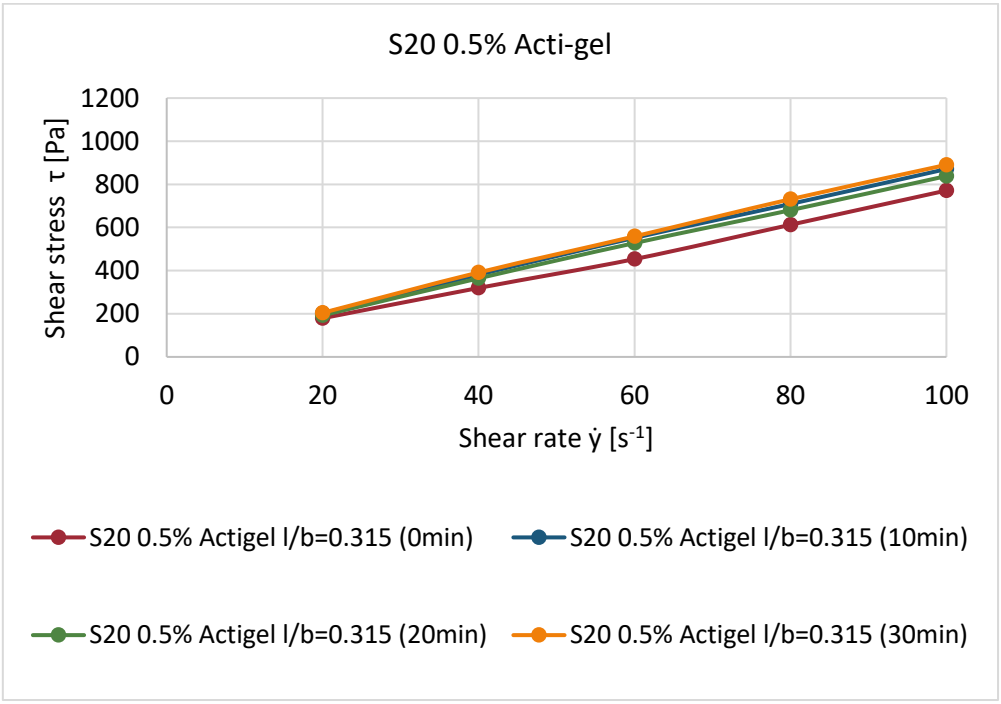

Fig. 5. 6: Mixture 3 S20 with 0.5% Acti-gel and l/b-ratio of 0.315 (shear stress vs shear rate)

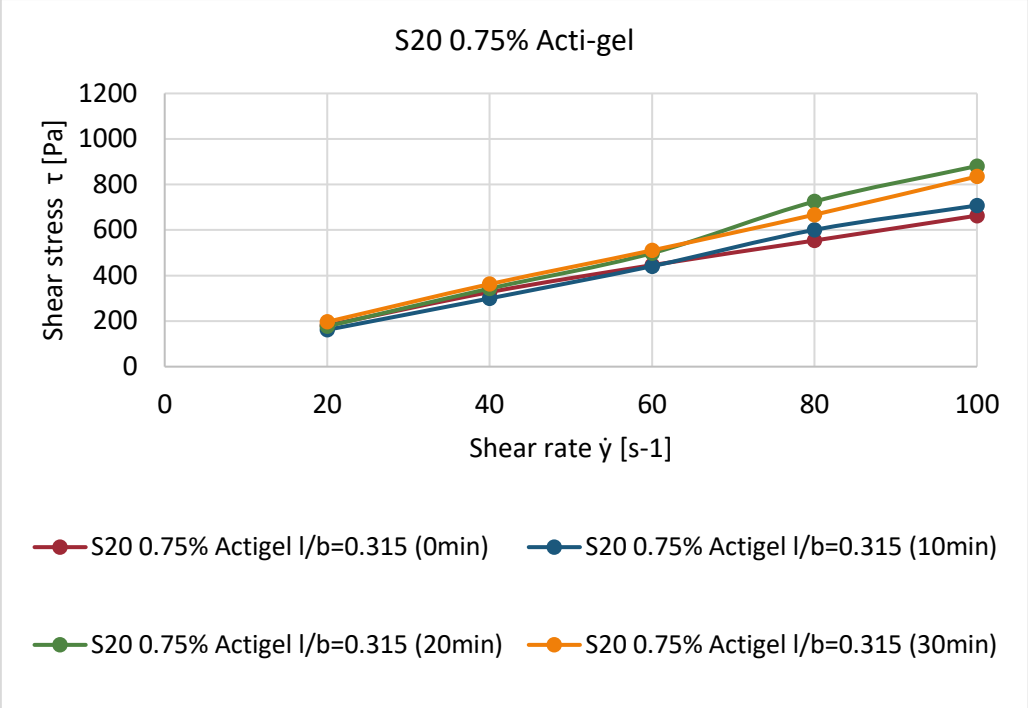

Fig. 5. 7: Mixture 4 S20 with 0.75% Acti-gel and l/b-ratio of 0.315 (shear stress vs shear rate)

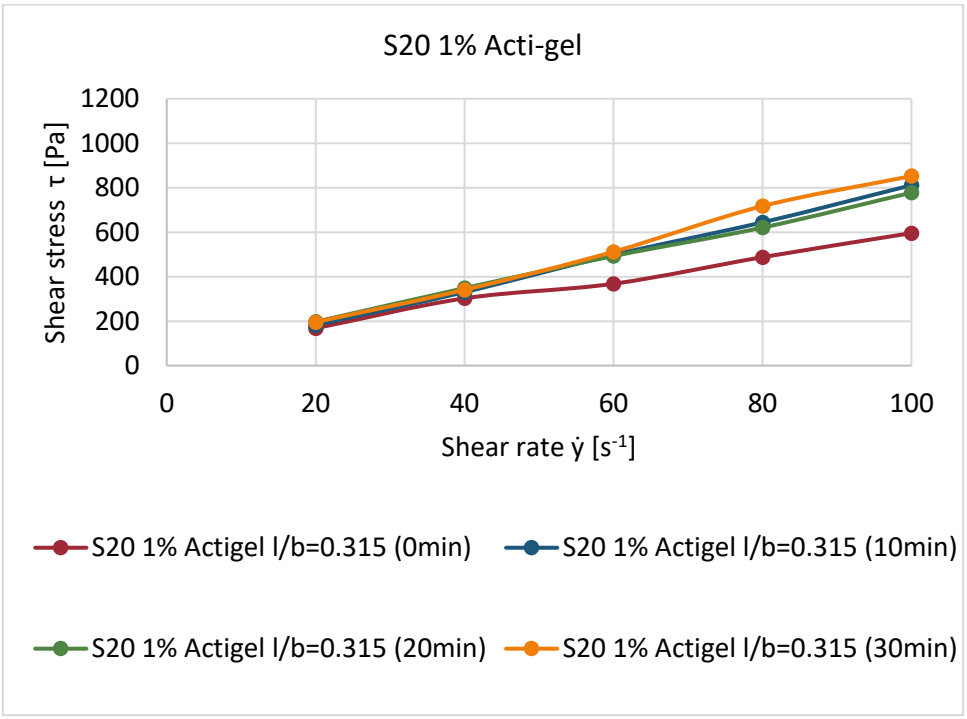

Fig. 5. 8: Mixture 5 S20 with 1% Acti-gel and l/b-ratio of 0.315 (shear stress vs shear rate)

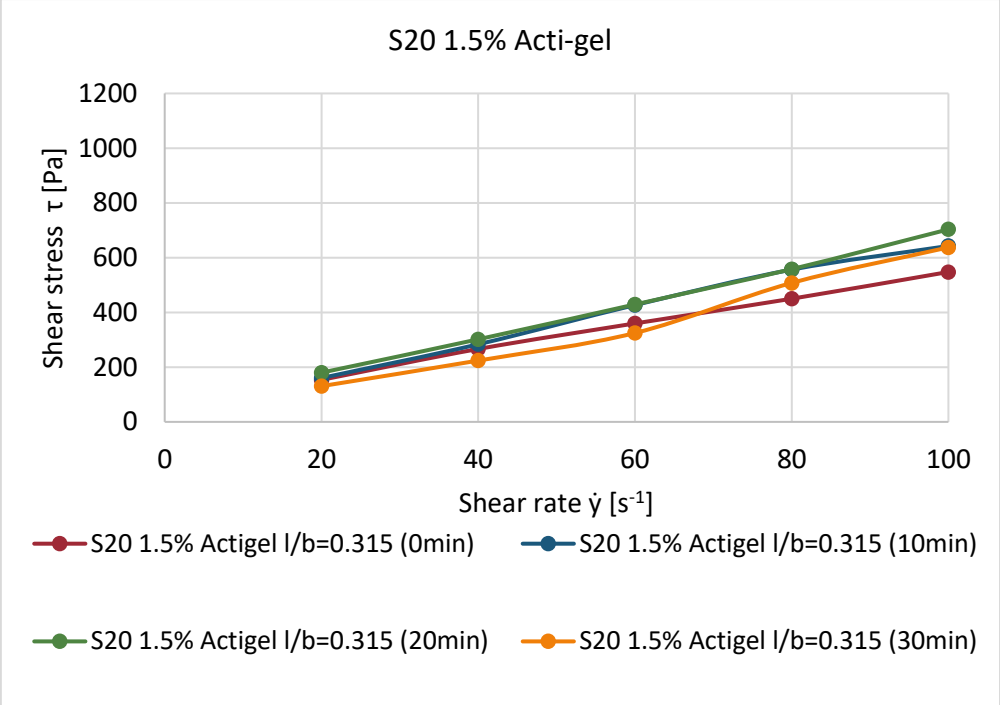

Fig. 5. 9: Mixture 6 S20 with 1.5% Acti-gel and l/b-ratio of 0.315 (shear stress vs shear rate)

5.2.3 Ram extruder

A ram extruder system with a rigid barrel having smooth surface and capillary dies with different lengths was developed to study the extrusion properties of fresh paste mixtures. The setup of the ram extruder is shown in Figure 5.10. The ram extruder in Figure 5.10 and 5.11 consists of an assembly, barrel, die's and a piston. It is assembled on the Instron universal testing machine. The ram extruder can be used in the laboratory as a form of rheometer to provide a means of characterizing the bulk yield stress (σ_0) and shear yield stress(τ_0) of paste- like materials. The total extrusion pressure gives an indication of the rheology of semi-solid pastes because a higher pressure will be required to extrude stiffer paste. For this type of ram extruder, an initial setting time of 90 minutes is required for a mixture design.

Fig. 5. 10: Ram extruder test setup

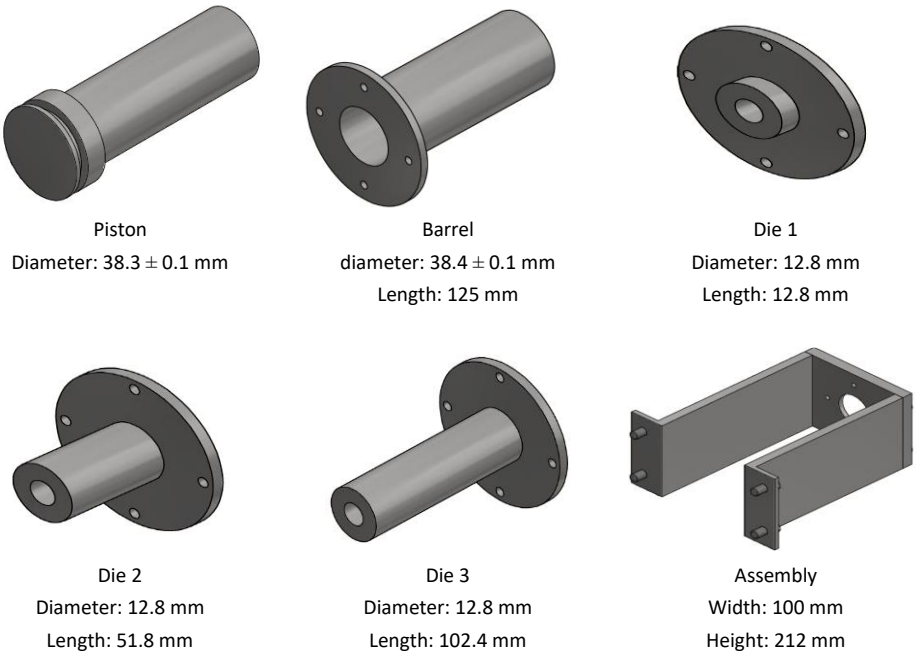

Fig. 5. 11: Ram extruder components

The ram extrusion mechanism can be illustrated by the Benbow-Bridgewater model (Eq. 3) based on the assumption of plastic deformation in the die entry and die land, as it is shown in Figure 5.12 and Figure 5.13. [76]
The ram extruder has been applied for cementitious mortars. However, until now no geopolymer pastes was tested with the ram extruder.

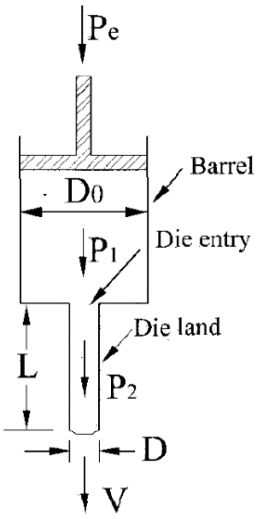

Fig. 5. 12: Ram extrusion and pressure drops

Fig. 5. 13: Example of Ram extruder paste extrusion

$$P_e = P_1 + P_2 = 2\,ln\left(\frac{D_0}{D}\right)(\sigma_0 + \alpha V^m) + \frac{4L}{D}(\tau_0 + \beta V^n) \quad [3]$$

P_e: total Pressure drop [kPa]

P_1: die entry pressure [kPa]

P_2: die land pressure [kPa]

D_0: barrel diameter [mm]

D: die diameter [mm]

L: die Land length [mm]

V: Extrusion velocity of the paste [mm/s]

σ_0: initial bulk yield stress [kPa]

τ_0: initial wall shear yield [kPa]

α: factor characterizing the effect of velocity on bulk yield strength. It is a measure for the dependence of the flow resistance to the extrudate velocity in the die entry.

β: factor characterizing dynamic behavior of the sliding stresses and it shows some velocity or shear rate
dependent properties of the pastes.

n & m: flow index to calibrate the pseudo-plasticity of the pastes

5.2.3.1 Testing procedure

The paste mixture is mixed with a mechanical stirrer for 5 minutes (2 minutes binder and 3 minutes alkaline activator solutions) and immediately move to the ram extruder. The fresh mixture is then lumped into the barrel. To remove air bubbles, each lump is tamped down by hand with a steel tamper. After the barrel is completely filled with the fresh mixture, the experimental procedure is then initiated. The average piston pressure during extrusion is taken as the total extrusion pressure. Each mixture is tested with the three dies shown in Figure 5.11. The piston speed is changed on a specific position, as it is shown in Figure 5.16. The piston speed is changed from 2 mm/s, 1 mm/s, 0.5 mm/s to 0.25 mm/s.

5.2.3.2 Experimental results

The ram extruder gives a better understanding of the total pressure on the piston and the buildability of the paste. Due to limited knowledge about the extrusion of geopolymer paste and how to improve the extrudability and buildability for 3D printing, four S20 paste mixtures were examined with different percentage of Acti-gel, see Table 5.1. Mixture 1, 3, 4 and 5 with 0%, 0.5%, 0.75% and 1% of Acti-gel are tested. The Acti-gel, with rod-shaped magnesium aluminum silicate particles, is examined on geopolymer pastes to find out if it can help in improving the extrudability and simultanously the buildability.
The volumetric flow rate of the barrel and die is illustrated in Figure 5.14. The volumetric flow rate of the barrel and the die are not similar because both have different diameters. The fluid speed in the barrel depends on the piston speed and the fluid speed in the die can be calculated using Eq. 4- 8.

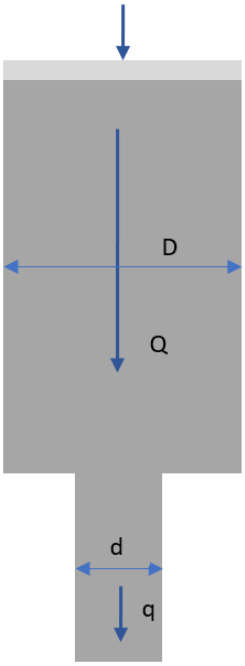

Fig. 5. 14: Volumetric flow rate in barrel (Q) and die (q)

$$\boldsymbol{Q_{barrel} = q_{die}} \quad [4]$$

$$V_b * A_{barrel} = V_{die} * A_{die} \quad [5]$$

$$V_{barrel} * \frac{\pi * D^2}{4} = V_{die} * \frac{\pi * d^2}{4} \quad [6]$$

$$V_{barrel} * D^2 = V_{die} * d^2 \quad [7]$$

$$V_{die} = \frac{V_{barrel} * D^2}{d^2} \quad [8]$$

Q: volumetric flow rate in barrel [mm^3/s]

q: volumetric flow rate in die [mm^3/s]

V_{barrel}: piston speed/fluid speed [mm/s]

V_{die}: fluid speed in die [mm/s]

D: barrel diameter [mm]

d: die diameter [mm/s]

A_{barrel}: area barrel [mm^2]

A_{die}: area die [mm^2]

Due to the fast-alkaline activation process of the binders, the rheological properties of the S20 mixture, with 80% of NaOH solution and 20% $NaSiO_3$ solution, are changing rapidly. It is not possible to compare the average pressure of three successive tests with 5 to 7 minutes interval time between each extruding test. Because of this, only the first test (time interval of 0 min after mixing) of each mixture is taken for the calculation of the initial shear yield stress (τ_0) and the initial bulk yield stress(σ_0). The graphs of the tested mixtures with the three different die lengths are shown in Figure 5.17 to Figure 5.19. From the obtained results, for each tested S20 mixture, the most stable total pressure is selected of three different fluid flow speeds in the barrel, see Table 5.2. For the three-fluid flow speeds the average of the total pressure was determined. This average pressure was plotted against the die length to die diameter ratio (L/D), see Figure 5.20 to Figure 5.23. The purpose of this step is to simplify Equation 3 by assuming m and n as 1 to obtain the initial wall shear yield stress (τ_0), initial bulk yield stress (σ_0), the die entry P1 and die land pressure P2. By assuming m and n as 1, Equation 3 can be seen as a linear function, see Figure 5.15. The a and b values of the linear function are calculated as follows Eq. 9-1 0:

$$\boldsymbol{a = 4(\tau_0 + \beta V)} \quad [9]$$

$$\boldsymbol{b = 2 \ln\left(\frac{D_0}{D}\right)(\sigma_0 + \alpha V)} \quad [10]$$

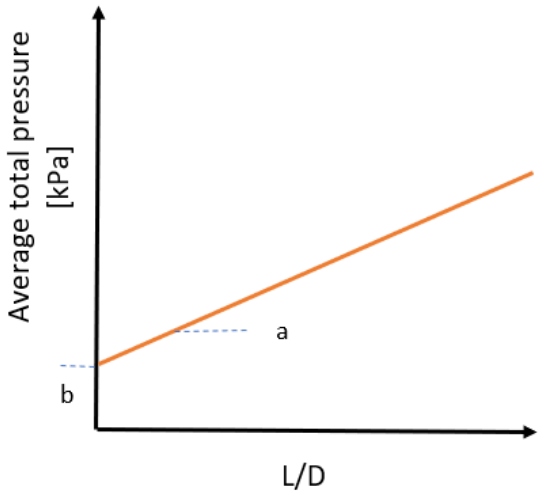

Fig. 5. 15: Linear function average total pressure vs. L/D ratio

The nature of the results obtained from the ram extruder shows an increase in the pressure with a time interval of 5 to 7 minutes between each test performed on a mixture (see Appendix F). An increase in the die length of the ram extruder results in accumulative increase in the piston pressure during the process of extruding the mixtures. It is very important to point out here that this paste mixtures are sticky without the Acti-gel because more extrusion pressure is required to be exerted when the die length increases, see Figure 5.17 to Figure 5.19. The addition of Acti-gel gives more stable flowability of the mixture with increasing the piston pressure of the ram extruder. This behavior confirmed the logical approach which stated that the Acti-gel, under conditions of shear, improves the flow conditions which in turn enhances the pumpability and workability (lower viscosity upon shear force) of the mixture, see section 3.4.2. This gives a positive advantage to use the Acti-gel in such kind of applications.
As a preliminary approach, the flow index parameters n and m of Benbow-Bridgewater model were selected to be as 1. However, all the mixtures behaved non-linearly, see Figure 5.20 to Figure 5.23. This assumption for n and m to be 1 needs more refinement to obtain better values for the shear yield stress (τ_0) and initial bulk yield stress (σ_0). This might be achieved by repeating the tests of each mixture at least 5 times.

Table 5. 2: Fluid flow speed in barrel and die

Fluid flow speed in barrel [mm/s]	Fluid flow Speed in die [mm/s]
1	9
0.5	4.5
0.25	2.25

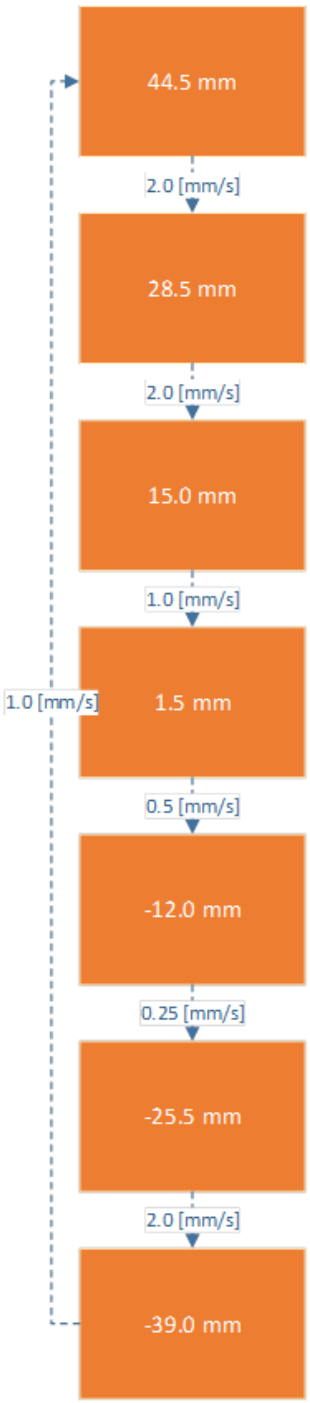

Fig. 5. 16: Ram extruder Position vs. piston speed

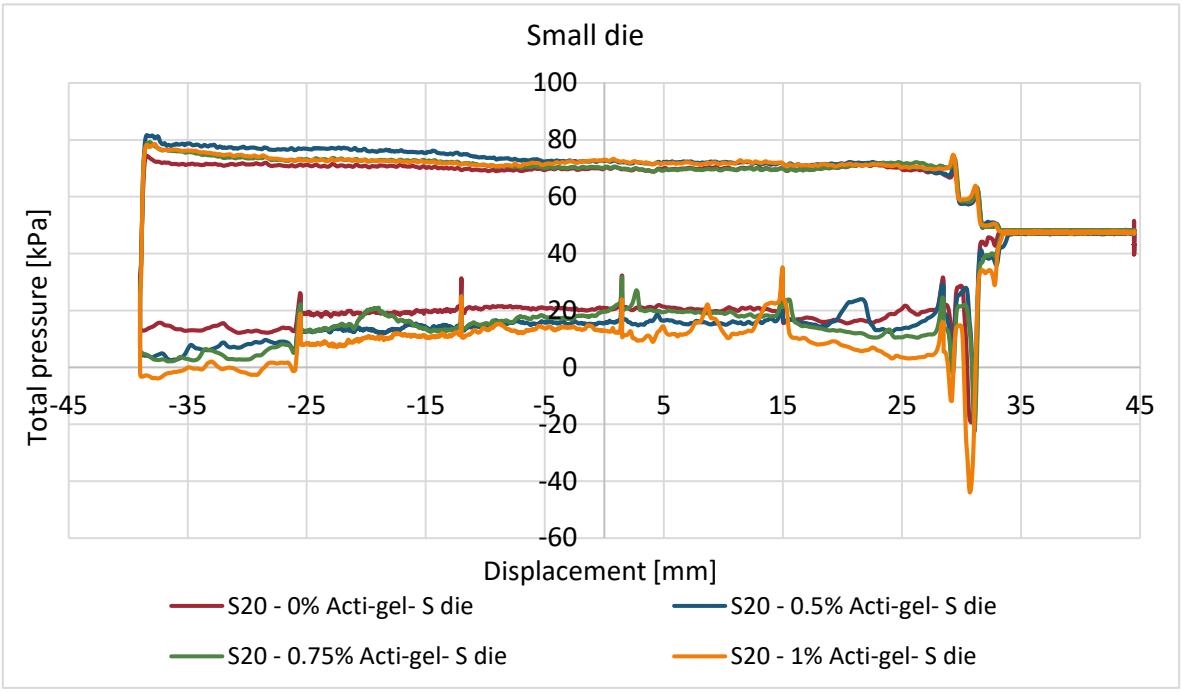

Fig. 5.17: S20 paste mixture with 0%, 0.5%, 0.75% and 1% of Acti-gel tested with small die on 0 min time interval

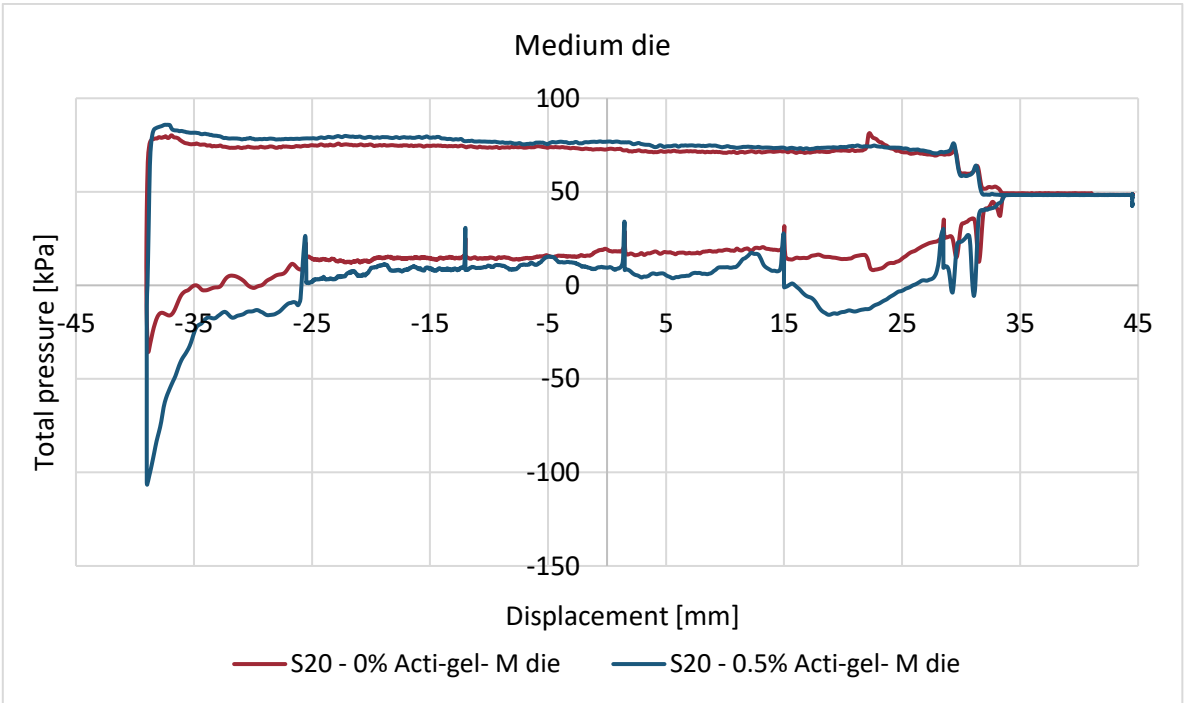

Fig. 5. 18: S20 paste mixture with 0%, 0.5%, 0.75% and 1% of Acti-gel tested with medium die on 0 min time interval

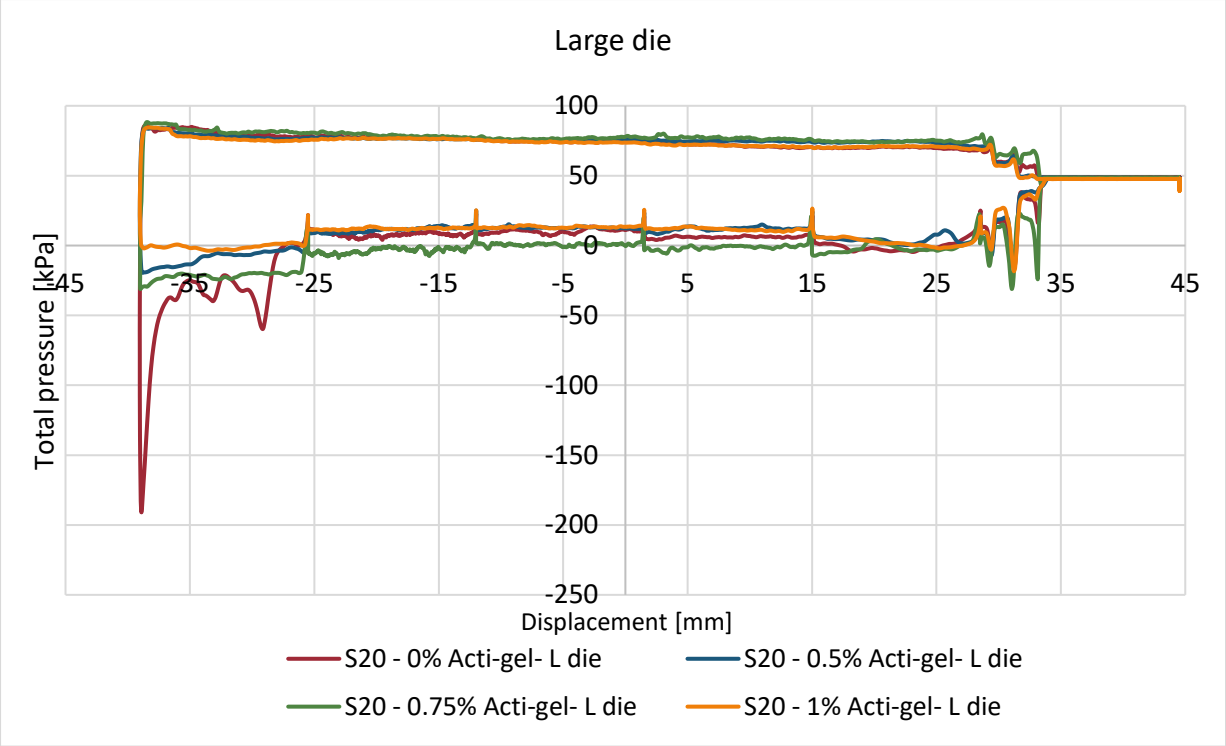

Fig. 5.19: S20 paste mixture with 0%, 0.5%, 0.75% and 1% of Acti-gel tested with large die on 0 min time interval

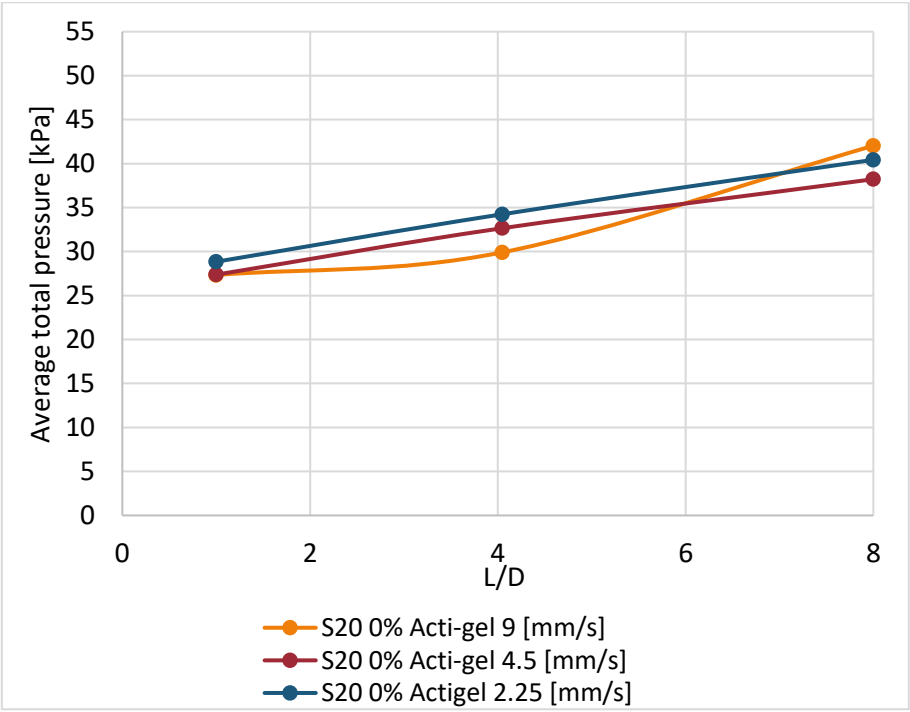

Fig. 5. 20: Average total pressure vs. L/D S20 paste mixture with 0% of Acti-gel

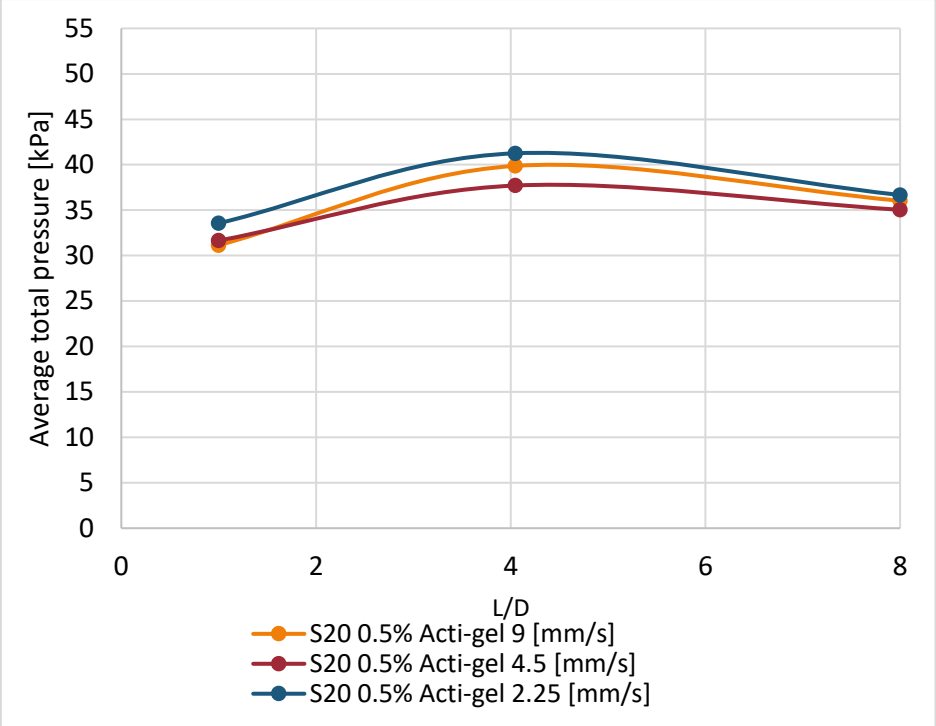

Fig. 5.21: Average total pressure vs. L/D S20 paste mixture with 0.5% of Acti-gel

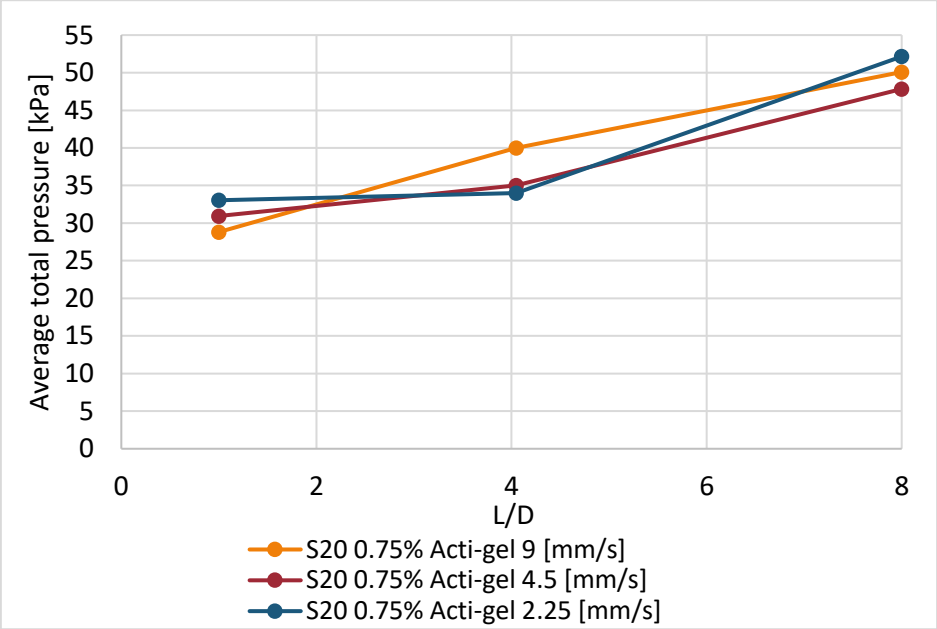

Fig. 5.22: Average total pressure vs. L/D S20 paste mixture with 0.75% of Acti-gel

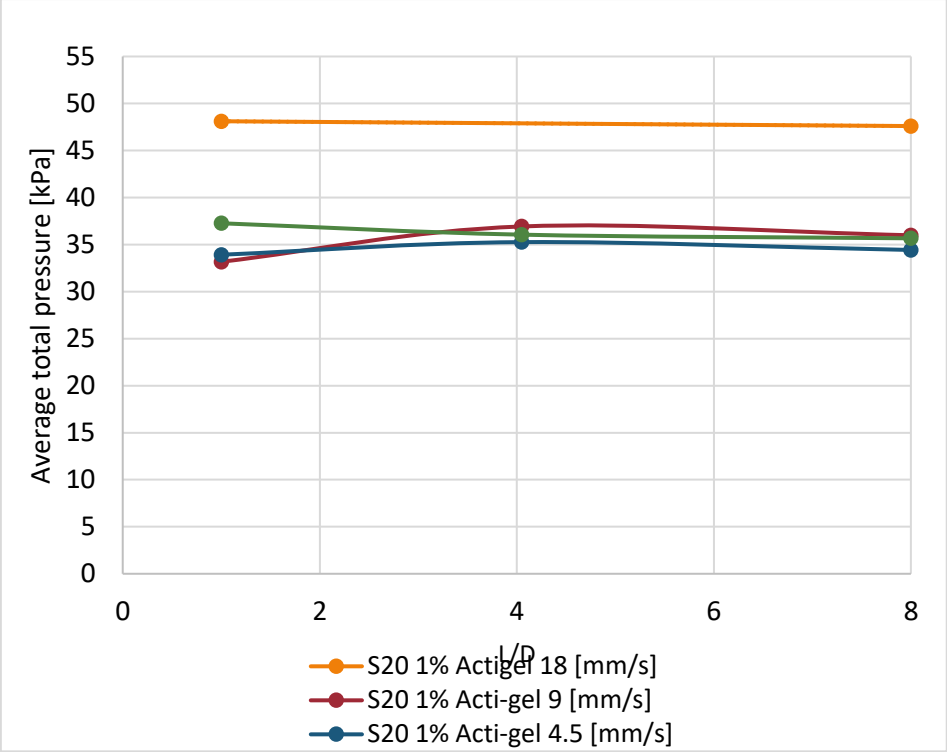

Fig. 5. 23: Average total pressure vs. L/D S20 paste mixture with 1% of Acti-gel

5.3 3D PRINTING OF A PASTE MIXTURES

5.3.1 Introduction

Mixture 1, 3, 4 and 5 in Table 5.1 were further examined on extrudability and buildability in a small 3D printer, as shown in Figure 5.24. Due to the fact that there is no Eurocode for 3D printing materials, it is necessary to create and adopt a special protocol for the process of examining the paste mixtures to be used in 3D printing process and for each specific 3D printer. The 3D printer which has been used in this work is specialized for laboratory applications. The technical specification of this 3D printer is stated in Table 5.3. Moreover, the nozzle of this printer can only be adjusted manually in the vertical direction and the platform in the horizontal direction.

To choose the best S20 paste mixture for 3D printing purpose on the bases of buildability and extrudability, the four mixtures were tested in the fresh state on 4 layers structure using the above-mentioned 3D printer. From these tests, one mixture was chosen to be examined on open time and 28 days tensile bonding strength of two layers.

a Nozzle
b Material container
c Platform
d Screwblade

Fig. 5. 24: 3D printer

Table 5. 3: Specifications of concrete pastes 3D printer

Maximum speed	Minimum speed	Nozzle size	Maximum sample size
1.6 cm/s	> 0 cm/s	Ø18 mm Length (L) =28 mm	250mm* 70mm

5.3.2 4 layers buildability of S20 paste mixtures

The S20 paste mixtures with 0%, 0.5%, 0.75% and 1% of Acti-gel, with respect to the total binder weight, are examined on 4 layers buildability with time interval of 2 minutes between each layer. The l/b- ratio could be lowered to 0.315 for a good flowability to fulfill the technical requirements of the used 3D printer. The layers have a total length of 20 cm. One of the properties of Acti-gel is that it provides the mixtures with shape stability and more creamy texture. The 4 layers were evaluated on the bases of the layer/Filament width and total height.

The reason for such test is to choose one of these four mixtures to be examined further on open time test and 28 days tensile bonding strength between two filaments.

It has been noticed that the buildability is noticeably improved when the percentage of Acti-gel becomes higher, see Tables 5.4 to Table 5.7 and Figure 5.25 to Figure 5.28.

The lower specific layer showed a support to the layers above in the fresh state. However, when comparing 0.75% and 1% of Acti-gel, more than 0.75% of Acti-gel showed no improvement to the buildability during the extruding process. Furthermore, due to the fact that the Acti-gel has surface water adsorption, the width of the layers started to decrease. A comparison between the different cases of tests, shown in Tables 5.4 to Table 5.7, with respect to the filament width and total height, it is quite clear that the increase of Acti-gel

has positive impact on the filament width as well as the height development. This positive impact was valid until the percentage of Acti-gel reached the value of 1%.
This leads to choose 0.75% Acti-gel to be the optimal percentage for maximum buildability and extrudability of the S20 paste mixture because the width of the filaments persists the value of 5.5 cm and no real change in the average total height of the 4 layers, see Table 5.6. This can be considered to be another evidence to reflect the stable buildability and extrudability.
The S20 paste mixture is composed of 80% 4M NaOH, 20% Na_2SiO_3 alkaline solutions and l/b ratio of 0.315.

Table 5. 4: S20 paste mixture with 0% Acti-gel

0% Acti-gel			
Time [min]	**Filament width [cm]**	**Filament Length [cm]**	**Average height of 4 layers [cm]**
7	5.3	20	3.3
9	3	20	
11	3	20	
13	2.5	20	

Fig. 5. 25: 4 layers of S20 paste mixture with 0% Acti-gel

Table 5. 5: S20 paste mixture with 0.5% Acti-gel

0.5% Acti-gel			
Time [min]	**Filament width [cm]**	**Filament Length [cm]**	**Average height of 4 layers [cm]**
7	5.5	20	4.5
9	4.5	20	
11	3.75	20	
13	2.9	20	

Fig. 5. 26: 4 layers of S20 paste mixture with 0.5% Acti-gel

Table 5. 6: S20 paste mixture with 0.75% Acti-gel

0.75% Acti-gel			
Time [min]	**Filament width [cm]**	**Filament Length [cm]**	**Average height of 4 layers [cm]**
7	5.5	20	4.7
9	5.5	20	
11	5.5	20	
13	5.5	20	

Fig. 5. 27: 4 layers of S20 paste mixture with 0.75% Acti-gel

Table 5. 7: S20 paste mixture with 1% Acti-gel

1% Acti-gel			
Time [min]	**Filament width [cm]**	**Filament Length [cm]**	**Average height of 4 layers [cm]**
7	5.5	20	4.7
9	4.5	20	
11	4	20	
13	3.5	20	

Fig. 5. 28: 4 layers of S20 paste mixture with 1% Acti-gel

5.3.3 Open time test of chosen S20 mixture

The open time is identified as the time interval required for the mixture to maintain its good printability. Once disruption occurs during the extrusion process, open time is assumed to be ended. The chosen S20 paste mixture with 0.75% of Acti-gel and l/b-ratio of 0.315 was tested on open time. The test was performed every 5 minutes and the results are shown in Table 5.8 and in Figures 5.29 to Figure 5.30. The distance of the nozzle was 1 cm with plate speed of 1.6 cm/s. The preparation of the mixture till the extruding process took 8 minutes of time. The results show that the width of the filaments is changing every 5 minutes with 0.5 cm. The open time was examined till the mixture could not be extruded anymore on 43 minutes after mixing. The disruption of the filament started 33 minutes after mixing, which means the open time for good printability has ended.
Based on the setting time of the S20 paste mixture of 85 minutes (Table 4.5) and the open

time test; the 85 minutes setting time reflects the hardening of the casted mixture, whereas the open time test reflects the workability and extrudability for this specific 3D printer.

Table 5. 8: Open time test results of S20 paste mixture with 0.75% Acti-gel and l/b-ratio of 0.315

Time [min]	Filament width [cm]	Filament Length [cm]
0	5	20
5	4	20
10	3.5	20
15	3	20
20	2.5	20
25	2	20
30	1	20
35	0	20
Total open time		**33 minutes**

Fig. 5. 29: S20 paste mixture with 0.75% Acti-gel and l/b-ratio of 0.315

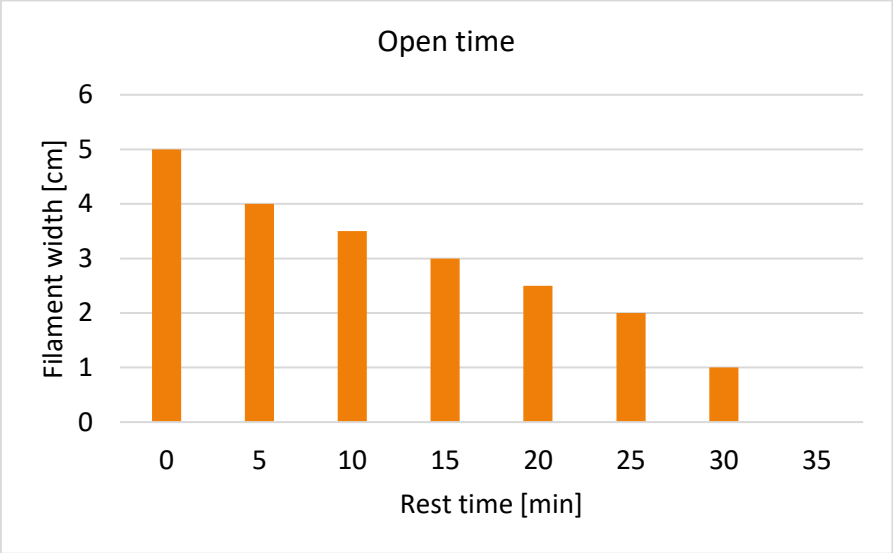

Fig. 5. 30: Filament width of S20 paste mixture with 0.75% Acti-gel and l/b-ratio of 0.315

5.3.4 Tensile bonding strength test for the S20 paste mixture

The tensile bonding strength of two layers of S20 paste mixture was examined on 28 days of cured specimens with specimens' dimension of 7mm * 35 mm. The test was performed on 10 minutes time gap between the two filaments/ layers. From Figure 5.31 it can be seen that the crack did not start at the adhesion location of the two layers. All the tested samples cracked near the glue. This might be due to the fact that the sticky nature of the geopolymer paste provides a good adhesion between the two layers. It is important to note that one of the properties of the Acti-gel is that it provides a superior cohesion of the mixtures. This can also influence the adhesion between the layers. Another reason is that the glue heats up the specimens, which causes extra tensile stresses at the glue location, see Figure 5.32. The specimen cracks at the weakest spot, which can be seen in Figure 5.31. However, the average tensile strength of three tested specimens cured for 28 days displayed a strength of 1.32 MPa, see Figure 5.33.

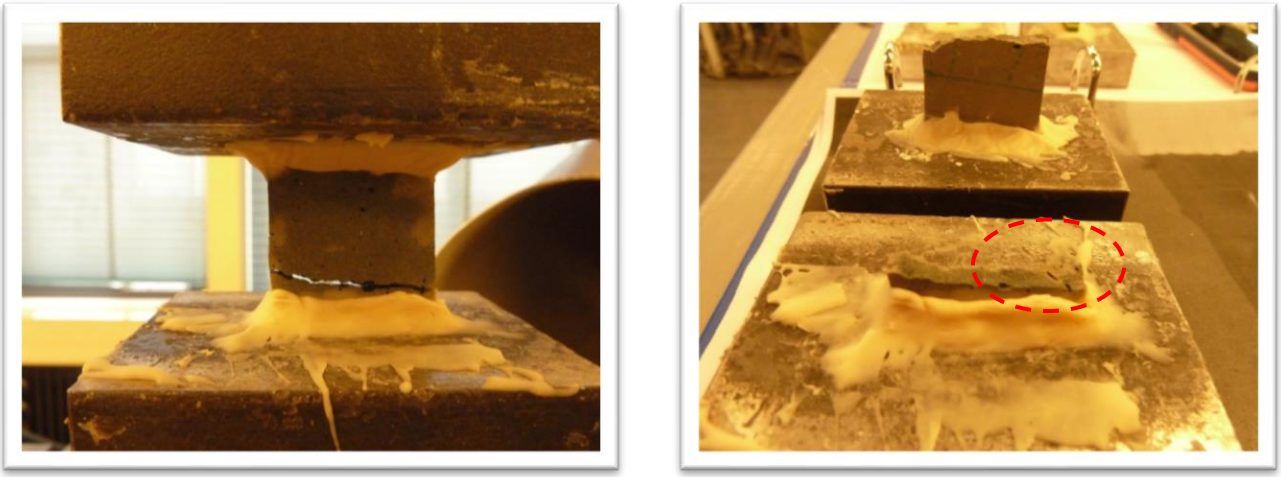

Fig. 5. 31: Tensile bond strength of two layers with a time gap of 10 minutes

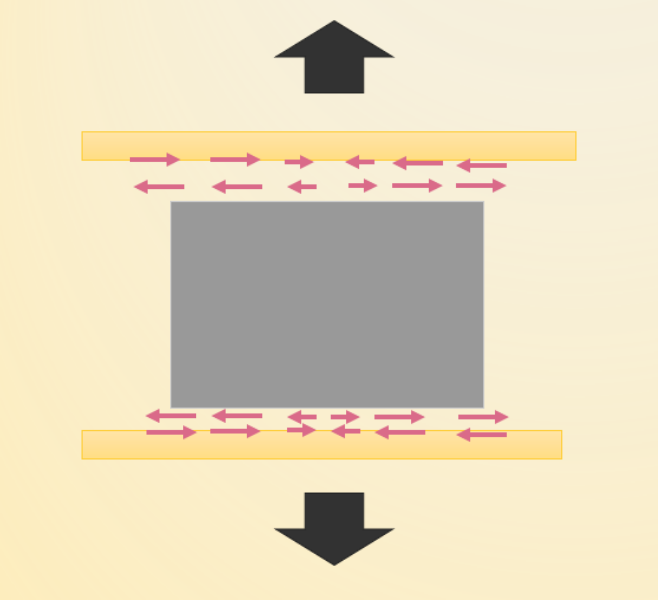

Fig. 5. 32: Tensile stresses on the tested specimens (7mm 35 mm)*

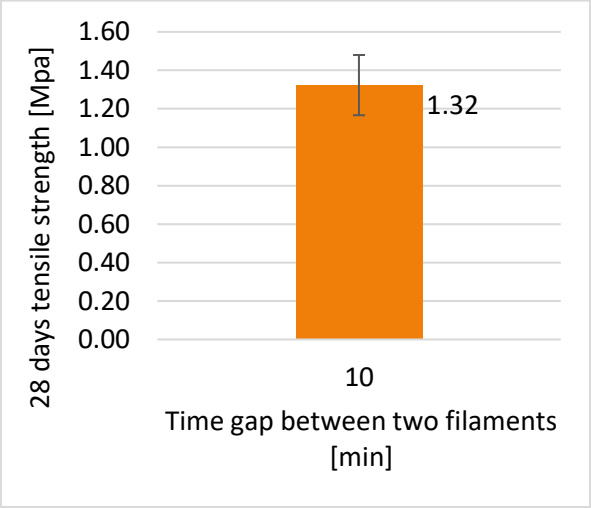

Fig. 5. 33: Tensile bonding strength test of 28 days cured specimens (7mm 35mm) with a 10 minutes time gap between the two layers*

5.4 Concluding remarks

For the selected paste mixtures S20, a rheometer tests were carried out. The obtained results from these tests show, for similar value of shear rate, that the values of the shear stress increase linearly with time. It has also been noticed that for each specific time interval, the mixtures exhibited a shear thinning behavior. As it is illustrated in Figure 5.4 to Figure 5.9, the shear yield stress is quite small. This means that this material requires very slight stress to make it flowable, which inflicts its applicability in the extruding process for the purpose of 3D printing.

Results from another rheological test on the S20 paste mixtures, the ram extruder, showed an increase in the extruding pressure between time intervals of 5 to 7 minutes. Increasing the die length of the ram extruder results in accumulative increase in the pressure during the extruding process of the mixtures. However, the added Acti-gel improved the stability of the flow conditions, with an increase in piston pressure, which in turn enhanced the pumpability and workability. This gives a positive advantage for using the Acti-gel to enhance the rheological properties of the mixtures for the purpose of 3D printing.

The S20 paste mixtures with 0%, 0.5%, 0.75% and 1% of Acti-gel, with respect to the total binder weight, are examined on 4 layers buildability with time interval of 2 minutes between each layer by using a specific 3D printer.
The buildability of the 4 layers is improved with 0.75% percentage of added Acti-gel and the width of the layers persists the value of 5.5 cm with no real change in the average total height of the 4 layers structure. This can be considered to be another evidence to reflect the stable buildability and extrudability.

The open time test can be considered as another factor to evaluate the workability and extrudability of the mixture for a specific 3D printer. The S20 mixture with 0.75% added Acti-gel and l/b-ratio of 0.315 showed a disruption of the extruded filament after 33 minutes during the open time test. This open time were achieved without adding any additives to the mixture. Comparing the results of the plastic viscosity to the open time test, the extrudability of the mixture is not anymore valid beyond 8.8 Pa.s plastic viscosity. This short open time of 33 minutes for such geopolymer mixture design needs a fast-performing 3D printer. This might help in achieving construction projects within short time.

A tensile bonding strength of two layers of S20 paste mixture was examined on 28 days of cured specimens. This test shows 1.32 MPa of tensile strength and a good adhesion between the two layers. This might be due to the sticky nature of the geopolymer mixture and/ or the positive influence of the Acti-gel which gives a superior cohesion to the used mixture in the 3D printer.

Chapter 6

6 Conclusions

One of the main objectives of this work is to find out the feasibility of using two kinds of byproducts (BFS and FA), as a construction materials, in the field of 3D printing. The aim was to find a paste mixture design that can be optimized for this purpose. Experiments were carried out to study the influence of the binders and alkaline solutions (NaOH and Na_2SiO_3) ratios on the early age mechanical strength development and the setting time. Six mixtures were tested by adjusting the ratio between the FA and BFS and keeping all the other parameters constant. The addition of a higher percentage of BFS of the total binder amount linearly increased the compressive strength of the tested specimens. However, the setting time decreased exponentially as more BFS was added to the total binder amount.

For this work and based on the specifications of the 3D printer, the rheological properties, setting time and mechanical strength development were adjusted to be more applicable for 3D printing. This has been achieved by changing the ratio of the alkaline solutions of the paste mixtures.
Among the different selected paste mixtures, the S20 (80% FA and 20% BFS) was chosen for further optimization to be tested on rheological properties (ram extruder test) that requires an initial setting time of 90 minutes. The selected alkaline solution ratios (Na_2SiO_3/NaOH) were 0, 0.25, 0.43, 1, 2.33 and 4. The 90 minutes setting time was achieved with (Na_2SiO_3/NaOH) and (SiO_2/Na_2O) ratios of 0.25 and 0.82. The compressive strength of 5MPa of this mixture was obtained after 3 days of curing the specimens.

This mixture was further investigated on rheological properties with a plate rheometer and a ram extruder by adding 0%, 0.5%, 0.75% and 1% of Acti-gel with respect to the total binder amount.
The obtained results from the rheometer show, for similar value of shear rate, that the values of the shear stress increase linearly with time. However, the shear yield stress is quite small. This means that this material requires very slight stress to make it flowable. This has a direct relation to the added Acti-gel which lowers the shear stress when a load is applied to the mixture. The effect of the Acti-gel was noticeable even for addition of small quantities. This would inflict its applicability in the extruding process for the purpose of 3D printing.

Results from another rheological test on the S20 paste mixtures, the ram extruder, showed an increase in the extruding pressure between time intervals of 5 to 7 minutes. Increasing the die length of the ram extruder results in accumulative increase in the pressure during the extruding process of the mixtures. However, the added Acti-gel improved the stability of the flow conditions, with an increase in piston pressure, which in turn enhanced the pumpability and workability. This gives a positive advantage for using the Acti-gel to enhance the rheological properties of the mixtures for the purpose of 3D printing.

The S20 paste mixtures with 0%, 0.5%, 0.75% and 1% of Acti-gel was tested on fresh state 4 layers buildability with a time interval of 2 minutes between each layer. For these mixtures, the lowest l/b-ratio was obtained for good extrudability has a value of 0.315. Based on the results, the Acti-gel improved the buildability especially by the addition of 0.75% Acti-gel. This mixture had no noticeable changes in the width of the subsequent layers. This can be considered to be another evidence to reflect the stable buildability and extrudability by adding Acti-gel to the mixture.

The open time test was carried out on the S20 mixture with 0.75% Acti-gel. This test showed a disruption of the extruded filaments after 33 minutes. This open time were achieved without adding any additives to the mixture. Comparing the results of the plastic viscosity to the open time test, the extrudability of the mixture is not anymore valid beyond 8.8 Pa.s plastic viscosity. This short open time of 33 minutes for such geopolymer mixture design needs a fast-performing 3D printer. This might help in achieving construction projects within short time.

A tensile bonding strength of two layers of S20 paste mixture was examined on 28 days of cured specimens. This test shows 1.32 MPa of tensile strength and a good adhesion between the two layers. This might be due to the sticky nature of the geopolymer mixture and/ or the positive influence of the Acti-gel which gives a superior cohesion to the used mixture in the 3D printer.

Chapter 7

7 Recommendations

The 3D printing in the field of construction is still in its innovative stages. The obtained results from this project gave better insight on some important aspects with respect to 3D printing. Therefore, few recommendations might in light researchers in this field to improve future research projects:

- Two types of extrusion 3D printers (for pastes and mortars) are recommended to test the buildability, extrudability (flowability) and open time of the mixtures.
- The printers need to have different nozzle diameter and different nozzle shapes to test the mixture designs.
- Depending on the mixture designs a plate rheometer and cylindrical rheometer is recommended to test at least 3 times the rheological properties of each mixture design.
- If the mixtures cannot be tested with the rheometer due to wall slip forming, ram extruder can be an alternative for testing the rheological properties of the mixture designs. However, it is important to mention that it requires allot of time compared to testing the mixtures with the rheometer.
- To test the tensile bonding strength of two layers, a new type of glue is necessary that does not produce exotherm heat release.
- Different type of additives to improve the buildability, setting time and open time of geopolymer mixture designs is required for future research.
- Addition of fibers to the paste mixture can help improve the strength development as well as the buildability of the geopolymer mixture designs.

Chapter 8

8 References

[1] Afvalstoffenstatistieken (2017)). Information found from:

http://ec.europa.eu/eurostat/statistics-explained/index.php/Waste_statistics/nl#Afvalstoffenstatistieken

[2] Olivier J.G.J, Schure K.M., Peters J.A.H.W. (2017), 'Trends in global CO_2 and total greenhouse gas emissions'. Information found from:
http://www.pbl.nl/sites/default/files/cms/publicaties/pbl-2017-trends-in-global-co2-and-total-greenhouse- gas-emissons-2017-report_2674.pdf

[3] Cement&BetonCentrum. Information found from:
http://www.cementenbeton.nl/marktinformatie/cementmarkt

[4] Okoye F.N. (2016),' Geopolymer Binder: A veritable alternative to Portland cement', *Materials today*, Department of Civil Engineering, Federal Polytechnic, Oko, Nigeria, Proceedings, vol.4, pp. 5599-5604.

[5] Komnitsasa A. (2011),' Potential Of Geopolymer Technology towards green buildings and sustainable cities', *International conference on Green buildings and Sustainable Cities*, Technical University Crete, Department of Mineral Resources Engineering, 73100 Chania, Greece.

[6] Egger S.,' Determining a sustainable city model', *Environmental Model Software*, vol.621, pp.1235-46.

[7] Pacheco-Torgal F., Labrincha J.A., Leonelli C., Palomo A., Chindaprasirt P. (2015), 'Handbook of Alkali-Activated cements, Mortars and Concretes', *Woodhead Publishing*.

[8] Aldin, Z., Nedeljković, M., Luković, M., Liu, J., Blom, K., & Ye, G. (2017), 'Optimization of a geopolymer mixture design for a reinforced cantilever concrete bench', *9th International Symposium on Cement and Concrete (ISCC)*.

[9] Thaarrini J., Dhivya S. (2016), 'Comparative Study on the Production Cost of Geopolymer and Conventional Concretes', *International Journal of Civil Engineering Research*, vol. 7, Number 2, pp.117-124.

[10] Muttashar M., Lokuge W., Karunasena W. (2014), 'Geopolymer Concrete: The Green alternative with suitable structural properties', *23rd Australasian conference on the mechanics of structures and materials (ACMSM23)*, Byron Bay, NSW, Southern Cross University, Lismore, NSW, vol. 1, pp. 101-106.

[11] McLellan B.C., Williams R.P., Lay J., Van Riessen, A. (2011), 'Costs and carbon emissions for geopolymer pastes in comparison to ordinary Portland cement', *Journal of Cleaner Production*, vol. 19, no. 9, pp. 1080-90.

[12] International Energy Agency (iea), Cement Technology Roadmap 2009, 'Carbon emissions reductions up to 2050'.Information found from:
https://www.iea.org/publications/freepublications/publication/Cement.pdf

[13] Joshi S., Kadu M. (2012), 'Role of Alkaline Activator in Development of Eco-friendly Fly Ash Based Geo Polymer Concrete', *International Journal of Environmental Science and Development*, vol. 3, no. 5, pp. 417-21.

[14] Subramanian N. (2007), 'Sustainability-Challenges and solutions', *Indian ConCreTe Journal*, vol. 81, no.12, pp.39-50.

[15] Guo X., Shi. Dick W.A. (2010), 'Compressive strength and microstructural characteristics of class C fly ash geopolymer', *Cement and Concrete Composites*, vol. 32, no. 2, pp. 142-7.

[16] Hardjito D., Wallah S.E., Sumajouw D.M., Rangan B.V. (2004), 'On the development of fly ash-based geopolymer concrete', *ACI Materials Journal-American Concrete Institute*, vol. 101, no. 6, pp. 467-72.

[17] Nasvi M., Gamage R.P. Jay S. (2012), 'Geopolymer as well cement and the variation of its mechanical behavior with curing temperature', *Greenhouse Gases: Science and Technology*, vol. 2, no. 1, pp. 46-58.

[18] Yost J.R., Radlińska A., Ernst S., Salera M. (2013), 'Structural behavior of alkali activated fly ash concrete. Part 1: mixture design, material properties and sample fabrication', *Materials and structures*, vol. 46, pp. 435–47.

[19] Kong D.L., Sanjayan J.G. (2008), 'Damage behavior of geopolymer composites exposed to elevated Temperatures', *Cement & Concrete Composites*, vol.30, pp.986–99.

[20] Kumar S., Kumar R., Mehrotra S. (2010), 'Influence of granulated blast furnace slag on the reaction, structure and properties of fly ash based geopolymer', *Journal of Materials Science*, vol. 45, no. 3, pp. 607-15.

[21] Li Z., Liu S. (2007), 'Influence of slag as additive on compressive strength of fly ash-based geopolymer', *Journal of Materials in Civil Engineering*, vol. 19, no. 6, pp. 470-4.

[22] Manjunath G., Giridhar C. (2011), 'Compressive Strength Development in Ambient Cured Geopolymer Mortar', *International Journal of Earth Sciences and Engineering*, vol. 4, no. 6, pp. 830- 4.

[23] Akhilesh P., Marepally V.R, Padmakanth P. (2012), 'Geopolymer concrete', Information found from: https://www.slideshare.net/akhileshpadiga/geo-polymer-concrete

[24] Mustafa Al Bakri Abdullah M., Kamarudin H., Binhussain M., Yahya Z. (2013),'Comparison of Geopolymer Fly Ash and Ordinary Portland Cement to the Strength of Concrete', *Journal of Computational and Theoretical Nanoscience*, vol. 19, no.12, pp.3592-3595.

[25] Olivia M, Nikraz H. (2012), 'Properties of fly ash geopolymer concrete designed by Taguchi method', *Materials & Design*, vol. 36, pp. 191-8.

[26] Bhikshma V., Koti R.M., Srinivas R., (2012), 'An experimental investigation on properties of geopolymer concrete (no cement concrete)', *Asian Journal of Civil Engineering (Building and Housing)*, vol. 13, no. 6, pp. 841-53.

[27] Hardjito D., Wallah S.E., Sumajouw D.M., Rangan B.V. (2005), 'Fly ash-based geopolymer concrete', *Australian Journal of Structural Engineering*, vol. 6, no. 1, pp. 77-84.

[28] Mane S., Jadhav H. (2012), 'Investigation of Geopolymer mortar and concrete under high temperature', *International Journal of Emerging Technology and Advanced Engineering*, vol. 2, no. 12, pp. 384-90.

[29] Kong D.L., Sanjayan J.G. (2010), 'Effect of elevated temperatures on geopolymer paste, mortar and concrete', *Cement and concrete research*, vol. 40, no. 2, pp. 334-9.

[30] Guerrieri M., Sanjayan J.G. (2010), 'Behavior of combined fly ash/slag-based geopolymers when exposed to high temperatures', *Fire and Materials*, vol. 34, no. 4, pp. 163-75.

[31] Zhao R., Sanjayan J. (2011), 'Geopolymer and Portland cement concretes in simulated fire', *Magazine of Concrete Research*, vol. 63, no. 3, pp. 163-73

[32] Nath P., Sarker P.K. (2017), 'Flexural strength and elastic modulus of ambient- cured blended low calcium fly ash geopolymer concrete', *Construction and Building materials*, vol. 130, pp.22-31.

[33] Wallah S. (2010), 'Creep behavior of fly ash-based geopolymer concrete', *Civil Engineering Dimension*, vol. 12, no. 2, pp. 73-8.

[34] Shaikh A.U.A., Afshang A., 'Corrosion Durability of Geopolymer Concretes Containing Different Concentrations of Alkaline Solution', Curtin University, Perth, Australia. Information found from: http://hosted.arinex.com.au/abstracts/cia2013/pdf/411310015Final00053.pdf

[35] Olivia M., Nikraz H.R. (2011), 'Corrosion performance of embedded steel in Fly Ash Geopolymer concrete by impressed voltage method', Incorporating Sustainable Practice in Mechanics of Structures and Materials, pp.781-786.

[36] Mathew B.J., Sudhakar M., Natarajan C. (2013),'Strength, Economic and Sustainable Characteristics of Coal Ash- GGBS Based Geopolymer Concrete', International Journal of Computational Engineering Research, vol 3, Issue.1.

[37] Arbi K. Nedeljkovic M., Zou Y., Ye G. (2016), 'A review on the Durability of Alkali-Activated Fly Ash/ Slag Systems: Advances, Issues, and Perspectives', Industrial & Engineering Chemistry research (I&EC research).

[38] Provis J. L., Bernal S. A. (2014),' Geopolymers and Related Alkali Activated Material', Annu. Rev. Mater. Res., vol. 44, p. 299.

[39] Provis J. L., van Deventer J. S. J, (2014) 'Alkali Activated Materials', State of-the-Art Report, *RILEM week* TC 224- AAM; Springer: Dordrecht, the Netherlands.

[40] Scrivener K. L., Kirkpatrick R. J. (2008), 'Innovation in use and research on cementitious material', Cement Concrete Research. Vol. 38, p.128.

[41] Turner L.K., Collins F.G. (2013),'Carbon dioxide equivalent (CO_2-e) emissions: A comparison between geopolymer and OPC cement concrete', *Construction and Building materials*, vol.43, pp. 125-130.

[42] Wu B., Wu D., 'Test study on hydration temperature of compound concrete made of demolished concrete lumps and fresh concrete', *6th International workshop on performance, protection & strengthening of structures under extreme loading*, *PROTECT2017*, Guangzhou (Canton), China, Procedia Engineering, vol. 210, pp. 120-125.

[43] Geopolymer Institute (2017), 'Why Alkali-Activated Materials are NOT Geopolymers?'.

Information found from:
https://www.geopolymer.org/faq/alkali-activated-materials-geopolymers].

[44] Shi C., Fernandez-Jimenez A., Palomo A. (2011),' New cements for the 21st century: the pursuit of an alternative to Portland cement', Cement and Concrete Research, vol.41, pp. 750-763.

[45] Pacheco-Torgal F., Labrincha J.A., Leonelli C., Palomo A., Chindaprasirt P. (2015), 'Introduction to handbook of alkali-activated cements, mortars and concretes', *Woodhead Publishing*, p.49-73.

[46] Nedeljkovi M., Lukovic M., van Breugel K., Hordijk D., Ye G. (2018), 'Development and application of an environmentally friendly ductile alkali-activated composite', *Journal of Cleaner Production*, vol.180, p.524-538.

[47] Information found from:
https://en.wikipedia.org/wiki/Coke_(fuel)#/media/File:Koks_Brennstoff.jpg

[48] Tata steel, raw materials. Picture found from:
https://www.tatasteeleurope.com/en/services/specialist/tata-steel-consulting/raw-materials

[49] Indiamart, Picture found from:
https://www.indiamart.com/paras-metallurgical/foundry-flux-raw-material.html

[50] Provis J.L, van Deventer J.S.J. (2009), 'Geopolymers: Structures, Processing, Properties and Applications, Ed. Woodhead Publishing, 1st edition, University of Melbourne, Australia.

[51] Wan H., Shui Z., Lin Z. (2004), 'Analysis of geometric characteristics of GGBS particles and their influences on cement properties', *Cement and Concrete Research*, vol. 34, Issue 1, p. 133-137.

[52] Khan S.U., Nurudin M.F., Ayub T., Shafiq N. (2014),'Effects of different mineral admixtures on the properties of fresh concrete', *The Science World Journal*, vol. 4.

[53] Information found from:
https://en.wikipedia.org/wiki/Fly_ash

[54] Information found from:
http://www.monolithic.org/blogs/construction/fly-ash-properties-and-uses

[55] Trindade A.C.C., de Andrade Silva F., Alcamand H.A., Borges P.H.R., 'On the Mechanical Behavior of Metakoalin Based Geopolymers Under Elevated Temperatures', *materials research*, vol.20, Sao Carlos, ISSN 1980-5373.

[56] Garcia-Lodeira I., Palomo A., Fernandez-Jimenez A., '2-An overview of the chemistry of alkali-activated cement- based binders', *Handbook of Alkali-Activated cements*, Mortars and Concretes, pp.19-47.

[57] Palomo A., Grutzeck M.W., Blanco M.T. (1999), 'Alkali-activated fly ashes—a cement for the future', Cement and Concrete Research, vol.29, pp.1323–1329.

[58] Duxon P., Fernández-Jiménez A., Provis J.L., Lukey G.C., Palomo A., van Deventer J.S.J. (2007), 'Geopolymer technology: the current state of the art', Journal of Material Science, vol. 42, pp. 2917–2933.

[59] Khale D., Chaudhary R. (2007), 'Mechanism of geopolymerization and factors influencing its development: a review', *Journal of Material Science*, vol. 42, pp.729–746.

[60] Richardson I.G., 'Tobermorite/Jennite- and tobermorite/calcium hydroxide- based models for the structure of C-S-H: applicability to hardened pastes of tricalcium silicate, β-dicalcium silicate, Portland cement, and blends of Portland cement with blast furnace slag, metakaolin, or silica fume', Cement and Concrete Research, vol.34, Issue 9, pp.1733-1777.

[61] Palomo A., Krivenko P., Garcia-Lodeiro I., Kavalerova E., Maltsev O., Fernández-Jiménez A.,' A review on alkaline activation: new analytical perspectives', vol.64, no.315.

Information found from:
http://materconstrucc.revistas.csic.es/index.php/materconstrucc/article/viewArticle/1492/1762

[62] Glukhovsky V., (1994), 'Ancient, modern and future concretes', First International Conference Alkaline Cements and Concretes, Kiev, Ukraine, vol.1, pp. 1-8.

[63] The Editors of Encyclopaedia Britannica .Information found from:
https://www.britannica.com/science/water-glass

[64] Palomo A., Fernández-Jimenez A., Kovalchuck G. (2005), 'Some key factors affecting the alkali activation of fly ash', 2nd International Symposium of Non-Traditional Cement and Concrete, Brno, Czech Republic.

[65] Provis J. L., Bernal S. A. (2014),'Binder Chemistry – Blended Systems and Intermediate Ca Content', In J. L. Provis & J. S. J. van Deventer (Eds.), Alkali Activated Materials: State-of-the-Art Report, RILEM TC 224-AAM, Dordrecht: Springer Netherlands, pp. 125-144.

[66] Garcia-Lodeiro I., Palomo A., Fernández-Jiménez A., Macphee D.E. (2011),'Compatibility studies between N-A-S-H and C-A-S-H gels: study in the ternary diagram Na2O-CaO-Al2O3-SiO2-H2O', *Cement and Concrete Research*, vol.41,pp. 923-931.

[67] Presentation of Bijani A.,'Sustainable Design Graduation Studio –P5'.

[68] Ma G., Li Z., Wanga Li. (2018), 'Printable properties of cementitious material containing copper tailings for extrusion-based 3D printing', Construction and Building Materials, vol. 162, pp.613–627.

[69] Winsun, WinSun China builds world's first 3D printed villa and tallest 3D printed apartment building, Information found from:
http://www.3ders.org/articles/20150118-winsun-builds-world-first-3d-printed-villa-and-tallest-3d-printed-buildingin-china.html (2015).

[70] WASP, the first adobe building. Information found from:
http://www.wasproject.it/w/en/3d-printersprojects/(2016).

[71] Information found from:
https://www.cemexventures.com/2017/12/14/benefits-of-3d-printing-in-construction/

[72] Information found from:
https://blog.inkjetwholesale.com.au/3d-printing/disadvantages-3d-printing/

[73] Rubio M, Sonebi M, Amziane S, (2017),'Fresh and rheological properties of 3D printing bio-cement-based materials', *2nd International Conference on Bio-Based Building Materials*, Rilem, vol. 119, Clermont Ferrand, France.

[74] Nedeljkovic M., Arbi K., Zuo Y., Ye G. (2016),'Microstructural and mineralogical analysis of alkali activated fly-ash- slag pastes', *3rd International Conferences on Microstructure Related Durability of Cementitious Composites:* Nanjing, *China, RILEM publications* S.A.R.L, pp.1-10.

[75] Paul S.C., Tay Y.W.D., Panda B., Tan M.J. (2017), 'Fresh and hardened properties of 3D printable cementitious materials for building and construction', Archives of civil and mechanical engineering, vol.18, pp.311-319.

[76] Zhou X., Li Z. (2005), 'Characterization of rheology of fresh fiber reinforced cementitious composites through ram extrusion', *Materials and Structures, vol.38, pp.17-24.*

[77] Pacheco-Torgal F., Labrincha J.A., Leonelli C., Palomo A., Chindaprasirt P. (2015), 'Introduction to handbook of alkali-activated cements, mortars and concretes', *Woodhead Publishing*, p. 23

[78] Ma Y., (report 2013), 'Microstructure and Engineering properties if Alkali Activated Fly Ash', TU Delft.

Chapter 9

Appendix A: BFS Particle size distribution (PSD)

Donner Technologies — **DIPA-2000**

Particle Size & Concentration Analysis: Laser Channel

Customer:

Setup created by:	user	Setup Date:	Nov 08 2016 11:18AM (GMT+2)
Measured by:	user	Measure Date:	May 04 2018 17:16PM (GMT+2)
Printed by:	user	Print Date:	May 04 2018 18:13PM (GMT+2)
System Model:	DIPA-2000 S/N:60298	SW Version:	2.3.4.0

Sample Name:	**BFS_zainab-1(SUM)**	Result ID#:	**6451**
Sample Type:	HAO	Setup Name:	dry powder (v127)
Server Name:	TUD10531		

Comments:

Laser lens:	A100	Video lens:	CWx20
Meas. Range:	0.1 - 200.0	Stirrer:	None
Meas. Time:	540 Sec.	Status:	Standard
Cell Type:	DCM-104A Liquid flow (10x10mm)	Accessories:	LFC-101
Calibration mode:	Not Active	Particles existence:	Active. Stabilization time (10 sec.)
Illumination:	Exposure: 2, Intensity: 16	Image control:	Gain:97, Contrast:230, Brightness:187
Cleaning Test:	Not Active		

Meas. Mode: AND:Time(180 Sec.),Conf. (95, 10 Sec., Volume) Completed

Preparation instructions: Add the sample to the LFC-101 container.

Statistics Info (ID#:6451)

Concentration:	2.3e+005 #/ml	Concentration:	9.0e+000 ppm
Solids:	4.52e-004	Specific Area:	3.2e-005 cm2/ml

Mean diameter by:	Size(um)	STD(um)	Conf.(%)	Dimension	D10(um)	D50(um)	D90(um)	Mode(um)
Length, D[1,0]	1.48	1.54	100.00	Number	0.59	1.17	2.64	0.59
Length weighted, D[2,1]	3.08	4.13	100.00	Length	0.73	1.61	6.30	1.32
Surface, D[2,0]	2.13							
Surface Weighted, D[3,2]	8.61	8.47	100.00	Surface	1.32	4.83	22.41	1.46
Volume, D[3,0]	3.39							
Volume Weighted, D[4,3]	16.94	9.75	100.00	Volume	3.81	16.84	29.87	18.16

Volume Percentage Table (ID#:6451) (Status: Full scale)

Under(%)	Size	Under(%)	Size	Under(%)	Size	Under(%)	Size
0.00	0.15	30.00	10.54	55.00	18.16	80.00	26.07
5.00	2.64	35.00	12.15	60.00	19.92	85.00	27.97
10.00	3.81	40.00	13.77	65.00	21.09	90.00	29.87
15.00	5.13	45.00	15.38	70.00	22.84	95.00	32.51
20.00	6.74	50.00	16.84	75.00	24.46	100.00	41.00
25.00	8.64						

Volume Histogram and Cumulative Undersize (ID#:6451) (Full scale)

Mean: 16.94 um STD: 9.75 um Conf.: 100.00 %

Volume Histogram and Cumulative Undersize (ID#:6451) (Full scale)
D10 : 3.81 um D50: 16.84 um D90: 29.87 um

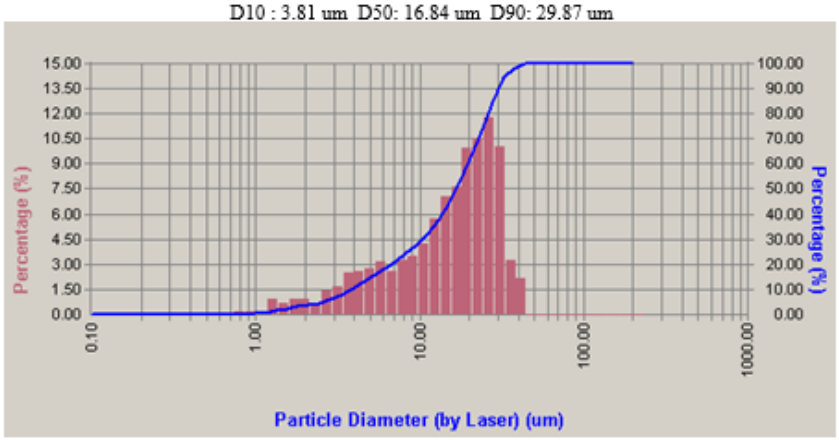

Number Percentage Table (ID#:6451) (Status: Full scale)

Under(%)	Size	Under(%)	Size	Under(%)	Size	Under(%)	Size
0.00	0.00	30.00	0.73	60.00	1.32	90.00	2.64
10.00	0.59	40.00	0.88	70.00	1.46	100.00	41.00
20.00	0.73	50.00	1.17	80.00	1.76		

Number Histogram and Cumulative Undersize (ID#:6451) (Full scale)
Mean: 1.48 um STD: 1.54 um Conf.: 100.00 %
D10 : 0.59 um D50: 1.17 um D90: 2.64 um

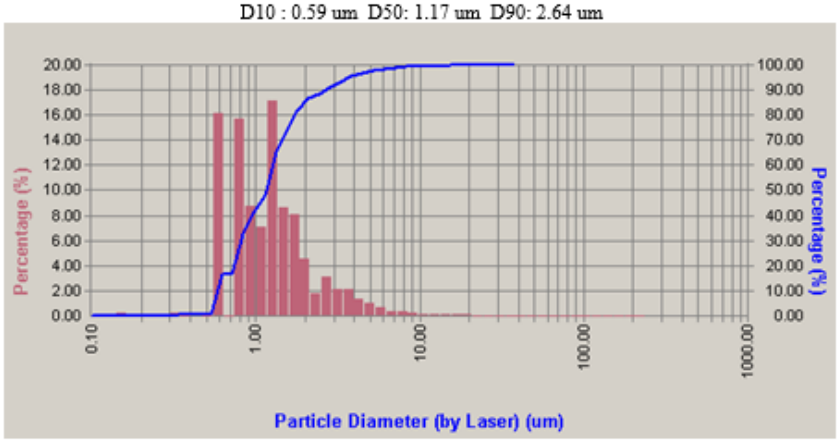

Appendix B: FA Particle size distribution (PSD)

Donner Technologies — **DIPA-2000**

Particle Size & Concentration Analysis: Laser Channel

Customer:

Setup created by:	user	Setup Date:	Nov 08 2016 11:18AM (GMT+2)
Measured by:	user	Measure Date:	Apr 27 2018 11:44AM (GMT+2)
Printed by:	user	Print Date:	Apr 27 2018 11:47AM (GMT+2)
System Model:	DIPA-2000 S/N:60298	SW Version:	2.3.4.0

Sample Name:	**fly ash ordered by marija(SUM)**	Result ID#:	**6426**
Sample Type:	HAO	Setup Name:	dry powder (v127)
Server Name:	TUD10531		

Comments:

Laser lens:	A100	Video lens:	CWx20
Meas. Range:	0.1 - 200.0	Stirrer:	None
Meas. Time:	540 Sec.	Status:	Standard
Cell Type:	DCM-104A Liquid flow (10x10mm)	Accessories:	LFC-101
Calibration mode:	Not Active	Particles existence:	Active. Stabilization time (10 sec.)
Illumination:	Exposure: 2, Intensity: 16	Image control:	Gain:97, Contrast:230, Brightness:187
Cleaning Test:	Not Active		

Meas. Mode: AND:Time(180 Sec.),Conf. (95, 10 Sec., Volume) Completed

Preparation instructions: Add the sample to the LFC-101 container.

Statistics Info (ID#:6426)

Concentration:	2.1e+005 #/ml	Concentration:	6.4e+001 ppm
Solids:	3.19e-003	Specific Area:	8.4e-005 cm2/ml

Mean diameter by:	Size(um)	STD(um)	Conf.(%)	Dimension	D10(um)	D50(um)	D90(um)	Mode(um)
Length, D[1,0]	2.25	3.11	100.00	Number	0.58	1.45	4.64	0.72
Length weighted, D[2,1]	6.54	10.88	100.00	Length	1.01	3.62	13.48	1.30
Surface, D[2,0]	3.84							
Surface Weighted, D[3,2]	24.63	27.03	100.00	Surface	2.90	12.90	65.08	4.20
Volume, D[3,0]	7.13							
Volume Weighted, D[4,3]	54.30	34.25	100.00	Volume	11.31	48.12	98.42	137.12

Volume Percentage Table (ID#:6426) (Status: Full scale)

Under(%)	Size	Under(%)	Size	Under(%)	Size	Under(%)	Size
0.00	0.14	30.00	31.89	55.00	54.21	80.00	85.81
5.00	6.38	35.00	35.95	60.00	60.45	85.00	87.55
10.00	11.31	40.00	41.02	65.00	65.66	90.00	98.42
15.00	17.10	45.00	45.37	70.00	72.91	95.00	117.56
20.00	22.61	50.00	48.12	75.00	77.11	100.00	137.27
25.00	27.40						

Volume Histogram and Cumulative Undersize (ID#:6426) (Full scale)

Mean: 54.30 um STD: 34.25 um Conf.: 100.00 %

Volume Histogram and Cumulative Undersize (ID#:6426) (Full scale)
D10 : 11.31 um D50: 48.12 um D90: 98.42 um

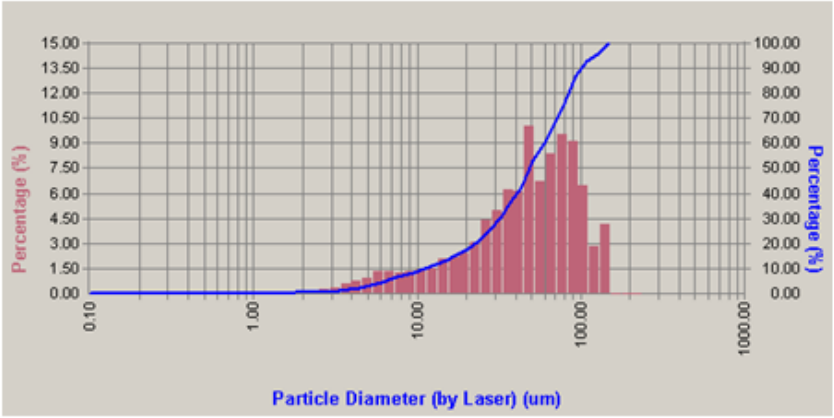

Number Percentage Table (ID#:6426) (Status: Full scale)

Under(%)	Size	Under(%)	Size	Under(%)	Size	Under(%)	Size
0.00	0.00	30.00	0.87	60.00	1.59	90.00	4.64
10.00	0.58	40.00	1.16	70.00	2.17	100.00	137.27
20.00	0.72	50.00	1.45	80.00	3.19		

Number Histogram and Cumulative Undersize (ID#:6426) (Full scale)
Mean: 2.25 um STD: 3.11 um Conf.: 100.00 %
D10 : 0.58 um D50: 1.45 um D90: 4.64 um

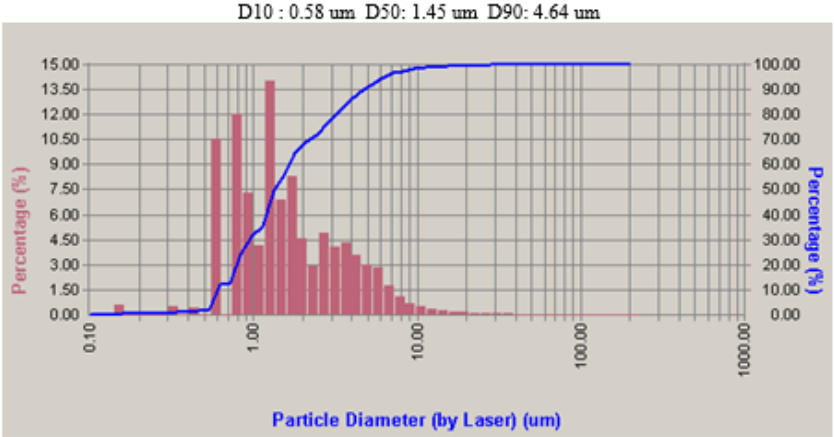

Appendix C: Waterglass (Na_2SiO_3)

TECHNICAL DATA SHEET

BRENNTAG

SODIUM SILICATE 37-38 °BE

Product code: MS16283 | Date of issue: 14/01/2014 | Replaces: 13/07/11

FORMULA : SiO_2 3,3/3,5 Na_2O (CAS : 1344-09-8 / EINECS : 215-687-4)
Custom tariff no.: 28.39.19.00

Main uses

- Detergent industry
- Laundries
- Ceramic – refractories
- Building and insulating materials
- Paper mills
- Cardboard industries
- Manufacture of catalysts and white fillers
- Oil refining
- Impregnation
- De-inking
- Flotation process
- Paint and enamel industries
- Soil reinforcements
- Agriculture
- Manufacture of silica-gel
- Water purifying plants
- Cement industries
- Fireproofing
- Mining industries

COMPOSITION

SiO_2	: 26,3 - 27,5	% ≙ 26,9 wt% = 44,77 mol%
Na_2O	: 7,8 - 8,2	% ≙ 8,0 wt% = 12,907 mol%

PHYSICAL PROPERTIES

Density (20°C)	: 1,34 – 1,36	kg/l
Viscosity (20°C)	: 80 – 100	cp

1 cp = 1 mPa.

CHEMICAL ANALYSIS

Beaumé	: 37 – 38	°BE
Mol ratio	: 3,3 / 3,5	

PACKING

Can be obtained in bulk, IBC's, drums and cans.
Other packing are available on request.

$\rho = 1,35$ kg/l.
$weight_{can} = 27$ kg.
$V = \frac{27}{1,35} = 20$ liter.

STORAGE

Dry warehouse, keep the temp. above 0 °C.

SAFETY REGULATION

The safety data sheet is available on request.

1/1

BRENNTAG N.V. • Nijverheidslaan 38 • BE-8540 DEERLIJK
Tel. +32(0)56/77.69.44 • Fax +32(0)56/77.57.11 • info@brenntag.be • www.brenntag.be
BTW nr. : BE0405317567 • KvK Deerlijk no.: HRKortrijk 76927
BRENNTAG Nederland B.V. • Donker Duyvisweg 44 • NL-3316 BM DORDRECHT
Tel. +31(0)78/65.44.944 • Fax +31(0)78/65.44.919 • info@brenntag.nl • www.brenntag.nl
BTW nr. : NL001375945B01 • KvK Dordrecht no.: 30112931

1/1

Appendix D: Acti-gel properties

Acti-Gel 208®

Mineral Additive

High Performance Rheology Modifier and Mix Stabilizer

Product Description

Acti-Gel® 208 is a low-dose rheology modifier and anti-settling agent that stabilizes mixtures, provides superior aggregate suspension, and dramatically improves the performance and paste quality of concretes. When fully dispersed, Acti-Gel® 208 particles form a unique lattice 'microstructure' that supports slightly higher yield stress and thixotropy, resulting in a greater ability to suspend both cement particles and aggregate with reduced segregation and bleed. Under conditions of shear, flow conditions are enhanced resulting in improved pumpability and workability. Some designs may result in a reduction in measured slump. Please see optimizing recommendations below.

Acti-Gel® 208 is made from a highly purified Mg-aluminosilicate using a patented process. It is non-swelling and shear stable in both low and high salt environments and between pH 2-13.

Acti-Gel® 208 is neutral setting and will not affect air contents.

Acti-Gel® 208 complies with ASTM C 494, Type S.

MADE IN USA

Packaging

Acti-Gel® 208 is supplied in powder or suspension form.

Applications:

- **Self-consolidating concretes (SCCs)**
- **Pre-cast concrete**
- **Shotcrete (wet and dry-mix)**
- **Slip-form pavements, extruded curb, etc.**
- **Deep foundations/anti-washout, underwater applications**
- **Lightweight concrete, and more.**

Benefits:

- **Unsurpassed concrete stability,**
- **Reduces unwanted bleeding, eliminates mortar halo in SCCs,**
- **Suspends both coarse and fine particles and manufactured or gap-graded aggregates,**
- **Improves surface finish; dramatically reduces bug holes,**
- **Superior cohesion for low rebound shotcrete; thicker applications and higher lifts,**
- **Dramatically reduces airborne particles in sprayed applications,**
- **Higher green strength for shape stability in slip-cast,**
- **Reduced form-work pressure in SCC applications,**
- **Easily pumps low-slump concrete,**
- **Recovers unstable or over-activated designs.**

Performance

Acti-Gel® 208 is a thixotropic material that suspends particles, reduces segregation, and dramatically stabilizes concretes. During mixing or emplacement, flow is greatly enhanced due to its shear-thinning behavior. On removal of shear, the rate of thixotropic rebuilding of the lattice structure is exceptionally fast, which provides i) superior cohesion, ii) rapid development of green strength and shape stability, iii) excellent anti-washout properties, and iv) reduction in hydrostatic pressure.

When used in an optimized mix design, Acti-Gel® 208 has been shown to increase early strength, reduce shrinkage, decrease rapid chloride permeability, and reduce efflorescence – all with outstanding workability and off-form finish. Please contact your local representative for recommendations.

ActiveMinerals INTERNATIONAL, LLC®
Integrity. Innovation. Teamwork. Execution.

34 Loveton Circle, Suite 100, Sparks, Maryland 21152
Tel: 800-258-2600 * Fax: 815-333-2997
info@activeminerals.com

www.activeminerals.com

Properties

Acti-Gel® 208: An excellent high solids suspending agent for concretes.

- ✓ Anti-settling and anti-segregation control
  - Unsurpassed concrete stability,
  - Eliminates bleed,
  - No mortar halo.

Properties

Acti-Gel® 208: Superior flowability and passing ability

- ✓ Rheology modifier *('low yield point, shear thinning')*
  - High structural stability *when static*, but…
  - Flows easily *when mixed, pumped*, or *extruded.*

Key! ⟹ *When shear is removed*, structural stability immediately returns.

⟹ Higher green strength, faster

⟹ Improved adhesion and greatly improved cohesion

⟹ Superior anti-washout control

Table 1. Typical Properties

Physical	
pH	8.50-9.25
Sp. Grav. (powder)	2.29
Sp. Grav. (24% suspension)	1.154

Table 2. Chemical Composition

Oxide composition	*wt. %*
SiO_2	50.2
Al_2O_3	9.8
MgO	9.1
Fe_2O_3	3.2
CaO	3.0
Na_2O	0.6
K_2O	0.6
TiO_2	0.4
P_2O_5	0.7
LOI	22.0
Water sol. Cl^-	<0.001
Acid sol. Cl^-	0.007

Appendix E: Rheometer test results

Mixture 1:

Table E. 1: Rheometer results of mixture 1 with 0% Acti-gel at 0 minutes after mixing

S20 0% Acti-gel l/b=0.315 (0 min)				
Shear rate	Shear stress (τ)	Apparent viscosity (μ)	Plastic viscosity (η)	Torque
[1/s]	[Pa]	[Pa·s]	[Pa·s]	[μNm]
20	135.2	6.8	6.1	415
40	252.9	6.3		775.9
60	376.6	6.3		1155
80	501.7	6.3		1539
100	624.8	6.2		1919

Table E. 2: Rheometer results of mixture 1 with 0% Acti-gel at 10 minutes after mixing

S20 0% Acti-gel l/b=0.315 (10 min)				
Shear rate	Shear stress (τ)	Apparent viscosity (μ)	Plastic viscosity (η)	Torque
[1/s]	[Pa]	[Pa·s]	[Pa·s]	[μNm]
20	161.9	8.1	7.7	496.2
40	319.1	8.0		979.1
60	483.8	8.1		1483
80	617.1	7.7		1894
100	780.2	7.8		2393

Table E. 3: Rheometer results of mixture 1 with 0% Acti-gel at 20 minutes after mixing

S20 0% Acti-gel l/b=0.315 (20 min)				
Shear rate	Shear stress (τ)	Apparent viscosity (μ)	Plastic viscosity (η)	Torque
[1/s]	[Pa]	[Pa·s]	[Pa·s]	[μNm]
20	199.8	10.0	9.2	612.9
40	371.5	9.3		1139
60	551	9.2		1690
80	727.2	9.1		2231
100	939.1	9.4		2878

Table E. 4: Rheometer results of mixture 1 with 0% Acti-gel at 30 minutes after mixing

S20 0% Acti-gel l/b=0.315 (30 min)				
Shear rate	Shear stress (τ)	Apparent viscosity (μ)	Plastic viscosity (η)	Torque
[1/s]	[Pa]	[Pa·s]	[Pa·s]	[μNm]
20	204.7	10.2	10.2	627.6
40	418.8	10.5		1284
60	602.7	10.1		1850
80	804.9	10.1		2470
100	1024	10.2		3140

Mixture 2:

Table E. 5: Rheometer results of mixture 2 with 0.2% Acti-gel at 0 minutes after mixing

S20 0.2% Acti-gel l/b=0.315 (0 min)				
Shear rate	Shear stress (τ)	Apparent viscosity (μ)	Plastic viscosity (η)	Torque
[1/s]	[Pa]	[Pa·s]	[Pa·s]	[μNm]
20	188.3	9.4	7.0	577.5
40	334.8	8.4		1027.3
60	467.6	7.8		1437
80	601.3	7.5		1844
100	746.9	7.5		2292

Table E. 6: Rheometer results of mixture 2 with 0.2% Acti-gel at 10 minutes after mixing

S20 0.2% Acti-gel l/b=0.315 (10 min)				
Shear rate	Shear stress (τ)	Apparent viscosity (μ)	Plastic viscosity (η)	Torque
[1/s]	[Pa]	[Pa·s]	[Pa·s]	[μNm]
20	113.99	5.7	6.2	349.7
40	245.5	6.1		752.8
60	324.9	5.4		996
80	472.7	5.9		1449
100	609.6	6.1		1871

Table E. 7: Rheometer results of mixture 2 with 0.2% Acti-gel at 20 minutes after mixing

S20 0.2% Acti-gel l/b=0.315 (20 min)				
Shear rate	Shear stress (τ)	Apparent viscosity (μ)	Plastic viscosity (η)	Torque
[1/s]	[Pa]	[Pa·s]	[Pa·s]	[μNm]
20	190.4	9.5	9.1	584.1
40	372.7	9.3		1144
60	545.3	9.1		1673
80	728.6	9.1		2236
100	919.4	9.2		2820

Table E. 8: Rheometer results of mixture 2 with 0.2% Acti-gel at 30 minutes after mixing

S20 0.2% Acti-gel l/b=0.315 (30 min)				
Shear rate	Shear stress (τ)	Apparent viscosity (μ)	Plastic viscosity (η)	Torque
[1/s]	[Pa]	[Pa·s]	[Pa·s]	[μNm]
20	200.4	10.0	9.1	614.6
40	377.9	9.4		1160
60	547.5	9.1		1682
80	724.8	9.1		2223
100	930.5	9.3		2855

Mixture 3:

Table E. 9: Rheometer results of mixture 3 with 0.5% Acti-gel at 0 minutes after mixing

S20 0.5% Acti-gel l/b=0.315 (0 min)				
Shear rate	Shear stress (τ)	Apparent viscosity (μ)	Plastic viscosity (η)	Torque
[1/s]	[Pa]	[Pa·s]	[Pa·s]	[μNm]
20	179.3	9.0	7.4	550.1
40	319.7	8.0		981.5
60	453.5	7.6		1391
80	612.6	7.7		1879
100	771.4	7.7		2366

Table E. 10: Rheometer results of mixture 3 with 0.5% Acti-gel at 10 minutes after mixing

S20 0.5% Acti-gel l/b=0.315 (10 min)				
Shear rate	Shear stress (τ)	Apparent viscosity (μ)	Plastic viscosity (η)	Torque
[1/s]	[Pa]	[Pa·s]	[Pa·s]	[μNm]
20	201.7	10.1	8.4	619.2
40	381.1	9.5		1168
60	551.9	9.2		1694
80	709.1	8.9		2176
100	871.1	8.7		2673

Table E. 11: Rheometer results of mixture 3 with 0.5% Acti-gel at 20 minutes after mixing

S20 0.5% Acti-gel l/b=0.315 (20 min)				
Shear rate	Shear stress (τ)	Apparent viscosity (μ)	Plastic viscosity (η)	Torque
[1/s]	[Pa]	[Pa·s]	[Pa·s]	[μNm]
20	192.9	9.6	8.1	591.5
40	364.3	9.1		1118
60	527.8	8.8		1618
80	680.3	8.5		2087
100	838.3	8.4		2572

Table E. 12: Rheometer results of mixture 3 with 0.5% Acti-gel at 30 minutes after mixing

S20 0.5% Acti-gel l/b=0.315 (30 min)				
Shear rate	Shear stress (τ)	Apparent viscosity (μ)	Plastic viscosity (η)	Torque
[1/s]	[Pa]	[Pa·s]	[Pa·s]	[μNm]
20	204.5	10.2	8.6	626.5
40	391.4	9.8		1201
60	558.8	9.3		1715
80	731.1	9.1		2242
100	890.5	8.9		2732

Mixture 4:

Table E. 13: Rheometer results of mixture 4 with 0.75% Acti-gel at 0 minutes after mixing

S20 0.75% Acti-gel l/b=0.315 (0 min)				
Shear rate	Shear stress (τ)	Apparent viscosity (μ)	Plastic viscosity (η)	Torque
[1/s]	[Pa]	[Pa·s]	[Pa·s]	[μNm]
20	181	9.1	6.0	556
40	327	8.2		1004
60	446	7.4		1368
80	554	6.9		1698
100	663	6.6		2034

Table E. 14: Rheometer results of mixture 4 with 0.75% Acti-gel at 10 minutes after mixing

S20 0.75% Acti-gel l/b=0.315 (10 min)				
Shear rate	Shear stress (τ)	Apparent viscosity (μ)	Plastic viscosity (η)	Torque
[1/s]	[Pa]	[Pa·s]	[Pa·s]	[μNm]
20	161.7	8.1	6.8	496
40	299.7	7.5		919.6
60	441.1	7.4		1352
80	600.8	7.5		1843
100	707.6	7.1		2171

Table E. 15: Rheometer results of mixture 4 with 0.75% Acti-gel at 20 minutes after mixing

S20 0.75% Acti-gel l/b=0.315 (20 min)				
Shear rate	Shear stress (τ)	Apparent viscosity (μ)	Plastic viscosity (η)	Torque
[1/s]	[Pa]	[Pa·s]	[Pa·s]	[μNm]
20	196.8	9.8	8.0	603.9
40	362.5	9.1		1111
60	510.7	8.5		1567
80	667.4	8.3		2048
100	835	8.3		2562

Table E. 16: Rheometer results of mixture 4 with 0.75% Acti-gel at 30 minutes after mixing

S20 0.75% Acti-gel l/b=0.315 (30 min)				
Shear rate	Shear stress (τ)	Apparent viscosity (μ)	Plastic viscosity (η)	Torque
[1/s]	[Pa]	[Pa·s]	[Pa·s]	[μNm]
20	177.3	8.9	8.8	544.6
40	343	8.6		1053.3
60	498.4	8.3		1527
80	725.1	9.1		2224
100	881.1	8.8		2704

Mixture 5:

Table E. 17: Rheometer results of mixture 5 with 1% Acti-gel at 0 minutes after mixing

S20 1% Acti-gel l/b=0.315 (0 min)				
Shear rate	Shear stress (τ)	Apparent viscosity (μ)	Plastic viscosity (η)	Torque
[1/s]	[Pa]	[Pa·s]	[Pa·s]	[μNm]
20	168.1	8.4	5.3	515
40	302.6	7.6		928.6
60	368.2	6.1		1131
80	487.8	6.1		1497
100	596	6.0		1830

Table E. 18: Rheometer results of mixture 5 with 1% Acti-gel at 10 minutes after mixing

S20 1% Acti-gel l/b=0.315 (10 min)				
Shear rate	Shear stress (τ)	Apparent viscosity (μ)	Plastic viscosity (η)	Torque
[1/s]	[Pa]	[Pa·s]	[Pa·s]	[μNm]
20	182.6	9.1	7.9	560.3
40	330.8	8.3		1015.3
60	498.3	8.3		1528
80	644.4	8.1		1978
100	811.4	8.1		2491

Table E. 19: Rheometer results of mixture 5 with 1% Acti-gel at 20 minutes after mixing

S20 1% Acti-gel l/b=0.315 (20 min)				
Shear rate	Shear stress (τ)	Apparent viscosity (μ)	Plastic viscosity (η)	Torque
[1/s]	[Pa]	[Pa·s]	[Pa·s]	[μNm]
20	197.2	9.9	7.3	604.7
40	348.6	8.7		1070
60	492.8	8.2		1511
80	620.7	7.8		1906
100	777.9	7.8		2387

Table E. 20: Rheometer results of mixture 5 with 1% Acti-gel at 30 minutes after mixing

S20 1% Acti-gel l/b=0.315 (30 min)				
Shear rate	Shear stress (τ)	Apparent viscosity (μ)	Plastic viscosity (η)	Torque
[1/s]	[Pa]	[Pa·s]	[Pa·s]	[μNm]
20	195.6	9.8	8.2	599.7
40	340.9	8.5		1045.2
60	512.3	8.5		1569
80	717.5	9.0		2200
100	852.6	8.5		2615

Mixture 6:

Table E. 21: Rheometer results of mixture 6 with 1.5% Acti-gel at 0 minutes after mixing

S20 1.5% Acti-gel l/b=0.315 (0 min)				
Shear rate	Shear stress (τ)	Apparent viscosity (μ)	Plastic viscosity (η)	Torque
[1/s]	[Pa]	[Pa·s]	[Pa·s]	[μNm]
20	153.5	7.7	4.9	471.2
40	266.3	6.7		817.5
60	359.6	6.0		1102
80	449.9	5.6		1379
100	547.6	5.5		1680

Table E. 22: Rheometer results of mixture 6 with 1.5% Acti-gel at 10 minutes after mixing

S20 1.5% Acti-gel l/b=0.315 (10 min)				
Shear rate	Shear stress (τ)	Apparent viscosity (μ)	Plastic viscosity (η)	Torque
[1/s]	[Pa]	[Pa·s]	[Pa·s]	[μNm]
20	160.2	8.0	6.0	492
40	283.4	7.1		869.3
60	426.7	7.1		1310
80	556.2	7.0		1707
100	642.7	6.4		1971

Table E. 23*: Rheometer results of mixture 6 with 1.5% Acti-gel at 20 minutes after mixing*

S20 1.5% Acti-gel l/b=0.315 (20 min)				
Shear rate	Shear stress (τ)	Apparent viscosity (μ)	Plastic viscosity (η)	Torque
[1/s]	[Pa]	[Pa·s]	[Pa·s]	[μNm]
20	179.8	9.0	6.5	551.2
40	301.6	7.5		925.3
60	429	7.1		1316
80	558.1	7.0		1710
100	703.3	7.0		2159

Table E. 24: Rheometer results of mixture 6 with 1.5% Acti-gel at 30 minutes after mixing

S20 1.5% Acti-gel l/b=0.315 (30 min)				
Shear rate	Shear stress (τ)	Apparent viscosity (μ)	Plastic viscosity (η)	Torque
[1/s]	[Pa]	[Pa·s]	[Pa·s]	[μNm]
20	130.5	6.5	6.3	400.3
40	224	5.6		686.8
60	324.6	5.4		995.9
80	507.6	6.4		1556
100	637.4	6.4		1956

Appendix F: Ram extruder test results

S20 0% Acti-gel
L/B= 0.315

$$P_e = P_1 + P_2 = 2\,ln\left(\frac{D_0}{D}\right)(\sigma_0 + \alpha V^n) + \frac{4L}{D}(\tau_0 + \beta V^n)$$

$$Q = Velocity(die) * A(die)$$

0% Acti-gel S die		
Speed	L/D	Pressure [kPa]
9	1.0	27.3
4.5	1.0	27.4
2.25	1.0	28.8

0% Acti-gel M die		
Speed	L/D	Pressure [kPa]
9	4.0	29.9
4.5	4.0	32.7
2.25	4.0	34.2

0% Acti-gel L die		
Speed	L/D	Pressure [kPa]
9	8.0	42.0
4.5	8.0	38.2
2.25	8.0	40.4

Fluid speed in die	
2.25 mm/s a	1.651
2.25 mm/s b	27.325
4.5 mm/s a	1.5427
4.5 mm/s b	26.041

τ0	0.44
β	-0.01
α	-0.26
σ0	13.00

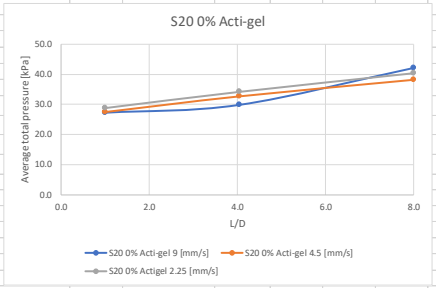

Barrel	
Diameter [mm] D0	38.4
Height [mm]	125
Radius [mm]	62.5
Area [mm2]	12271.8
Volume [mm3]	471238.9
Dies D [mm]	12.8
Radius R [mm]	6.4
L (S die) [mm]	12.8
L (M die) [mm]	51.8
L (L die) [mm]	102.4
Volume Die S [mm3]	1647.1
Volume Die M [mm3]	6665.6
Volume Die L [mm3]	13176.8
Ln D0/D	1.10
2*ln (D0/D0	2.20
L (S die) [mm]	12.8
L (M die) [mm]	51.8
L (L die) [mm]	102.4
Dies D [mm]	12.8
L/D S die	1
L/D M die	4.0
L/D L die	8

	Small die	Fluid speed in barrel
P1	27.43103051	2
p1	27.99527778	1
P1	28.27740142	0.5
p1	28.41846324	0.25
P2	1.66	2
P2	1.708	1
P2	1.732	0.5
P2	1.744	0.25
	Medium die	Fluid speed in barrel
P2	6.7178125	2
P2	6.9120625	1
P2	7.0091875	0.5
P2	7.05775	0.25
	Large die	Fluid speed in barrel
P2	13.28	2
P2	13.664	1
P2	13.856	0.5
P2	13.952	0.25

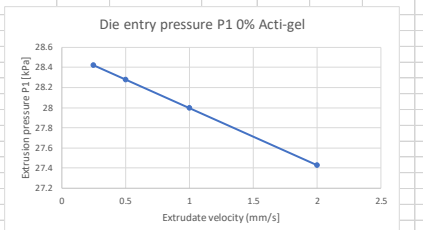

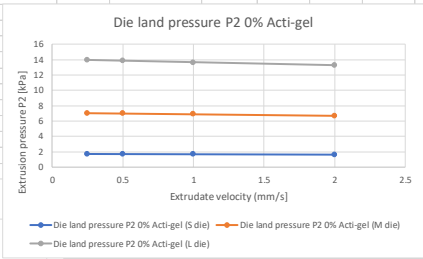

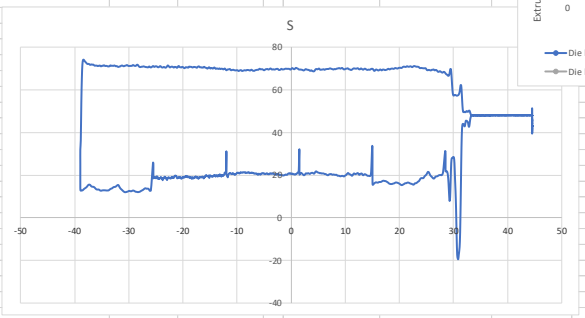

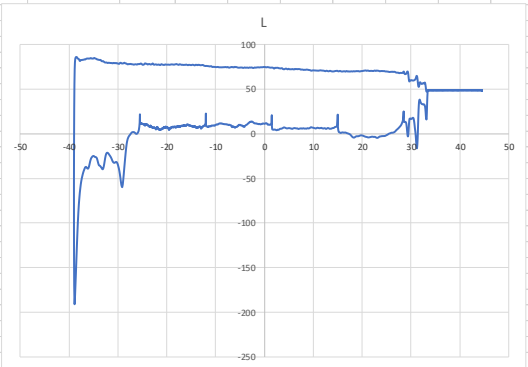

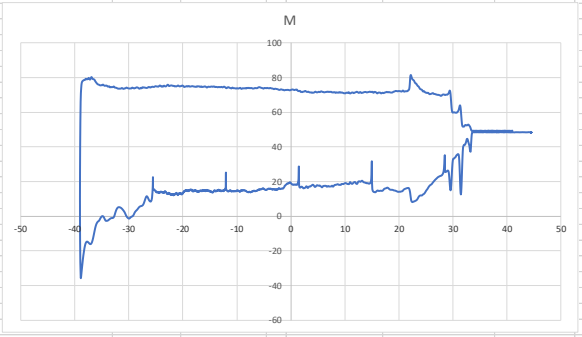

S20 0.5% Acti-gel
L/B= 0.315

$$P_e = P_1 + P_2 = 2\,ln\left(\frac{D_0}{D}\right)(\sigma_0 + \alpha V^m) + \frac{4L}{D}(\tau_0 + \beta V^n)$$

0.5% Acti-gel S die		
Speed	**L/D**	**Pressure [kPa]**
9	1	31.1
4.5	1	31.7
2.25	1	33.6

0.5% Acti-gel M die		
Speed	**L/D**	**Pressure [kPa]**
9	4.0	39.9
4.5	4.0	37.7
2.25	4.0	41.3

0.5% Acti-gel L die		
Speed	**L/D**	**Pressure [kPa]**
9	8.0	36.0
4.5	8.0	35.0
2.25	8.0	36.7

Fluid speed in die	
2.25 mm/s **a**	2.53
2.25 mm/s **b**	31.03
4.5 mm/s **a**	1.99
4.5 mm/s **b**	29.67

Ln D0/D	1.10
2*ln (D0/D0	2.20
L (S die) [mm]	**12.8**
L (M die) [mm]	**51.8**
L (L die) [mm]	**102.4**
Dies D [mm]	**12.8**
L/D S die	1
L/D M die	4.046875
L/D L die	8

Small die		Fluid speed in barrel
P1	31.13599	2
p1	31.73957	1
P1	32.04136	0.5
p1	32.19225	0.25
P2	2.59	2
P2	2.83	1
P2	2.95	0.5
P2	3.01	0.25

Medium die		Fluid speed in barrel
P2	10.48141	2
P2	11.45266	1
P2	11.93828	0.5
P2	12.18109	0.25

Large die		Fluid speed in barrel
P2	20.72	2
P2	22.64	1
P2	23.6	0.5
P2	24.08	0.25

τ0	**0.77**
β	**-0.06**
α	**-0.27**
σ0	**14.72**

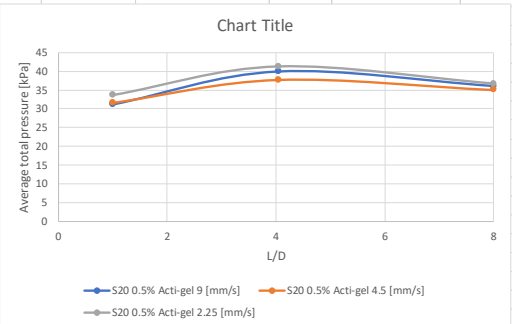

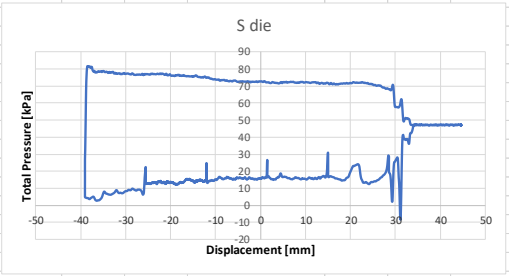

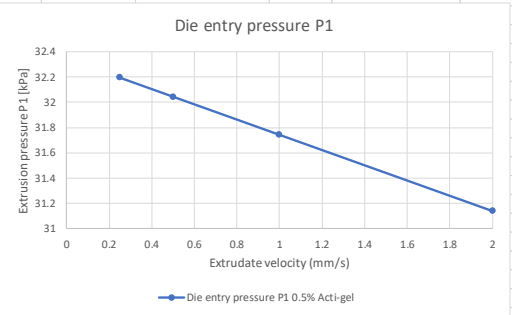

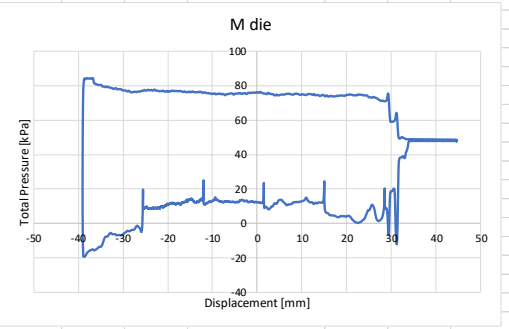

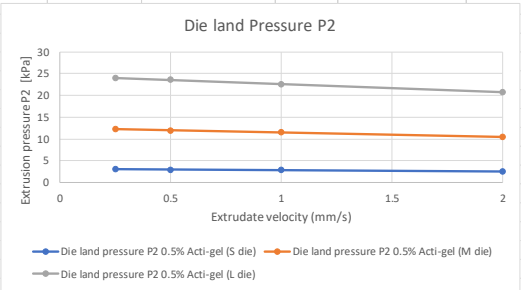

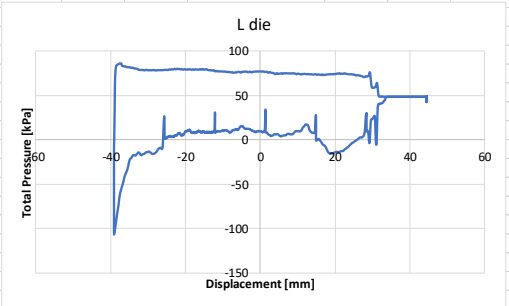

S20 0.75% Acti-gel
L/B= 0.315

0.75% Acti-gel S die		
Speed	L/D	Pressure [kPa]
9	1	28.8
4.5	1	30.9
2.25	1	33.0

0.75% Acti-gel M die		
Speed	L/D	Pressure [kPa]
9	4.0	40.0
4.5	4.0	35.0
2.25	4.0	34.0

0.75% Acti-gel L die		
Speed	L/D	Pressure [kPa]
9	8.0	50.09
4.5	8.0	47.83
2.25	8.0	52.15

Fluid speed in die	
2.25 mm/s a	2.82
2.25 mm/s b	27.47
4.5 mm/s a	2.45
4.5 mm/s b	27.26

Ln D0/D	1.10
2*ln (D0/D0	2.20
L (S die) [mm]	12.8
L (M die) [mm]	51.8
L (L die) [mm]	102.4
Dies D [mm]	12.8
L/D S die	1
L/D M die	4.046875
L/D L die	8

$$P_e = P_1 + P_2 = 2\ln\left(\frac{D_0}{D}\right)(\sigma_0 + \alpha V^m) + \frac{4L}{D}(\tau_0 + \beta V^n)$$

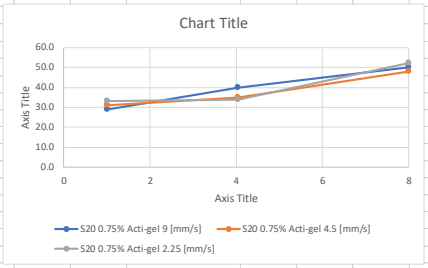

Small die		Fluid speed in barrel
P1	27.49164	2
p1	27.58492	1
P1	27.63156	0.5
p1	27.65488	0.25
P2	3.19	2
P2	4.67	1
P2	5.41	0.5
P2	5.78	0.25

τ0	1.54
β	-0.37
α	-0.04
σ0	12.58

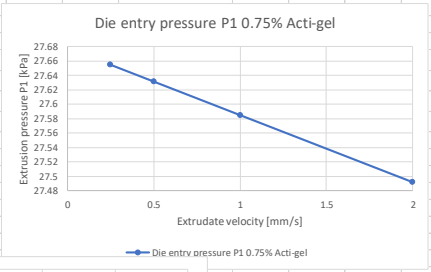

Medium die		Fluid speed in barrel
P2	12.90953	2
P2	18.89891	1
P2	21.89359	0.5
P2	23.39094	0.25

Large die		Fluid speed in barrel
P2	25.52	2
P2	37.36	1
P2	43.28	0.5
P2	46.24	0.25

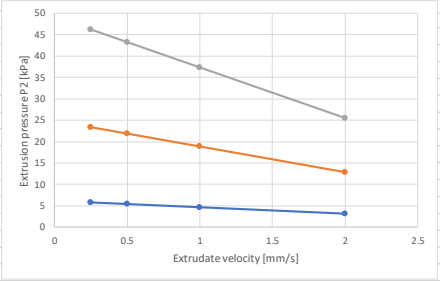

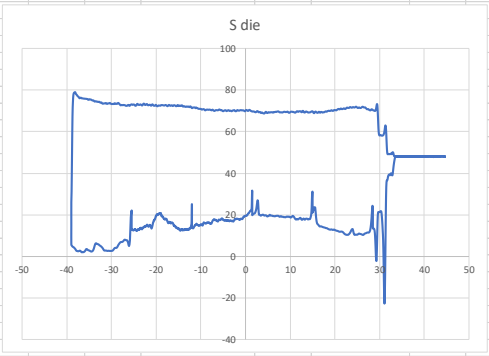

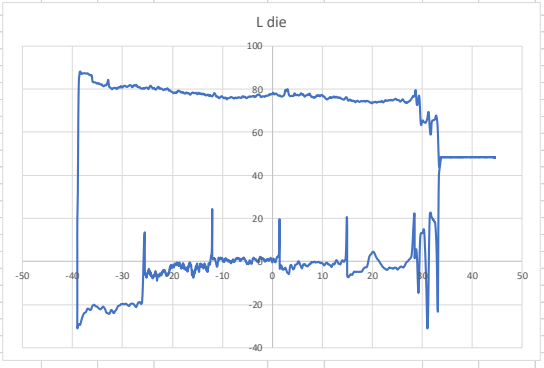

S20 1% Acti-gel
L/B= 0.315

1 % Acti-gel S die		
Speed	L/D	Pressure [kPa]
9	1	33.2
4.5	1	33.9
2.25	1	37.3
2	1	48.1

1 % Acti-gel M die		
Speed	L/D	Pressure [kPa]
9	4.0	36.9
4.5	4.0	35.3
2.25	4.0	36.1

1 % Acti-gel L die		
Speed	L/D	Pressure [kPa]
9	8	36.0
4.5	8	34.4
2.25	8	35.7
2	8	47.6

Fluid speed in die	
2.25 mm/s a	-0.222
2.25 mm/s b	37.296
4.5 mm/s a	0.06
4.5 mm/s b	34.28

Ln D0/D	1.10
2*ln (D0/D0	2.20
L (S die) [mm]	12.8
L (M die) [mm]	51.8
L (L die) [mm]	102.4
Dies D [mm]	12.8
L/D S die	1
L/D M die	4.047
L/D L die	8

$$P_e = P_1 + P_2 = 2\,ln\left(\frac{D_0}{D}\right)(\sigma_0 + \alpha V^m) + \frac{4L}{D}(\tau_0 + \beta V^n)$$

τ0	-0.13
β	0.03
α	-0.61
σ0	18.32

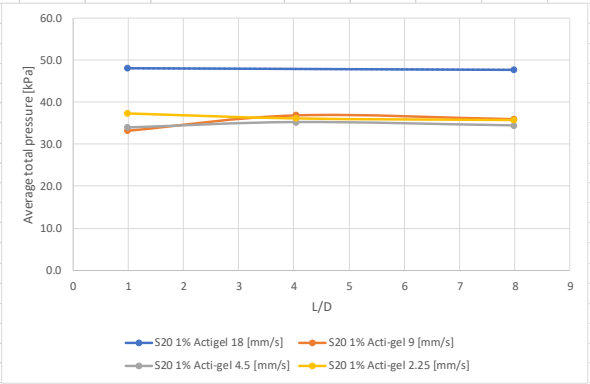

Small die		fluid speed in barrel
P1	37.63104	2
p1	38.97148	1
P1	39.6417	0.5
p1	39.97681	0.25
P2	-0.25334	2
P2	-0.37867	1
P2	-0.44133	0.5
P2	-0.47267	0.25

Medium die		fluid speed in barrel
P2	-1.02522	2
P2	-1.53242	1
P2	-1.78602	0.5
P2	-1.91282	0.25

Large die		fluid speed in barrel
P2	-2.02669	2
P2	-3.02934	1
P2	-3.53067	0.5
P2	-3.78134	0.25